Investigation of wind turbine generator's cables and their impact on waveform deterioration by means of experiment and circuit simulation

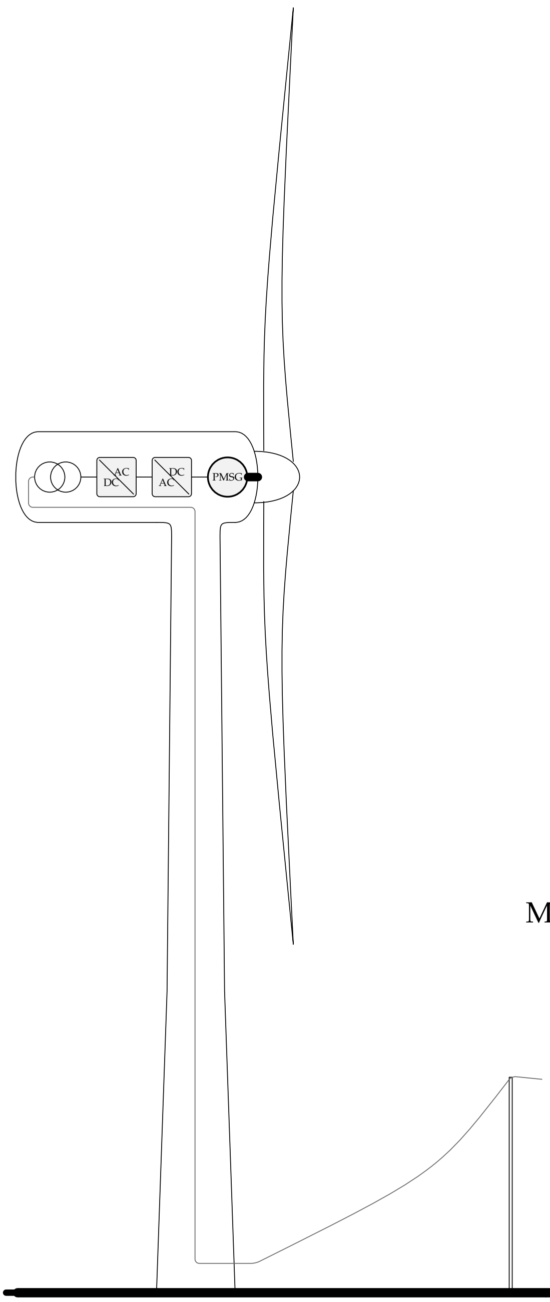

Master Thesis

WPS4-1050

Aalborg University

MSc Energy Engineering

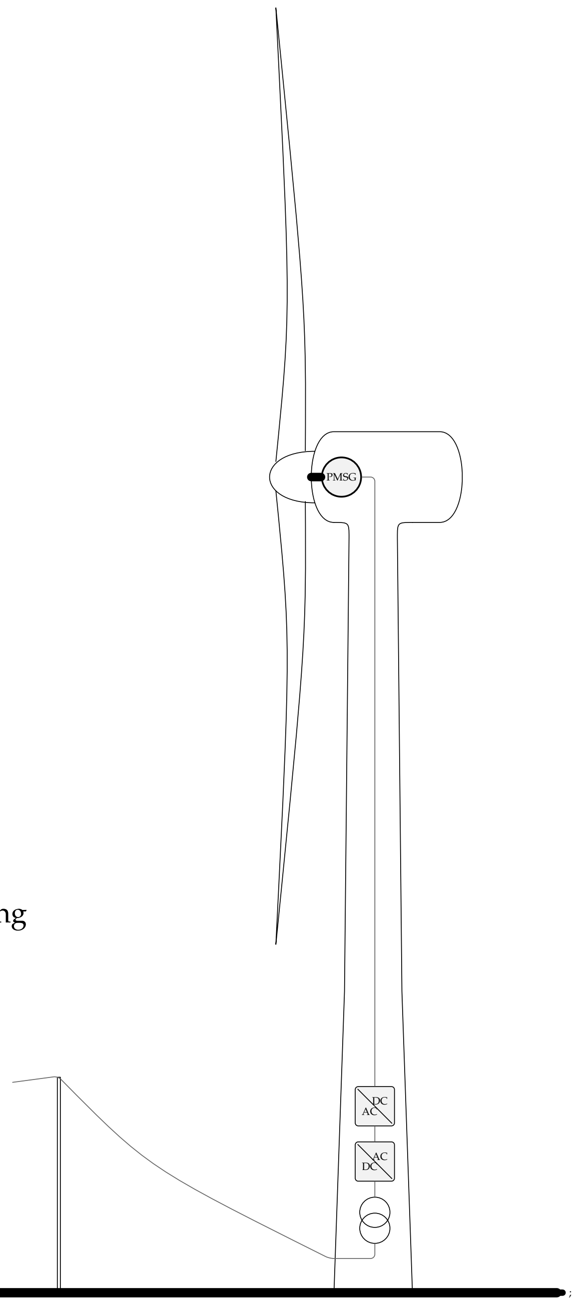

LaTeX has been used for typesetting the document. Figures and images including electrical circuits are created by the usage of Ti*k*Z. To process the data obtained, Matlab has been used. The circuit simulator PLECS was chosen for modelling.

AALBORG UNIVERSITY
STUDENT REPORT

MSc Energy Engineering
Specialization: Wind Power System
Aalborg University
http://www.aau.dk

Title:
Investigation of wind turbine generator's cables and their impact on waveform deterioration by means of experiment and circuit simulation

Theme:
Long cables, waveform deterioration, power converter, stability, wind power applications, permanent magnet synchronous generator, waveform reflection, *dV/dt* filter, HF-modelling, converter arrangement, tower base

Project Period:
Spring Semester 2019

Project Group:
WPS4-1050

Participant(s):
Lennart Beland
Tim Deininger

Supervisor(s):
Philip Carne Kjær, *AAU and Vestas A/S*
Kaiyuan Lu, *AAU*
Catalin-Gabriel Dincan, *Vestas A/S*

Page Numbers: 104

Date of Completion:
May 31, 2019

Abstract:

The evolvement of wind turbine power levels lead to an interest in investigating new physical conversion stage arrangements. One appealing distribution is moving the network decoupling back-to-back converter from nacelle to the tower base. This results in 100-200 m long cables between the generator in the nacelle and converter at ground level.
The motivation is to investigate resultant reflection effects due to long cables at the cable junctions in nacelle and tower base.
To investigate the cables impact, a low voltage setup emulates the above WTG topology and serves as a downscaled validation study. A circuit simulation of generator, cables and active rectifier is modeled in reflecting the experimental setup. Generator and cable components are parameterized by impedance fitting to the implemented model. Based on the validation, medium voltage simulation gives further insight for an expected application.
This gives the ability to assess the feasibility of a *dV/dt* filter. With the overvoltages suppressed, the generator is protected from harmful winding stresses.

Executive Summary

Introduction wise the issue of long cables between a converter and generator in wind turbines is given. Embedding the greater picture, the long cable is introduced due to rearrangement of generator and converter components in wind turbines, thus potentially reducing the levelized cost of energy. Following, the goal of the thesis is formulated, and the tools and environment for the solution is given.

A literature review of cable effects on pulses gives a theoretical frame of the voltage doubling phenomena. The overvoltage, leads to high rates of voltage change and a high frequency ringing at the generator terminal and a current distortion at the converter terminal. These issues are the result of an impedance mismatch between generator and cable. This could introduce high overvoltage ranging multiple p.u..

This thesis introduces a cable mode, which includes all important quantified behaviors. The sensitivity of the cable structure is investigated, and it is concluded, that utilizing the proposed high frequency transmission line model with 10 model sections yields sufficient accurate results for the purposes of this thesis. The relation between rise time and cable length (equivalent to traveling time) results in a certain overshoot when neglecting the damping behavior.

Following, common mode voltages and currents are considered, explaining a noise source in the system. It is proposed that a high frequency generator model should result in an accurately modeled damping behavior of the cable oscillation. Thus, a combination of fundamental dq0 model and a high frequency model should result in a universal usable model. A solution to suppress reflections in a cable, can be a *dV/dt* filter. A very simple topology is a LRC filter which can be used to prove the idea of suppressing the overshoot at the generator terminal.

To Characterize the experimental setup and thus match the simulation, impedance measurements are conducted for the cable and the generator. This methodology leads to very accurate results for the cable model. The obtained parameter yields the traveling time with an error of 0.7%. An identified problem is the scalability of the cable to length, where a difference of the line inductance between a short and a long cable of 20% is observed. For the generator parameterization did the model structure not correspond completely to the measured data. Nevertheless,

the resulting integrated model represents the reflection factor of the impedance mismatch with 5% error. This damping factor can be adjusted to yield realistic results.

The resulting waveform deterioration introduces two issues into the system. On the one hand introduced the long cable noise into the current measured at the converter terminal. This means that the sampling for a controller is potentially impacted. On the other hand, does the voltage doubling phenomena lead to additional insulation stress of the generator. For the investigated system both the dV/dt and the Voltage peak increase by 75%.

Thus, the previously proposed filter is introduced into the system. Even though this filter introduces power losses of over 1% into the system and is therefore not economical, the principle of a dV/dt filter as solution to the voltage doubling phenomena is demonstrated. The overshoot decreases 70% and the rate of voltage change decreases 10-fold. Additionally, the current noise is decreased to a level similar of a short cable.

Finally, a future use case of long generator cables is developed and due to the lack of actual data all parameters for the model are estimated. Thus, the expected behavior of a cable in a multi megawatt medium voltage environment is estimated. It can been seen, that despite the different cable parameter, the general behaviour of cable and filter in the new environment is similar to what was seen previously. Thus it is expected that the reflection behaviour of a long cable needs to be investigated further to prove the meaningfulness of this turbine topology.

Contents

List of Figures

List of Tables

List of Abbreviations and Symbols

Acronyms

ASM ...... Asynchronous Machine

DFIG ..... Double Feed Induction Generator

ESR .... Equivalent Series Resistance

FS .... Full Scale

HF .... High Frequency

IGBT ..... Insulated-gate bipolar transistor

IM .... Induction Machine

LCOE .... Levelized Cost Of Energy

MV .... Medium Voltage

OC .... Open Circuit

PMSG .... Permanent Magnet Synchronous Generator

PWM ..... Pulse Width Modulation

SC .... Short Circuit

Physical Symbols

Γ_g .... Reflection coefficient at generator side .... [ ]

Γ_{con} .... Reflection coefficient at converter side .... [ ]

μ .... Permeability .... [H/m]

μ_r .... Relative Permeability .... [ ]

ω_m .... Mechanical angular rotor speed .... [rad/s]

$\overline{V}_{l-l}$ ...... Peak line to line Voltage ......[V]

ϕ_d, ϕ_d ..... d- and q-axis stator flux linkage ......[Wb]

ϕ_m .... Permanent magnet flux linkage ......[Wb]

σ .... Logarithmic decay ......[ ]

θ_m .... Electrical angular rotor position ......[rad]

ε .... Permittivity ......[F/m]

ε_r .... Relative Permittivity ......[ ]

ζ .... Damping factor ......[ ]

c .... Speed of light ......[299 792 458 m/s]

$C^{'}$ .... Capacitance per unit length......[F/m]

C_f .... Filter Capacitance......[F]

$C^{'}_{px}$ .... Parallel Capacitance, while x = 1 for f_{low} and 2 for f_{high} ......[F/m]

C_{t_r} .... Capacitance for rise time emulation ......[F]

f_0 .... Cable oscillation (resonance) frequency ......[Hz]

f_d .... Damped oscillation frequency ......[Hz]

$f_{damp,osci}$ .. Damped oscillation function ......[Hz]

f_{high} ...... Highest test frequency in impedance measurement ......[Hz]

f_{low} .... Lowest test frequency in impedance measurement ......[Hz]

$f_{res,filter}$ ... Resonant frequency low-pass filter ......[Hz]

$G^{'}$ .... Conductance per unit length......[S/m]

i_d, i_q ...... d- and q-axis current ......[A]

I_0 .... Stall current ......[A]

I_N .... Rated current ......[A]

$L^{'}$ .... Inductance per unit length......[H/m]

l_c .... Cable length ......[m]

L_d, L_q ..... Rotor direct and quadrature axis PMSG inductance ......[H]

L_f	Filter inductance	[H]
$l_{critical}$	Critical cable length	[m]
M_0	Stall torque	[N · m]
M_N	Rated torque	[N · m]
n_{max}	Max permissible speed (mech.)	[1/min]
n_N	Rated speed	[1/min]
n_{opt}	Optimal speed	[1/min]
n_{pp}	Number of pole-pairs	[ ]
R'_{AC}	AC resistance per unit length	[Ω/m]
R_f	Filter resistance	[Ω]
R'_s	Series resistance per unit length	[Ω/m]
R_{ph}	Stator winding resistance	[Ω]
R'_{px}	Parallel Resistance, while x = 1 for f_{low} and 2 for f_{high}	[Ω/m]
R_{t_r}	Resistance for rise time emulation	[Ω]
$t_c r$	Critical rise time	[s]
T_e	Electromagnetic torque	[N · m]
t_r	Rise Time	[µs]
t_t	Traveling time of a pulse through cable	[µs]
t_{cycle}	Travel time for one oscillation cycle ($= 4t_t$)	[µs]
v_c	Pulse velocity (Propagation velocity) Cable	[m/µs]
v_{cm}	Common mode voltage	[V]
V_{damped}	Damped oscillatory voltage	[V]
V_{DC}	DC-link Voltage	[V]
$V_{o,\%}$	Voltage overshoot	[%]
$V_{refl,DC}$	Reflected voltage at generator terminal	[V]
$V_{refr,DC}$	Refracted voltage at generator terminal	[V]

v_{Xg} .... Phase-to-ground Voltage where X stands for phase U, V or W ....[V]

$x_{pp}(t, t + m\tau)$ Oscillation peak with extracted offset ....[V]

Z_0 .... Characteristic Impedance..[Ω]

$Z_{0,con}$ ..... Characteristic impedance Converter.............................[Ω]

$Z_{0,c}$ .... Characteristic impedance Cable ....[Ω]

$Z_{0,g}$ .... Characteristic impedance Generator ....[Ω]

$Z_{OC,meas}$ ... Measured value of open circuit impedance.......................[H]

$Z_{oc}^{'}$ .... Open circuit impedance......................................[Ω/m]

$Z_{SC,meas}$ ... Measured value of short circuit impedance.......................[H]

$Z_{sc}^{'}$ .... Short circuit impedance ....[Ω/m]

dV/dt ..... Rate of voltage rise ....[V/s]

a .... Radius of the conductor ....[m]

b .... Radius of the insulation ....[m]

λ_{mpm} ..... Magnet flux linkage ....[Wb]

Chapter 1

Introduction

The increase power consumption world wide, as well as political decisions demand more installed renewable energy capacities. Besides Hydro-, Solar- and Bio gas power, Wind energy is a promising candidate helping to fill that upcoming supply gap. [10, 32, 63]

With a growing share of power supplied by renewables it becomes more and more important, that these power plants contribute to grid stability. To meet those goals and also reduce the cost of energy, the trend of wind turbines is to raise the power level, while being more reliable, safe and expanding the lifetime expectations. [46]

The grid requirements and the attempt to maximize the energy yield of turbines lead to harsh demands of full power and speed control for WTGs. This lead to the point that the electrical drivetrain of multi-MW wind turbines can be generalized into two arrangements, both consisting of back-to-back converters. [25, 29, 34]

One, shown in figure 1.1a, is a doubly-fed induction generator (DFIG) with a partial-scale converter where approx. 30% of the power is converted. The other, as visualized in figure 1.1b, is the full-scale converter, where all power is converted. [9, 10, 47, 64]

The DFIG's main advantage of only converting partially the power declines, since power electronic converters are getting more efficient, reliable and sophisticated by means of withstand limits and switching frequencies.

By converting the full power with low voltage and high power levels, the fast switching devices are exposed to immense currents. This relates to large switching losses and parallel connected devices to withstand the current.

Nevertheless, the advantage of operating with a full-scale converter is to utilize PMSG involving the elimination of slip rings and simplified or even eliminated gearboxes. Those characteristics imply to maximize the power output and decrease the levelized cost of energy (LCOE), which is in correspondence to the preliminary mentioned future perspectives of WTGs.[9]

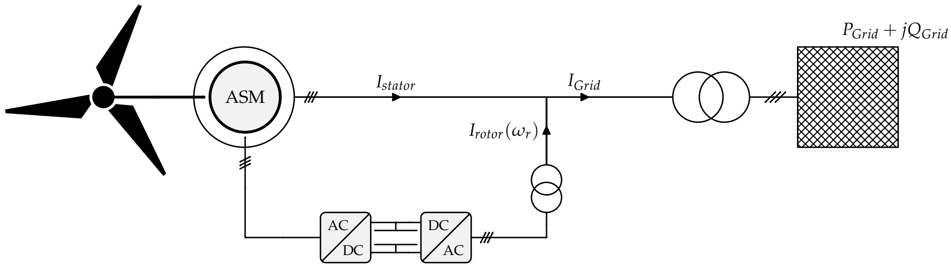

(a)

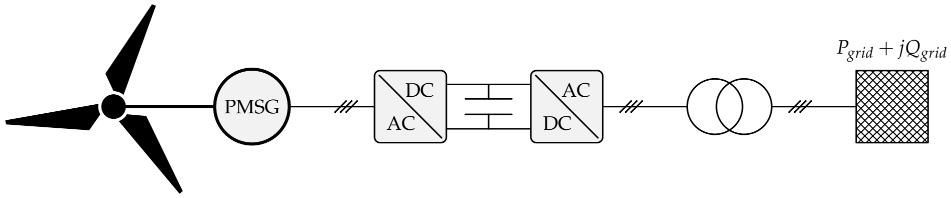

(b)

Figure 1.1: Schematic of: **a)** a partial-scaled Converter and **b)** a full-scaled Converter

Besides the benefit of a full-scale converter's operational flexibility [10, 27], around 20-30% of the downtime in modern wind turbines is related to component failure of converters [8, 18, 24]. By moving the converter stage from the nacelle down to the tower base it improves the accessibility of this high failure prone components which decreases the downtime of the WTG and thereby the LCOE [28, 60]. The relocation is visualized in figure 1.2.

With the WTG's evolvement to higher power levels, converter component failure rate is not expected to decline in near future. Medium voltage converters are a promising solution to circumvent the obstacles of high switching losses and high stress levels. Accompanying, this leads to WTG designs with medium voltage generators, making the step-up transformer redundant, decreasing the cost of energy for high power levels [52]. Though, low voltage is today still the mostly given level of operation [9].

An additional benefit of relocating the electrical components, including also filter and transformer, is to reduce the mechanical tension of the tower through the reduction of weight on WTG's upper part.

The importance of those benefits is confirmed by the trend of many wind turbine producers in cooperation with converter manufacturers of moving the electrical components down tower [cf. appendix A].

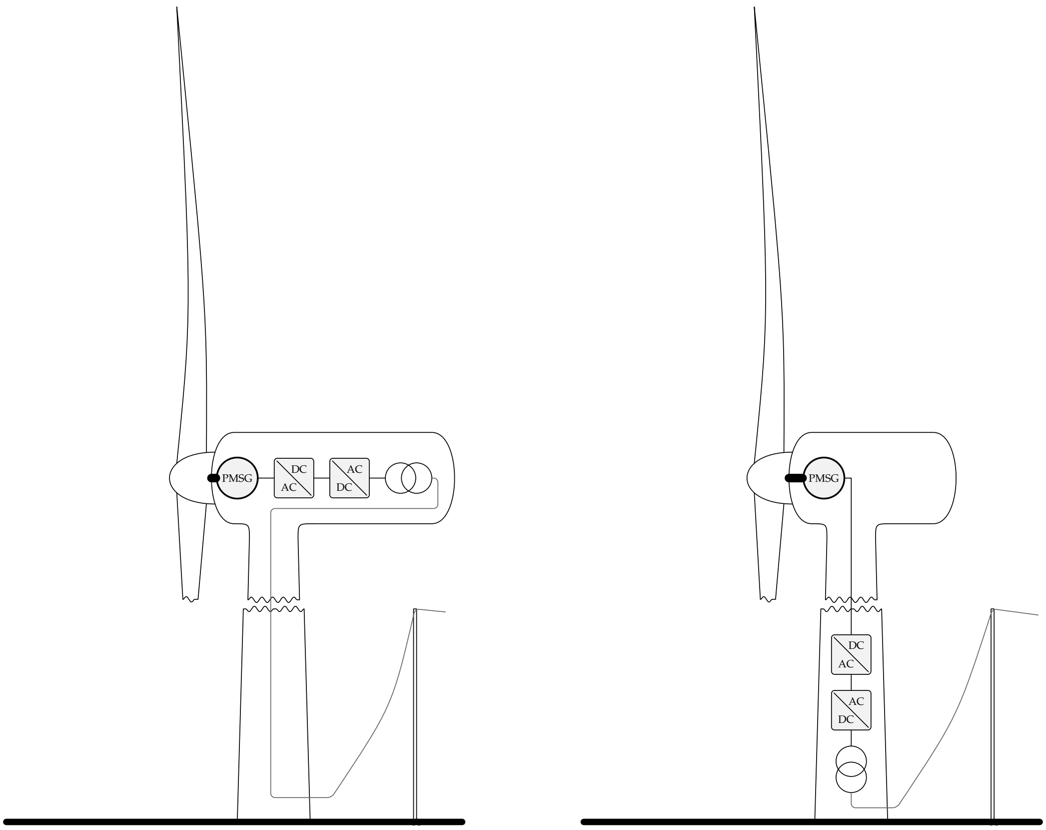

(a) **(b)**

Figure 1.2: Visualization of Wind turbine arrangements **(a)** Traditional arrangement **(b)** New arrangement with long generator cables

Anyhow, ground level components also introduce temperature fluctuations at the base of the tower - where the structural maximum stress momentum for a wind turbine lays - which is an other concern that should be considered. [25]

A further concern, addressed in this thesis, lays in the converter relocation resulting in long cables between the generator and converter. Now, not only the converter's input voltage has an influence on the generator's insulation, also its active rectifier's *dV/dt* (i.e. rise time) and the cable length can result in additional harmful overvoltages stressing the insulation [40].

The longer cable lengths contributes to a damped high-frequency ringing at the generator terminals due to the distributed nature of the cable's leakage inductance and coupling capacitance [56, 57], as shown in figure 1.3. These overvoltages can occur several hundred times per cycle, while most transmission line disturbances occur infrequently. Together, the rise time and repetition have the highest potential for insulating damage. [11, 40]

To reduce the affect on the generator's lifetime, design choices needs to be

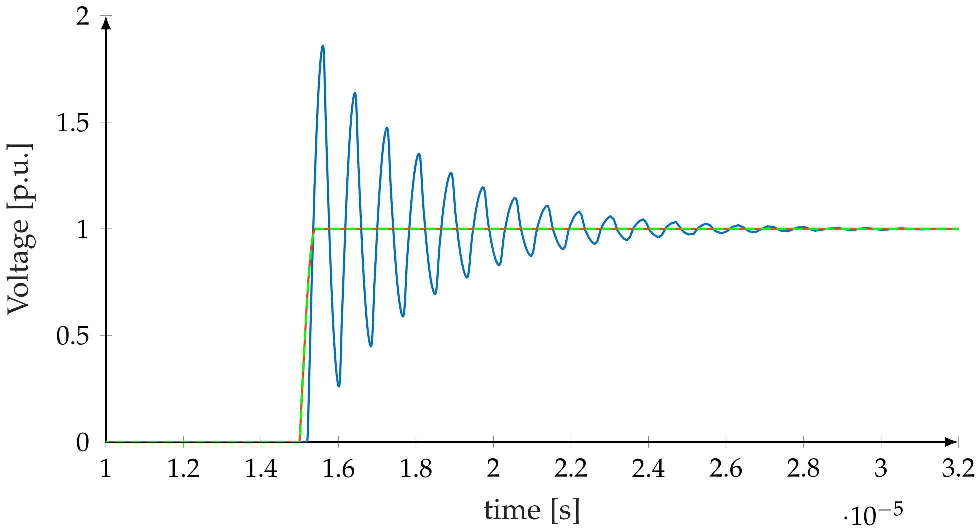

Figure 1.3: Line-line voltage waveform deterioration of an active rectifier's switching instance (——) when utilizing 3m short cable (- - -) and a 41m long cable (——) between converter and generator

reconsidered. In order to keep the design of the generator, the remaining part of the electrical drive train is investigated. While the repetition of the pulses of the converter is as high in the interest to reduce ripples of the modulated voltage, the rise time may be a factor to change. Implementing a filter reduces the rise time and thereby the effect of overvoltage at the generator terminal. Also, selective harmonic elimination PWM as a multi-level converter modulation technique seem promising to reduce the waveform deterioration. [58, 65]

Besides the generator issues, the waveform deterioration through a long cable might influence the indirect measurement of the shaft speed through voltage and current. Thus, additional effort, like the direct measurement of the rotational speed, is required for a reliable wind turbine control (e.g. maximum power tracking). [22]

As from the previous paragraphs apparent, a trend of increasing power levels and accordingly the application of PMSG and full-scale converters leads to a further trend of moving the converter stage down tower. This results in waveform deterioration due to long cables, which needs to be addressed. For commonly used technologies a comprehensive solution is not apparent, while keeping the LCOE in mind. A filter, down tower, at the active rectifier seems an appealing choice.

While the effect of long cables for motors is a well known topic, the question arises how a generator application changes the behavior. What effort of filtration is required due to the change of WTG arrangement? Does it influence the reliable performance of energy production? And do long cables have still the same behaviour in MV environment?

1.1 Problem Formulation

The evolvement of wind turbine power levels leads to an interest of investigating new arrangements of components. One appealing distribution is moving the network decoupling back-to-back converter from the nacelle to the bottom of the tower. This results in long cables between the generator in the nacelle and the converter at the tower base.

These long cables are known to introduce high frequency voltage ringing at the generator terminal and current distortion at the converter. The motivation is to evaluate a theoretical medium voltage application with the appreciated arrangement. Hence, the resultant influence of voltage and current waveform deterioration in steady-state must be quantified.

To verify the effect of waveform deterioration a 3 phase 2 level low voltage converter setup, connected to a permanent magnet synchronous generator is employed. The setup shall quantify the problem. Estimating an up-scaled medium voltage application, a circuit simulation shall emulate the observed behaviour, validated through experimental research. Finally this gives the ability to answer the uncertainty of required filtering effort to suppress the previously mentioned waveform deterioration.

1.2 Scope of the Thesis

1.2.1 Objectives

To investigate the cable's impact, a low voltage setup shall emulate the above WTG topology and serve as down scaled preface study. This includes:

- Quantify cable behaviour relative to length
- Modify pre-existent laboratory setup to needs by including a long cable and a dV/dt filter.
- Select appropriate cable model to include obligatory properties
- Model laboratory setup in circuit simulator (figure 1.4)
- Verify model through laboratory setup
- Tune a suitable filter to counterbalance long cable's effect
- Scale circuit simulation up to medium voltage level to extrapolate the cables influence

1.2.2 Utilized Tools and Environment

A pre-existend student laboratory setup is chosen as launch, located in the drive laboratory (Pon. 107) at Aalborg University. A Permanent Magnet Synchronous Machine (PMSM) is connected to an Induction Motor (IM), both being able to work either in motoring or generating mode. The Danfoss FC302 converter is controlled by mixed RISC/DSP digital controllers (dSPACE DS1103 PPC). A rectifier supplies bidirectional all converters by rectifying the grid voltage or feeding the energy back. Figure 1.4 is visualizing the schematic of the setup.

The oscilloscope used in experimental measurements is "Tektronix DPO2014" rated up to 100Mhz and 1GS/s. For voltage measurements the differential probes "Tektronix P5200" are used which are rated to up to 1300V are utilized. For current measurements the probes "Tektronix TCP0030A" are used which are rated up to 30 A RMS/50 A peak and has a bandwidth of up to 120 MHz. For LCR measurements the Impedance analyzer "Keysight E4990A" is used, which works in a frequency range between 20Hz to 120MHz.
The employed software tools are:

- Matlab for data processing,
- dSPACE Simulink interface for controlling the experimental set up,
- Plecs as circuit simulator.

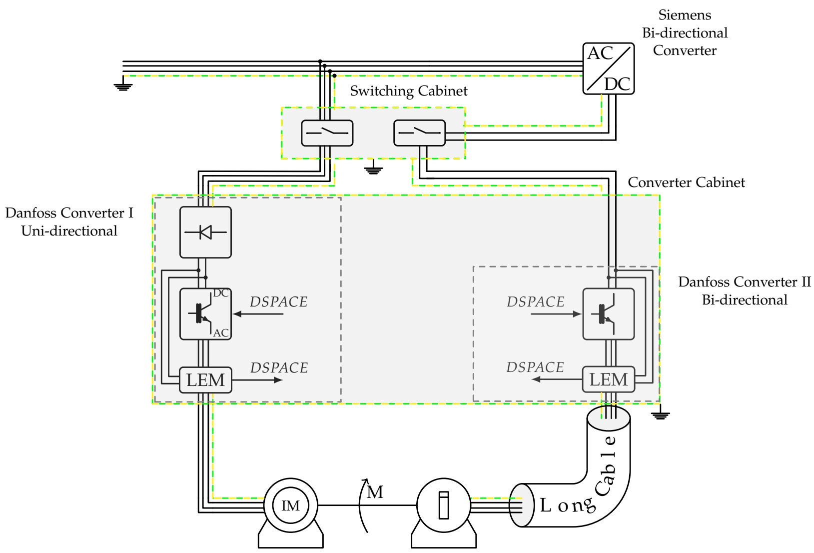

Figure 1.4: Schematic of laboratory setup

1.3 Project Limitations

- The whole wind turbine is not implemented in the laboratory setup. To emulate the torque of the rotor an Induction Motor is used.
- The grid is not modeled, the only used components are torque, generator, long cable and active rectifier. The active rectifier is connected to a constant DC voltage, emulating the DC link of the back-to-back converter.
- The pre-existend laboratory setup is modfied by connecting cables of two lengths between PMSG and converter
- The pre-existent control structure is considered as black box and utilized as that.
- No data for MV cables and Generator were present at the stage of analyzes, therefore the component values were estimated.
- All measured voltages in this thesis are measured line to line except stated otherwise.

1.4 Thesis Structure

The structure of this thesis is as follows:

- In chapter 2 the influence of cables on a pulse is investigated theoretically. This includes the investigation of the reflected wave phenomena, the effect of the rise time on it and the resulting damping behaviour.
- In chapter 3 the theoretical knowledge is summarized into a cable model. Special focus is on the influence of the model structure on the accuracy of the results and the relation between length rise time and overshoot.
- In chapter 4 further influences of the overall system on the resulting waveforms are discussed. A generator model is employed to model the reflection factor. As a result a filter is proposed including a tuning scheme.
- In chapter 5 the experimental setup is characterised, and thus the previous presented theory and model is verified. Then a conclusion of the experimental waveform deterioration through a long cable is drawn and the performance of the simulation is discussed.
- In chapter 6 the L-RC filter topology is tuned to counteract the cables influence and meet the requirements of the generator. The expected behaviour is also verified experimentally.

- In chapter 7 an 10 MW wind turbine environment is explored, and the previous given results are scaled to a higher power and voltage level by estimating or scaling new parameters for the model. This is meant to show the expected influences of long cables in a possible future application.
- Chapter 7 and 8 are discussing the obtained results and concluding the thesis.

Chapter 2

Cable Effects due to Converter Arrangement

The following chapter outlines relevant theory, concerning long generator cables. First the main effects of long generator cables are pointed out. Followed by the dominant deterioration effect, the Voltage reflection phenomena. Concluding, the damping behaviour of the voltage reflection is expressed.

As stated above [cf. chapter 1] in certain circumstances long cables will lead to voltage overshoots up to doubling of the initial voltage and increase thereby the *dV/dt* and introduce high frequency ringing at the generator terminals.

The involved effects can be summarized as:

- pulse rise time
- distributed cable parameter (characteristic impedance)
- cable length
- generator impedance

Whereby, the interconnection between the listed effects increases with the advances of power electronic devices, reflected in higher switching frequencies as well as faster rise times t_r [1] of PWM converters. These high switching frequencies and rise times lead to steep pulses with less time to damp oscillations before the next pulse.

The oscillations occurs due to a change of characteristic impedance at the connection point leading to a point of discontinuity. The generator has a rather high characteristic impedance, compared to the cable. Due to charging of parasitic capacitance within the generator, a current decrease in the higher impedance region

[1] The rise time is defined by IEC to the time required for the voltage to rise from 10% to 90% of the peak voltage. This thesis follows this definition. The definition is visualized in appendix B

is at this point the result. Extra charge accumulates at this point, when the capacitance is not able to discharge and charge due to the steep pulse. This leads to an increase of voltage (i.e. overvoltage). When the change of impedance occurs within a system due to energy conservation law, additional to the charge accumulation, the wave is reflected. Thereby, a high frequency ringing at the generator terminal is the consequence. [7, 36, 44]

The magnitude of these ringings is a function of the wave's traveling time t_t and the pulses' rise time t_r. Thereby, the wave's traveling time is dependent on the cable's distributed parameters and length. This means, for a specific pulse a specific cable length exists, below which no wave reflection occurs [7, 39]. This length is denoted as critical cable length l_{cr}.

For example, the averaged switching frequency of ABB's ACS880 converter is 2 kHz, for a power of 8 MW, switching across 0–690 $\mathrm{V_{dc}}$ [4] in less than 0.1 µs. This short rise time t_r, also high rate of voltage rise (i.e. dV/dt), has an adverse effect on the generators insulation. [58]

In this case the critical cable length - to avoid high frequency ringing - is as short as 8 m. However, the critical cable length is expected to decrease due to the stated evolvement in power electronics. When the application demands to separate the converter from the generator further than l_{cr} allows, solutions are required.

One approach to counteract this phenomena is to slow down the rate of voltage increase and minimizing the peak voltage at the generator terminals. Additionally, matching the characteristic impedance of cable and generator could solve the issue.

2.1 Reflected Wave Phenomena

As stated, wave reflection occurs when a wave propagates through a cable reaches a point of discontinuity. The reflection is determined with the coefficient Γ, describing the characteristic impedance mismatch between generator and cable. The cable between generator and converter behaves like RL components at low frequencies. Though, due to the addressed high frequency behaviour related to the high dV/dt, the cable cannot only be described with this configuration.

Capacitive coupling between the power core of the cable and ground needs to be taken into account. In order to capture those high frequency components, the cable needs to be modeled with distributed constants in order to spread the components account for the characteristic impedance. Independent of the length, the characteristic impedance describes the cables geometry, layout and material (i.e. parameters) and frequency. The characteristic impedance is defined as: [13, 44]

$$Z_0\left(\omega\right) = \frac{\sqrt{R_s^{'} + j\omega L^{'}}}{\sqrt{G^{'} + j\omega C^{'}}} \simeq \frac{\sqrt{L^{'}}}{\sqrt{C^{'}}} \tag{2.1}$$

while $R_s^{'}$ is the resistance per unit length, $L^{'}$ is the inductance per unit length,

$G^{'}$ is the conductance of the dielectric per unit length, $C^{'}$ is the capacitance per unit length. The cable resistance $R_s^{'}$ does influence the wave velocity only slightly, therefore the cable model can be estimated lossless [31].

To describe the reflection coefficient it is sufficient to consider the two extreme cases of impedance mismatch: $\Gamma = \pm 1$. This is equivalent to open (infinite impedance) and short (zero impedance) circuited terminals.

The point of discontinuity between cable and generator behaves similar to an open cable[2], due to the comparable high characteristic impedance of the generator Hence, a positive reflection appears. [7, 56–58]. Considering figure 2.1a, points 2 and 4 are representing this.

Further, the converter and its DC-link capacitor's characteristic impedance, represented in figure 2.1a as voltage source, are close to zero[2] resulting in a negative reflected wave in which case the terminal voltage is zero. [44, 56, 57]

While considering a finite long cable with an infinite *dV/dt*, figure 2.1 visualizes the sequence of events to represent the wave reflection phenomena.

The initial voltage pulse is shown in 2.1b, where the voltage as well as the current wave travels with positive sign towards the receiving end.

Since the end is open, figure 2.1c shows that the voltage is reflected with equal sign. The current at an open circuit end is zero. With this boundary condition it can be derived that the the current is reflected with a negative sign. Thereby, the resulting current magnitude is kept zero. Here, it can be seen that the current reflection behaviour is inverse to the voltage reflection behaviour.

The second reflection is pictured in figure 2.1d. The voltage at the converter is clamped to the dc-link, resulting in a similar boundary condition, compared to the current, for the voltage reflection. Hence, the converter acts as short circuit[2] and the voltage is reflected with negative sign back into the direction of the generator's end. Since, the voltage is of negative sign, the accompanied current is of equally sign as the voltage (i.e. negative).

Followed by the reflection of the converter side (figure 2.1e), the wave reaches the generator side for the second time (i.e. third reflection). As said, the current is negative, and since the current, due to the open circuit must be zero, the current becomes positive to balance it. The positive current moving left, must be accompanied by a negative voltage. Finally, the third trace is equal to the first incident. Thus, the reflection does not need to be traced further.

This leads to the conclusion, that the voltage and the current is a composition of forward and backward travelling waves. Thus, at a given instant and point of the cable the resulting voltage and current magnitude consists of the superimposition of reflected components. [13]

When introducing a load/source at the far side of the cable, the reflection factor Γ is not equal to one anymore. Part of the wave's energy at the point of discon-

[2]For high frequency components

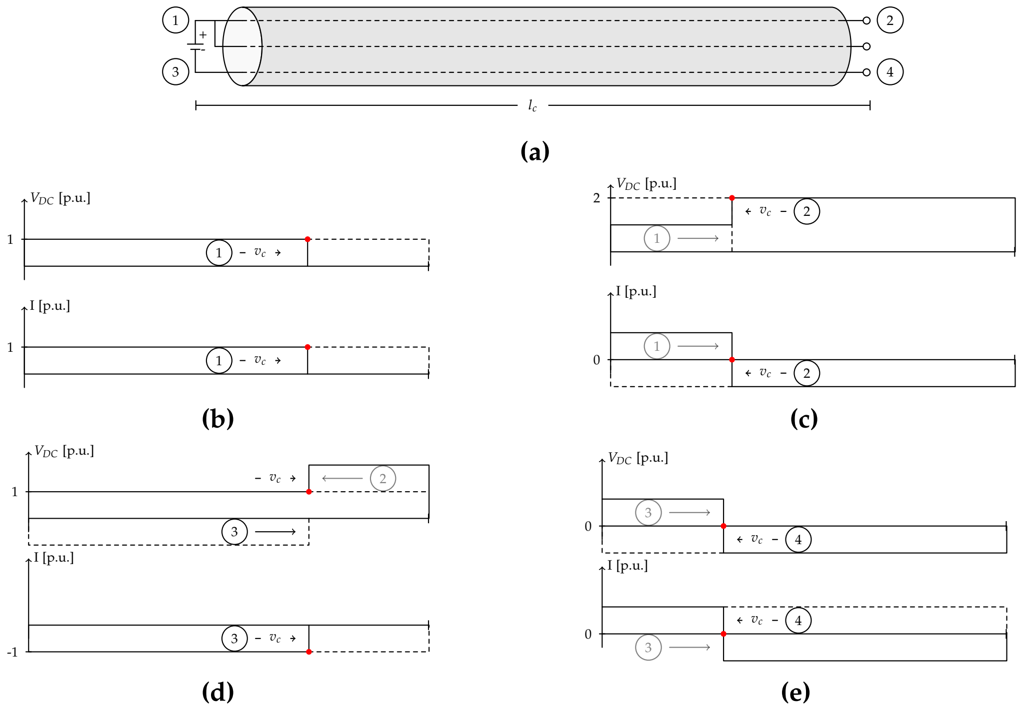

Figure 2.1: Waveform reflection within a cable (**a)**) for infinite generator's characteristic impedance and zero characteristic impedance of the converter: **b)** initial converter pulse, **c)** generator terminal reflection of the initial pulse, **d)** converter terminal reflection of the generator terminal reflected pulse, and **e)** second reflection of the pulse at the generator terminals. The ● indicates the present level. The x-axis is the cable length l_c

tinuity propagates past it (i.e. towards the generator). To comply with the law of energy conservation the remaining energy is reflected back as explained in figure 2.1. This relates to, that the refracted voltage ($V_{refr,DC}$) must be equal to the injected voltage (V_{DC}) plus the reflected voltage ($V_{refl,DC}$), while the same applies to the current. [13] See eq. 2.2:

$$V_{refr,DC} = V_{refl,DC} + V_{DC} \tag{2.2}$$

The reflection coefficient quantifies the amount of reflection and relates the characteristic impedance of the cable, $Z_{0,c}$ and the characteristic impedance of the generator, $Z_{0,g}$. This is expressed like:

$$\Gamma_g = \frac{Z_{0,g} - Z_{0,c}}{Z_{0,g} + Z_{0,c}} \tag{2.3}$$

As stated, the generator's characteristic impedance is larger than the cable's characteristic impedance, and as long as this applies, it is apparent from eq. 2.3 that $0 \leq \Gamma_g \leq 1$.

Being aware of the amount of reflection, $V_{refl,DC}$ is determined as:

$$V_{refl,DC} = \Gamma_g V_{DC} \tag{2.4}$$

As from 2.2 and 2.4 apparent, this results in:

$$V_{refr,DC} = \frac{2Z_{0,g}}{Z_{0,g} + Z_{0,c}} V_{DC} \tag{2.5}$$

At the converter side, Γ is constituted by the cable's and converter's characteristic impedance, which is specified as $Z_{0,con}$. The converter reflection coefficient is:

$$\Gamma_{con} = \frac{Z_{0,con} - Z_{0,c}}{Z_{0,con} + Z_{0,c}} \tag{2.6}$$

Similar to Γ_g, for Γ_{con} the reflection coefficient at the converter site is $-1 \leq \Gamma_{con} \leq 0$, as long as the converter's characteristic impedance is less than the cables (cf. eq. 2.6). Though, as stated above, $Z_{0,con} \simeq 0$ and thereby $Z_{0,con} \ll Z_{0,c}$, the reflection on the converter side is $\Gamma_{con} \simeq -1$.

Further, this indicates that theoretical voltage doubling could occur (cf. eq. 2.5) at the generator side, while the reflection attenuates at the converter side due to the negative sign.

2.2 Effect of PWM Rise Time (dV/dt)

As said in the introduction of this section, the overshoot's magnitude is not only constituted by the reflection coefficient, but also by the cable length, travelling time and the rise time of the PWM pulse. [11, 31, 39, 40]

The time for a pulse to travel from the source to the generator can be expressed as the travelling time [13, 44, 56]:

$$t_t = \frac{l_c}{v_c}, \tag{2.7}$$

while l_c is the cable length and v_c the propagation velocity. v_c is expressed like:

$$v_c = \frac{1}{\sqrt{L'C'}} \tag{2.8}$$

The propagation velocity is highly related to the distributed inductance $L^{'}$ and capacitance $C^{'}$ in an insulated conductor. Those components are calculated by using eq. 2.9 and 2.10, respectively [13]. In general, the cable parameters are determined by the cable construction, insulation type and conductor spacing [31].

$$C^{'} = \frac{2\pi\varepsilon}{\ln\left(\frac{b}{a}\right)} \tag{2.9}$$

$$L^{'} = \frac{\mu}{2\pi}\ln\left(\frac{b}{a}\right) \tag{2.10}$$

The variables a and b are the radius of the conductor and of the insulation, respectively [cf. figure 2.2].

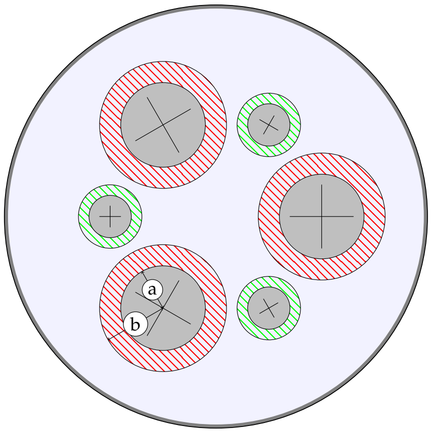

Figure 2.2: Cable cross section including radius of inductor and insulator

Inserting the capacitance and inductance into eq. 2.8, it is revealed, that the velocity in a lossless line is dependent on relative permittivity (ε_r) and relative permeability (μ_r), related to the speed of light c [13, 31]:

$$v_c = \frac{c}{\sqrt{\mu\varepsilon}} \Leftrightarrow v_c = \frac{c}{\sqrt{\mu_r\mu_0\varepsilon_r\varepsilon_0}} \Leftrightarrow v_c \simeq \frac{c}{\sqrt{\mu_r\varepsilon_r}} \quad \text{for } t_t \geq t_r \tag{2.11}$$

Considering a cable with $\mu_r = 1$ (copper) and $\varepsilon_r = 2.25$ (XLPE)
and inserting it into 2.11, results in:

$$v_c \simeq \frac{c}{\sqrt{2.25}} \simeq 200\,\mathrm{m/\mu s}, \tag{2.12}$$

which is typically near 50% of the speed of light [31, 44, 56, 57].

Resulting from the characteristic impedance missmatch (i.e. Γ) and the cable characteristic as described above, overvoltage occurs. The overvoltage is composed by two causes:

2.2.1 Overvoltage < $2V_{DC}$

Now, being able to determine the traveling time t_t, one can be aware of the moment at which the forward travelling voltage pulse has reached the point of discontinuity.

Considering the rise time t_r, the amplitude of the reflected pulse travelling towards the converter is now given as:

$$V_{refl,DC}(t = 2t_t) = \frac{t_t \Gamma_g V_{DC}}{t_r} \qquad \text{for } t_t < t_r \tag{2.13}$$

$$V_{refl,DC}(t = 2t_t) = \Gamma_g V_{DC} \qquad \text{for } t_t \geq t_r \tag{2.14}$$

As it can be seen in figure 2.1, the third wave reflection (i.e. at the generator terminal) has the opposite sign as the first reflection. When this wave reaches the converter before the first reflection reaches its voltage maximum the overshoot is suppressed by the ratio of t_t/t_r [cf. eq. 2.13]. This is the case when the rise time is longer than the time difference between these two reflections, being two times the traveling time.

The critical cable length is where the maximum voltage overshoot, for a certain rise time, occurs. Resulting from 2.7, the critical cable length can be derived [40, 44]:

$$l_{critical} = \frac{t_r v_c}{2} \tag{2.15}$$

It relates: the shorter the cable, the greater the suppression. Therefore, when $2t_t \geq t_r$, the pulse rise time is no longer acting on the reflected voltage [57].

The peak voltage at the generator terminal can after all be determined with the total voltage due to reflections after three transitions (two reflections) of the cable [35, 58]:

$$\overline{V}_{l-l}(t = 2t_t) = \frac{2 l_c \Gamma_g V_{DC}}{v_c t_r} + V_{DC} \qquad \text{for } t_t < t_r/2 \tag{2.16}$$

$$\overline{V}_{l-l}(t = 2t_t) = \Gamma_g V_{DC} + V_{DC} \qquad \text{for } t_t \geq t_r/2 \tag{2.17}$$

To determine no or minimum overvoltage, eq. 2.16 can be normalized, as:

$$\frac{\overline{V}_{l-l}}{V_{DC}} = \frac{2 l_c \Gamma_g}{v_c t_r} + 1 \tag{2.18}$$

Therefore,

$$\frac{2 l_c \Gamma_g}{v_c t_r} \ll 1 \tag{2.19}$$

Calculating the critical length With eq. 2.18, the reflection factor is included. Define the rise time as $t_r = 0.23\,\mu s$, $v_c = 200\,m/\mu s$ and $\Gamma_g \simeq 0.75$ and accept votage doubling, by rearranging eq. 2.19, the critical length can be found as:

$$l_{critical} = \frac{v_c t_r}{2\Gamma_g} \Leftrightarrow l_{critical} \simeq 30\,m \tag{2.20}$$

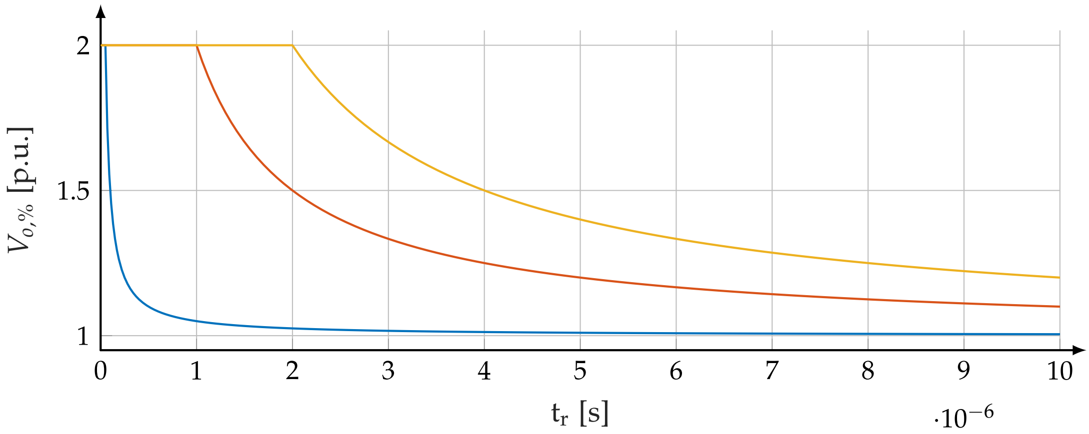

Figure 2.3: Overshoot vs rise time with $l_c = 5$ m (——), 100 m (——) and 200 m (——)

Figure 2.3 visualizes the worst case relation between the voltage overshoot and the rise time in relation for different cable lengths. This proves, that the issue of voltage overshoots gets more problematic with longer cables and/or faster rise times.

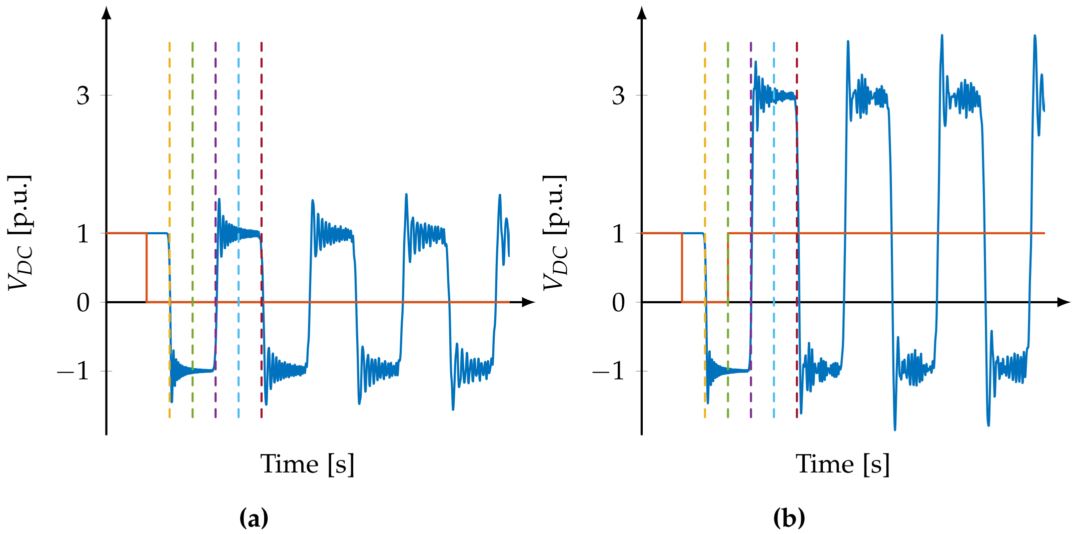

Figure 2.4: Natural oscillation of a cable with —— at the converter side initiating the starting wave and —— as the voltage at the generator side: **a)** single pulse leading to reflections **b)** double pulsing phenomena leading to overvoltages > $2V_{DC}$. Having - - - as first, - - - as second, - - - as third, - - - as fourth and - - - as fifth reflection

Summarizing the voltage doubling behaviour ($Vo \leq 2$):

- Reflections occur when pulses reach a characteristic impedance mismatch,
- The reflected amount and sign is quantified with the reflection factor Γ,
- If the cable length is smaller than $l_{critical}$, the negative reflections has a suppressing influence.

2.2.2 Overvoltages > $2V_{DC}$

Besides the doubling of V_{DC}, under certain circumstances the overvoltage may rise even higher. That is, when an ongoing pulse reflection is superimposed by a switching signal of the converter. When the reflected voltage pulse is arriving at the converter terminal after e.g. the second transition it is reflected back towards the generator. The reflected wave has the opposite sign due to $\Gamma_{con} = -1$. When the converter simultaneously switches the polarity, the edge of this new pulse is superimposed to the reflected voltage pulse leading to $2V_{dc}$. This voltage wave with double amplitude will be reflected at the generator terminal with $\Gamma_g = 1$ and can reach thereby an amplitude up to 4 p.u - leading to 3 p.u. overvoltage in the worst case. This behaviour is visualized in figure 2.4 and called double pulsing. [31, 44]

This double pulsing effect can be repeated multiple times successively which can lead to even higher overvoltages and should thereby with the modulation technique be avoided.

The effect for quadruple the overshoot is called double switching and occurs when a three phase system switches two inverter branches simultaneously at overmodulation. This leads to voltage polarity reversal, which can be up to 2 V_{DC}. This with voltage reflection then leads to the quadruple. [44]

This leads to, in contrast to overvoltages < $2V_{DC}$, that the carrier frequency and modulation technique has predominant effect for overvoltages > $2V_{DC}$, while the rise time t_r has a minor effect on the overvoltage. [31, 44]

Summarizing overvoltages ($2 \geq V_o \geq 4$):

- Cable characteristics only accountable for voltage doubling behaviour,
- Double pulsing leads to overshoots of 3 p.u.,
- Double switching leads to overshoots of 4 p.u.,
- Predominant influence is carrier frequency and modulation technique,
- The traveling time is the core concern for switching and modulation technique.

2.3 High Frequency Damping Behaviour

To avoid overvoltages higher than 2 p.u., oscillations needs to be damped and thereby the charge removed before the next pulse is applied. [31, 44]

The oscillation can be described by the interaction of the system's (mostly the cable's) capacitance and inductance bringing the system in resonance. The oscillation frequency of the reflected voltage pulses relates the cable's length to v_c. In order to complete one oscillation cycle, the wave needs to travel the cable four times [31, 44]:

$$t_{cycle} = 4t_t \tag{2.21}$$

Recalling eq. 2.8 and relating l_c and v_c, it results in:

$$f_0 = \frac{1}{t_{cycle}} = \frac{1}{4t_t} = \frac{v_c}{4l_c} = \frac{1}{4l_c\sqrt{L'C'}} \tag{2.22}$$

This shows, that the cable length is inversely proportional to the oscillation frequency. This may lead to unwanted problems, considering the cable length increases, the oscillation frequency decreases.

In real conductors one frequency dependent effect is described as skin effect. This effect relates the resistance to a frequency dependency. Taking the skin effect into account, it leads to a decrease of damping when increasing the cable length, since the ac resistance of an conductor increases for higher frequencies. Meaning, higher oscillation frequency leads to higher conductor AC resistance, since the charge moves to the surface of the conductor where its conductivity is less.

In addition to the skin effect, the proximity is an effect experienced at alternating currents. This is when the resultant magnetic field of the current flowing through the inductive part of the conductor induces eddy currents in the nearby conductors which will alter the overall distribution of the current flow. The eddy currents thereby reduces the current flow area, since the current is farthest away from the nearby conductors carrying current in the same direction. Closely bounded cables are thereby prone for this effect. Though, since it increases the damping of high frequencies through the increase of the AC resistance, this effect is pleasant for reducing remaining charges and thereby higher overvoltages than 2 p.u..

Those effects can be composed in order to determine the damping of the oscillation, as

$$\frac{V_o}{V_{DC}} = e^{-(R_{AC} l_c / 2Z_0)} = e^{-(K_p K_{skin}(f_0) R_s l_c / 2Z_0)}, \tag{2.23}$$

where V_o is the overshoot and R_{AC} the AC resistance consisting of the DC Resistance R_s, skin effect $K_{skin}(f_0)$, proximity effect K_p and l_c is the cable length.[31]

Further, [31] defines, through experimental validation, the AC resistance, with conductor diameter a, as:

$$R_{AC} = \frac{K_p 16.61 * 10^{-8} \sqrt{f_0}}{a} R_s \tag{2.24}$$

Dependent on the application by means of cable characteristic as well as length, this damping behaviour needs to be considered. However, Besides the direct damping effects of the cable, the reflection factor also introduce a damping component to a system.

When $|\Gamma| < 1$ (compare eq. 2.3 and 2.6) the reflected wave is reduced with every reflection. This damping behaviour can be extracted by the successive peaks of the oscillation. The damping of the peak magnitude introduced by the reflection factor is

$$y_{p,n} = \Gamma^n, \tag{2.25}$$

where n is the number of reflection and $y_{p,n}$ is the magnitude after the nth reflection at the generator side (i.e. half oscillation).

The overall damping of an oscillation can be described as logarithmic decay where the damping factor σ can be calculated as

$$\sigma = ln(\frac{x_{p,1}}{x_{p,2}}). \tag{2.26}$$

$x_{p,1}$ and $x_{p,2}$ are two peaks, which $m = 2n$ periods apart.

The damping factor σ can be converted into ζ which is commonly used as the damping factor for damped oscillations with the following equation

$$\zeta = \frac{\sigma}{2\pi}. \tag{2.27}$$

In order to identify the damping function $f_{damp,osci}$, the damping frequency can be calculated with the time difference between two peaks:

$$f_d = \frac{2\pi m}{\Delta t} \tag{2.28}$$

where m is the number of periods between the two selected peaks. The formula for a damped oscillation is then defined:

$$f_{damp,osci} = 1 + e^{-\zeta f_d \cdot t} sin(f_d \cdot t) \tag{2.29}$$

The relation between eq. 2.25 and eq. 2.29 can thereby be described by the relation between Γ and ζ and is given as

$$\Gamma = e^{-\pi \cdot \zeta}. \tag{2.30}$$

With the above given equations 2.25 - 2.30, the relation between theoretical calculated damping factor and experimental obtainable damping factor is given. This relation is later referred to again. For now, this relation is visualized with a simulated line to line voltage and eq. 2.29 and 2.26 in figure 2.5.

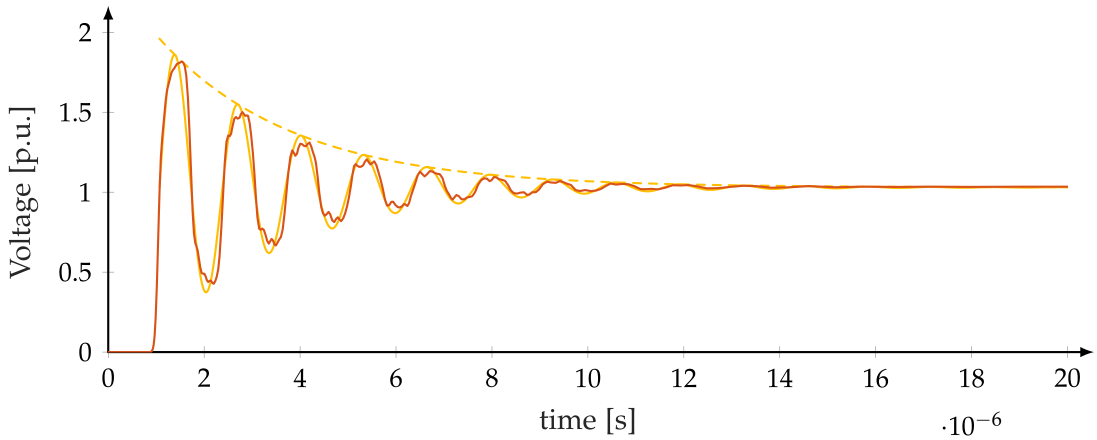

Figure 2.5: Simulated l-l voltage (——) vs eq. 2.29 (——) with eq. 2.26 (- - -)

Concluding, the effect of overvoltages can be described with two predominant mechanisms: when small wire gauges and great characteristic impedance difference of cable and generator are present, the predominant decay mechanism is through skin. While, in bigger generators its characteristic impedance increases and thereby the reflection factor Γ decreases since the characteristic impedance approximate [cf. eq. 2.3] the reflection factor is the predominant influence on overvoltages. Yet, higher power levels leads likely to greater cable diameter and thereby less AC resistance.

Chapter 3

Cable Model and its Responsiveness to Excitement

In this chapter the implemented cable model with the previous discussed characteristics is presented. Further, relevant aspects of the cable model are presented and determined. Finally, the reader should comprehend the important considerations of modelling a cable, while relating it to reflection theory.

3.1 Implemented Cable Model

As described in chapter 2, additionally to the RL components, capacitive coupling of the cable's core and ground needs to be considered, while the components needs to be spread in order to capture the high frequency components. References as [7, 11, 31, 38, 39, 44, 45, 56–58] gives over decades a description, that those effects can be captured by a lossy transmission line model.

In order to spread the components, several segments of the equivalent circuit shown in figure 3.1 can be used. Even though this is not a distributed element model, by following the above references the lumped parameter model gives reasonable precision when utilizing an adequate number of segments. The lumped model is advantageous, since less calculation power and thereby time is required. However, the result is also dependent on the segment number.

The reference [39] suggests to experimentally assess the power cable's parameters instead of estimating the parameters with equations related to the geometrical configurations. This method includes a frequency dependency in the calculations.

Also, the reference [39] proposed equations to extract the component values from the impedance measurements. The authors of this thesis take those equations as too inaccurate which is further explained in section 5.1.1, therefore are those equations presented in appendix E. In section 5.1.1 the numerical approach of extracting the component values is presented. Sufficient estimation of the cable

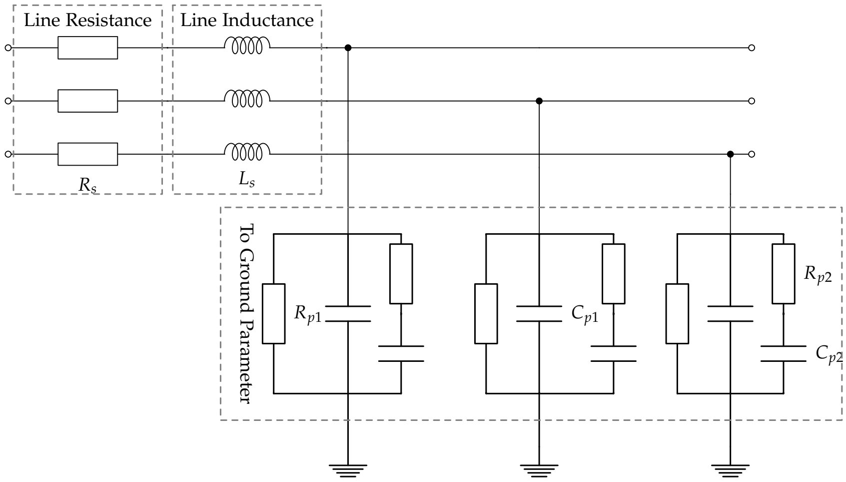

Figure 3.1: One section of the used transmission line model

parameters is essential in order to obtain accurate simulation results.

Even though the inaccurate estimation of the cable parameters, the argumentation of reference [39] using a HF-model to evaluate the overvoltage effect of the voltage pulse, could be followed. Considering the following equation:

$$f_{BW} = \frac{1}{\pi \cdot tr} \tag{3.1}$$

the bandwidth of the pulse can be estimated [44]. Having rise times of µs, would relate to the MHz region.

The apparent limitations of the chosen model are for one, that the previously discussed skin and proximity effects are not taken into account in this model, which may result in an inaccurate damping behaviour, and a slightly different waveform shape, between simulation and experiment, due to the frequency dependent damping.

Additionally some possible circuit components are not included into the model by simplifying the model. These assumptions are further evaluated in section 5.1.2.

In this section the sensitivity of different cable influences are explored. The overall goal of this section is to gain an understanding of how the different parameter influence its model, and how the different combinations may result in over voltages. This shall enclose assumption drawn in chapter 7 in order to determine a range of validity.

3.2 Sensitivity of selected Cable Model

The configuration of the model has a significant influence on the final behaviour of the cable model. Therefore different modelling aspects of the cable are explored in this section.

3.2.1 Number of Model Sections

The first choice, which needs to be considered when employing the cable model as depicted as schematic in figure 3.1 is the number of section. Two characteristics are taken into consideration. Once, the excitement of the cable model related to frequency components. The other, time domain waveforms, plotted in figure 3.2. Those two characteristics are surely correlated.Hence, they help together to determine the right number of sections.

As apparent from figure 3.2 and considering theory about resonance and harmonics, the increase of section numbers from one section (——) up to 200 (—— depicts, superimposing frequencies lead to a more square wave alike waveform. More harmonic components are overlayed and thereby compose the square wave. Reversely, this means, that higher cross excitements of the cable are considered. This is relevant, when considering the the frequency spectrum of the rising edge of the PWM pulse [cf. eq 3.1].

It has revealed, 10 section numbers (——) excite the cable model circuit above the rise time range and thereby is chosen in order to keep calculation power in the simulation down. The time domain thereby should not deceive, when comparing the full pulse reflection with a high rise time.

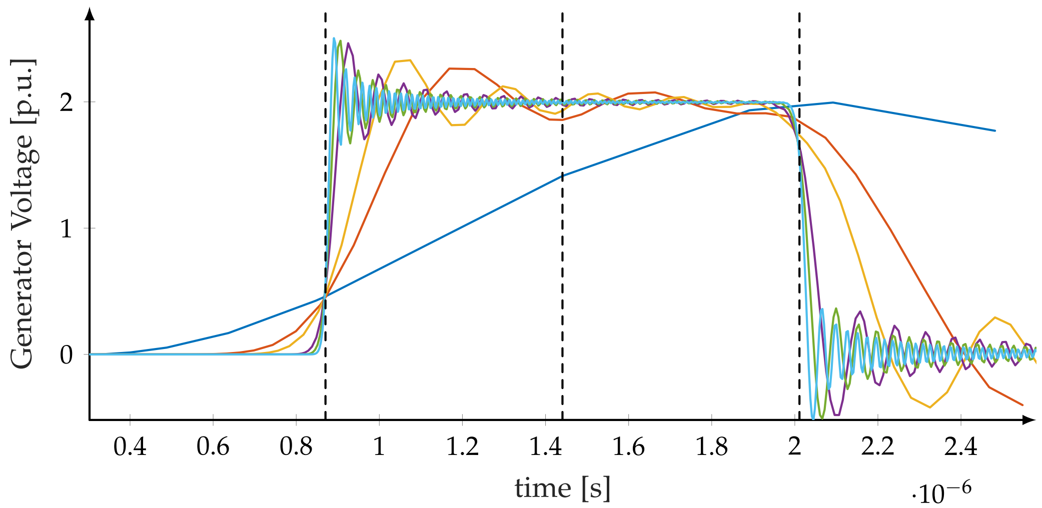

Figure 3.2: Cable model excitement for the same cable parameters with ideal step for different cable section number, as: 1 (——), 5 (——), 10 (——), 50 (——), 100 (——), 200 (——)

3.2.2 Model type

The next influence shown, is the configuration distinction between normal and high frequency cable model. The distinction between those two models were explained in section 3.1.

Figure 3.3 visualizes the two models in frequency domain for 10 section numbers. The overall influence is comparably small. Looking at figure 3.3a, it represents the cross influences between conductors, where the capacitive coupling is dominant. It is apparent, that the high frequency model (——) in the magnitude plot is in the lower frequency range divergent from the normal model (——). Further, in the phase plot of this figure, a difference between the two models is in the high frequency region apparent.

Moreover, in the conducting behaviour, shown in figure 3.3b, where the inductance has its dominant effect, a cross behaviour between inductance and capacitance is given. This is evident in the phase plot, where a slight difference in normal (——) and high frequency model (——) is given.

Even though the difference between those two models is minor, the high frequency model is chosen as basis for all simulations. This is due to the authors believe, it is an adequater representation of the cables behaviour, while calculation power in the simulation and parameterization of the components are of no significant surplus effort. Further, quantification of cross couplings, as explained in the paragraph above but also between generator components composed in the reflection factor, could not be fully detected, which gives further believe in choosing this model, following the authors.

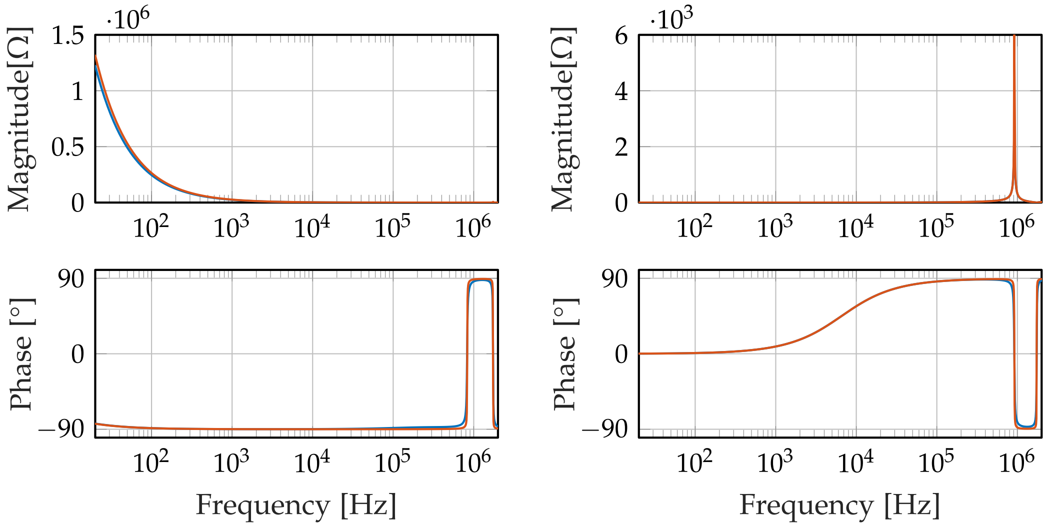

(a) **(b)**

Figure 3.3: Comparing the normal model (——) with the high frequency model (——) for **a)** open loop behaviour and **b)** closed loop behaviour

3.3 Influence of the relation between rise time and length

In this section the influence of the different cable parameters itself is depicted. This section shall help to compare and categorize different cables.

Recalling eq. 2.7 and 2.8, the travelling time is defined by the cables conducting ($L^{'}$) and coupling ($C^{'}$) part. Further, in conjunction with figure 2.1 it was explained that the reflection factor Γ, as well as the combination of travelling time and the pulse's rise time has a damping behaviour. This is in correlation to eq. 2.16, which gives the total overvoltage with the damping factor and the relation of t_t and t_r.

Those considerations yield for example in figure 3.4 for different rise times t_r. The restrictive boundaries for this figure is, that by emulating a pulse with a certain rise time, a linear slope is chosen. Further, just a single pulse, with the given rise

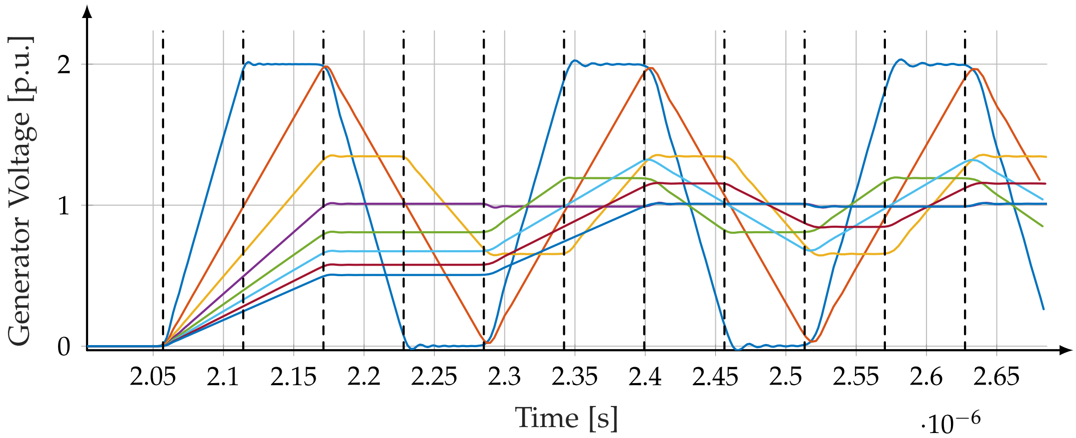

Figure 3.4: Time domain waveforms of reflections at generator terminal leading to over voltages for different rise times in correlation to travelling time, as: $t_r = 1 \cdot t_t$ (——), $2 \cdot t_t$ (——), $3 \cdot t_t$ (——), $4 \cdot t_t$ (——), $5 \cdot t_t$ (——), $6 \cdot t_t$ (——), $7 \cdot t_t$ (——) and $8 \cdot t_t$ (——). The travelling time is indicated by - - -

time, at the converter side is initiated, while a reflection coefficient of $\Gamma = 1$ is considered. The schematic for it can be seen in figure 5.12.

This initial step at the converter is not shown to depict only the significant behaviour and try to keep the image as clear as possible. As cross reference, figure 2.4 shows the correlation. However, this means that at 2.06 µs the pulse has reached the generator terminal [cf. figure 2.1c]. The vertical dotted lines (- - -) indicate successive travelling times and thereby reflections.

Examine the first case; $t_r = 1 \cdot t_t$ (——), it is apparent in figure 3.4, that the rise time takes the whole length of the cable to rise, before it reaches the converter terminal. Due to the reflection factor of $\Gamma = 1$, the pulse reaches 2 p.u. Further, the pulse stays at 2 p.u. when being reflected at the converter [cf. figure 2.1d and travelling back to the generator. At fourth reflection (3rd - - -) the sign changes due to the current, as in figure 2.1e and decays in $t_r = 1 \cdot t_t$. Due to no damping, this sequence continues from the beginning again.

By increasing the rise time to $t_r = 2 \cdot t_t$ it can be seen in figure 3.4 (——), that the pulse still reaches 2 p.u. Though, the constant state is not present any longer, by the same reflection behaviour. Now, increasing the rise time further, it can be seen, that the overshoot at the generator terminal is reduced.

Continuing with the increase of rise time, in figure 3.4 an additional behaviour is apparent, which is not considered in eq. 2.16. This is, when the rise time matches a quadruple multiple, the overshoot is no longer present, which means, that the overshoot stays at 1 p.u.

When increasing $t_r > 4 \cdot t_t$ a constant interval can be seen before the first overshoot is reached. For this interval the positive and negative reflection cancel each other, resulting in no change of voltage. This behaviour is especially distinctive for pulses with linear voltage slopes.

The above referred equation will only describe an exponential decay of overshoots related to the rise time-traveling time relation, by means of going trough each peak of figure 3.5. This figure visualizes particularly different overshoots for different traveling-rise time relations.

Due to the relation of traveling time and length [cf. eq. 2.7], a general estimation with the above explained traveling-rise time relation can be given relating the critical length and acceptable overshoot to a certain rise time.

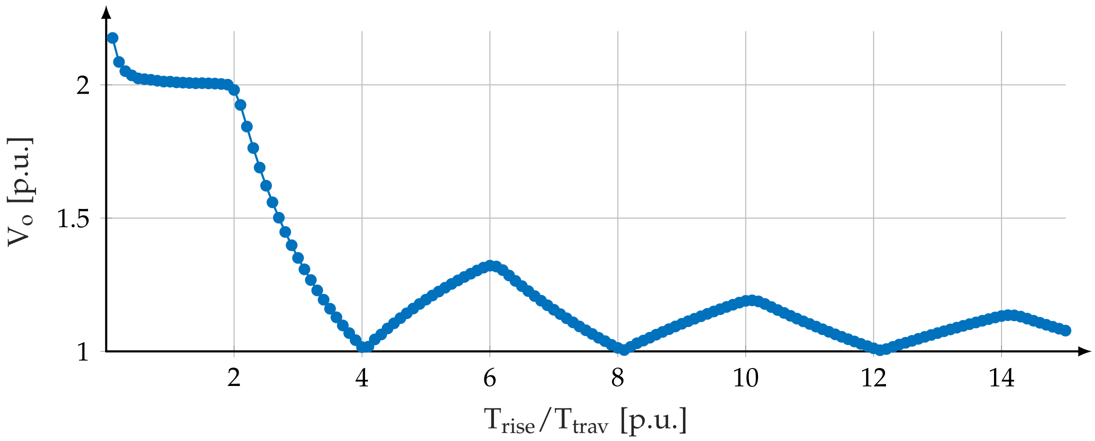

Figure 3.5: Travelling-rise time relation and its resulting over voltage with reflection factor $\Gamma = 1$. Summery of figure 3.4

Summarizing, it can be said that the section number should be evaluated on the pulses bandwidth. In this case this leads to a section number of 10. This gives a high enough frequency response. Further, no great differences between normal and high frequency model are apparent. However, due to unquantified cross couplings and no significant increase in calculation power, the high frequency model is chosen for further investigation. The eq. 2.16 gives a "worst-case" estimate of the overshoot. Though, it does not tell the whole story, since, as long as the rise time is a multiple quadruple, theoretically, voltage overshoot can be fully vanished.

Chapter 4

System Interaction Leading to Filter Scheme

In this chapter, the interaction of the analyzed setup is portrayed. This includes harmful current distribution, especially for the generator, within the system, due to unbalanced voltages. This guides to the conducted generator model and its considerations for an appropriate implementation. Finally, the considerations of this chapter and the previous chapters are concluded in a basic guide to counteract the depicted phenomena with a *dV/dt* filter, resulting in lesser overshoot.

4.1 Voltage and Current Paths in Back-to-Back Converter - Generator Setup

In an ideal and balanced system, only differential mode voltages and related currents are present. Differential mode is defined as the intended forth and back path within the system and thereby establishing a balanced current distribution within its system. That is, the vector sum of a three phase system always equals zero. Thus, the neutral point voltage equals zero. This is the case with purely sinusoidal waveforms.

By modulating a sine wave by PWM driven IGBTs through switching the DC-link voltage on and off, the fundamental waveform relates to the desired sine wave, which is symmetrical.

Though, the instantaneous switching interval are square waves, switched in a pattern where 3 switches are conducting simultaneously. These patterns in a 2-level converter allows the states: twice +V_{DC} and once -V_{DC} or vice versa or all off or on. Due to unbalanced switching states, the instantaneous sum of the voltages in the system is never symmetrical nor balanced, which relates to a non zero neutral point.

By implication, common mode voltages are always present and the current is forced to search its path. The common potential of all phases is related to ground, which means, the current is prone to search its path back to the source via the earth conductor and stray capacitances of the inverter. [1, 44]

Adding all three instantaneous phase-to-ground voltages together, the common mode voltage v_{cm} can be described as:

$$v_{cm} = \frac{v_{Ug} + v_{Vg} + v_{Wg}}{3} \tag{4.1}$$

Following eq. 4.1, the common mode voltage levels for a 2-level PWM converter are given as $\pm V_{DC}/3$ or $\pm V_{DC}$, visualized in figure 4.1).

The steep (common mode) voltage pulses relates to high frequency stray current pulses. The high frequency component searches its path outside the actual system through the stray capacitances of machines, cables and inverter. The capacitive impedance for high frequencies is low, while for low frequencies the impedance is high and thereby blocks the low frequencies. Therefore, the current flows through the return path (mostly earth) in a loop back to the source. [1, 33, 43]

A stray capacitance is every time present, when two conductive compotes are separated by an insulator. In a cable it is for instance the conductor to PE-conductor, separated by the insulation. In a generator it is the windings to frame, insulated by enamel coating and slot insulator, or shaft to frame, insulated by the bearings and its lubrication.

All those above named elements contain also inductive elements. The common mode current, flowing through those inductive parts, causes voltage drops that raises the generator frame potential above the source's ground potential of the converter frame. Thereby, also the generator's common mode voltage contributes to the potential difference. [1, 43]

As denoted in section 2.1, the voltage doubling is accounted by measuring line-to-line voltage. However, the overvoltage due to reflection can also be recorded by measuring line-to-ground. By measuring line-to-ground, this doubling phenomena can also be seen in the common mode voltage, which gives reasoning to consider those as well. [33, 43, 45]

The problem with common mode voltage and currents is, it causes, beside others: bearing damages due to lubrication irregularities by partial discharges and electromagnetic interference resulting in malfunctions of surrounding instrumentation, relating to major failure. While proper shielding of the motor cable and signal cables can help attenuate the effects, to further suppress the negative and damaging effects, filtering effort should be considered to reduce common mode currents. [43]

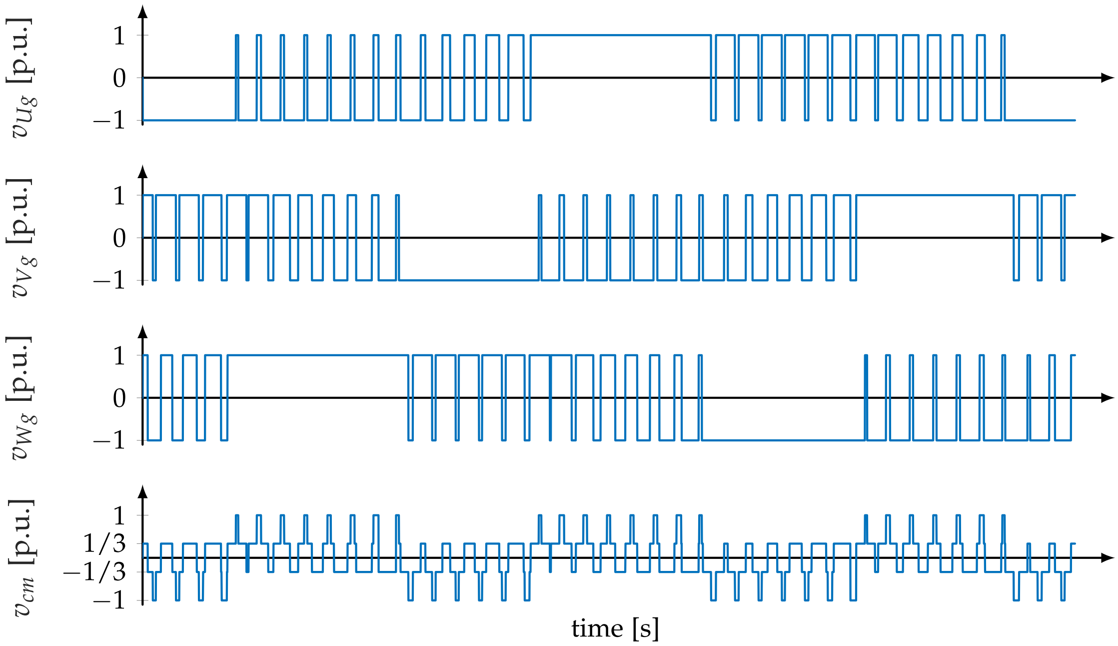

Figure 4.1: Composition of common mode voltage source through the 3 instantaneous switching stages of a 2-level converter. Base unit is V_{DC}.

4.2 Generator effect and model

The generator is responsible for two behaviours in a system operated with long cables. One is the operation point, being the fundamental waveform of voltage and current defined by its rotational frequency and magnitude. On the other hand, the generator's characteristic impedance in comparison to the cable's characteristic impedance is responsible for the reflection factor and through that for the damping and the overshoot at the generator terminal. To ensure longevity, standards limiting the overshoot are suggested.

The generator's characteristic impedance is related to the nominal power level of the machine. The lower the power rating is, the higher is the characteristic impedance and vice versa. [7, 14, 56] However, the characteristic impedance of the generator is in general shaped by its fundamental and parasitic components. Those influences can be separated in each representation or merged as a high frequency model of a PMSG.

The fundamental behaviour can be captured with a dq0-model [44], relating the stator inductance and current. The equivalent representation for the d-axis is visualized in figure 4.2, while the q-axis is identical due to the assumption of $L_d = L_q$. In order to obtain the flux linkage:

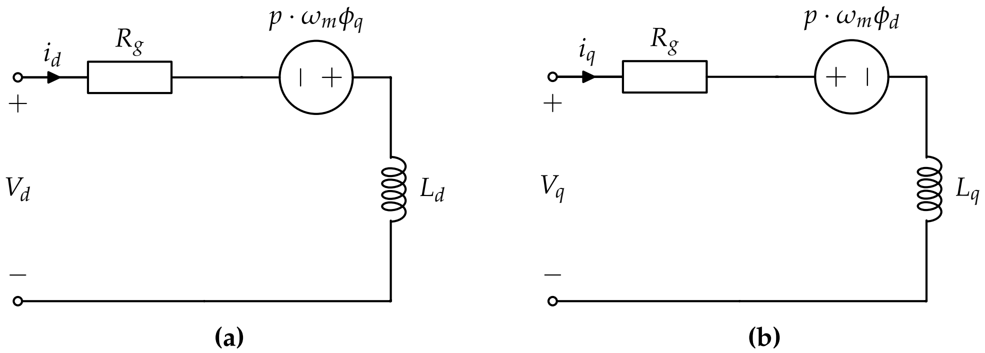

Figure 4.2: dq-axis PMSG equivalent circuit **a)** d-axis and **b)** q-axis representation

$$\phi_q = L_q i_q \tag{4.2}$$

$$\phi_d = L_d i_d + \phi_m^{'} \tag{4.3}$$

With the stator flux linkage, the electromagnetic torque is given as:

$$T_e = \frac{3}{2} p(\phi_d i_d - \phi_q i_d) \tag{4.4}$$

with p as polepairs. The mechanical rotor speed ω_m is calculated as:

$$\dot{\omega}_m = \frac{1}{J}(T_e - T_m) \tag{4.5}$$

$$\dot{\theta}_m = \omega_m \tag{4.6}$$

The mechanical torque is an input variable, as in the Plecs model [41]. The Plecs model is used as fundamental for simulation. Here, the mechanical parameters, as torque, rotor speed and angle and inertia, is measured. Those measurements are fed into an electrical model. This model measures the line to line voltage at the star point, transforms it with Park's transformation and relates finally the mechanical and electrical parameters as described above.

The output of the model is the calculated current, emulating the current generated by the rotor and stator. The current is transformed back to abc reference frame and fed into a current source. For further insight, reference [41] can be utilized.

Magnetic saturation, position dependent inductance as well as iron losses are not considered. Since saturation is neglected, the model can be assumed to be linear. [42]

The appealed model can be simplified, when the fundamental current is of no interest. Then, the generator can be modelled as a series resistance and inductance for each phase, connected in star. This model has been utilized by most of the papers in the literature regarding voltage reflection operated with frequency converters. [31, 44, 55].

However, this approach will only include the fundamental behaviour of the generator, excluding relevant parasitics, excited by the high *dV/dt*. A high frequency model could do that.

For the high frequency model, the reference paper [39] is adopted. This model is depicted in figure 4.3. There L_g and R_g are respectively the generators inductance and resistance and forming thereby the appealed fundamental characteristic of the generator.

The remaining branches are responsible to capture the addressed HF behaviour and forms together the dominant poles in the frequency repsonse, as: the C_t, L_t and R_t branch models the turn-to-turn inductance and capacitance of the stator coils. R_e is a parameter to model the eddy current losses. Last, C_{GND} and R_{GND} represent the coupling capacitance of all conductors to the generator's frame, including dissipating effects.

Using this model the generators behaviour can be approximated in a wide range of frequencies accurately.

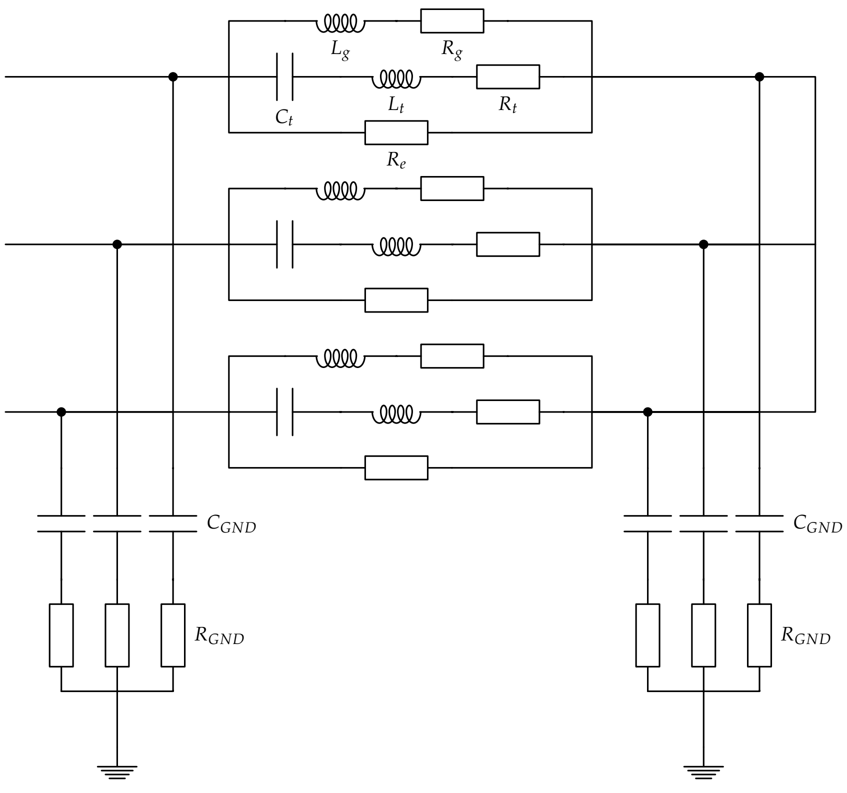

Figure 4.3: Schematic of the generator model

As apparent, the L_g R_g branch can be replaced with the dq0 - model to include the generator's fundamental behaviour into the model. This constitutes the final utilized model.

Concluding, the voltage distribution inside the machine's winding is not relevant to determine the overvoltage. It is rather important to capture the impedance as a function of frequency [39]. Thus, the generator model needs to be valid in the frequency range of the pulse's frequency spectrum, as in eq. 3.1. This can be appreciated when considering the reflection factor: the generator's impedance for high frequencies is low due to the capacitance nature (compared to the cable considerably higher).

Summarizing, the limitations of the generator model are:

- In this thesis it is assumed that the inductance of the generator is rotation angle independent, meaning $L_d = L_q$.
- The inductance of the generator is assumed to behave constant, meaning that the iron core saturation is neglected.
- The Current distribution within the generator is of no interest.
- The model uses Lumped parameters. It is fitted to impedance measurements and does not take the physical shape into account.
- The model is valid up to tens of MHz.

These simplifications and limitations are deemed to be acceptable because the emphasis is on the reflection behaviour in the cable due to the impedance mismatch.

4.3 Filter Topology

Because overvoltages are, as stated before, harmful for the generator/motor insulation standards to limit these are existent. Typical limitations are depicted in figure 4.4 by comparing different standards regarding generator overvoltages.

The european standards are IEC TS 600034-17, limits the overshoot for gerneal purpose 500 V machine when fed by frequency converters, which is by now replaces by IEC TS 600034-25. 25 A is for 500 V machine while 25 B is the limitation for 690 V machines. The american standards NEMA MG1 are limiations for definite purpose inverter fed motors. Overall NEMA and IEC suggest that the *dV/dt* is limited to less than 0.5 V/ns. When the limits are exceeded in the application, a filter should be used to protect the insulation. [14, 23]

In order to limit the overshoot and to stay with in the limitations, it is either possible to change the reflection factor through impedance matching, or to slow down the *dV/dt*. As apparent from figure 4.4, the limit of the overshoot is visualized over the rise time, directing to the approach of slowing down the rise time. A typical solution in literature are *dV/dt* filters [31, 37, 58].

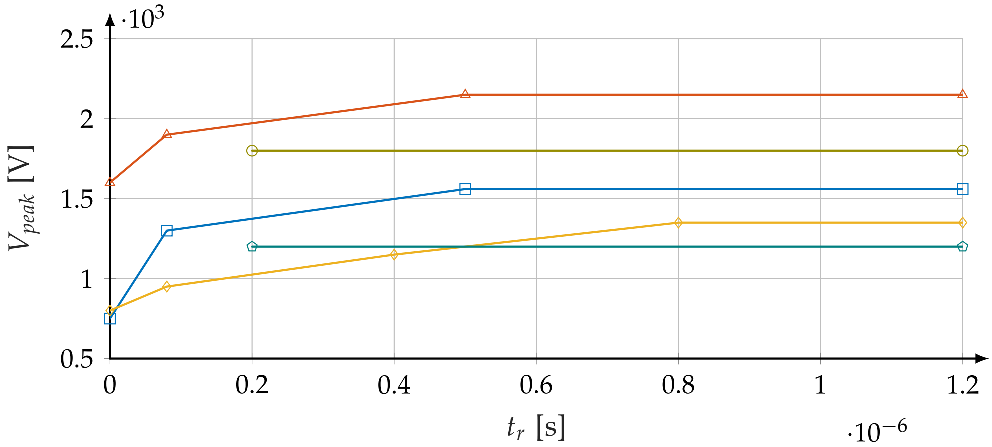

Figure 4.4: Overshoot limits for different rise times following different standards: IEC TS 600034-25 A (—□—), IEC TS 600034-25 B (—△—), IEC TS 600034-17 (—◇—), NEMA 400 V (—⬠—), NEMA 600 V (—○—)

Throughout the years many different topologies have been proposed for motor-inverter applications. A simple approach of a *dV/dt* filter is a LCR filter. Due to its simplicity, this topology is still practicable and chosen to be implemented in this thesis. The approach is to quantify the effort of filtration needed to suppress the voltage doubling effect. The equivalent circuit is depicted in figure 4.5. It can be seen, that the filter is connected to the converter's output.

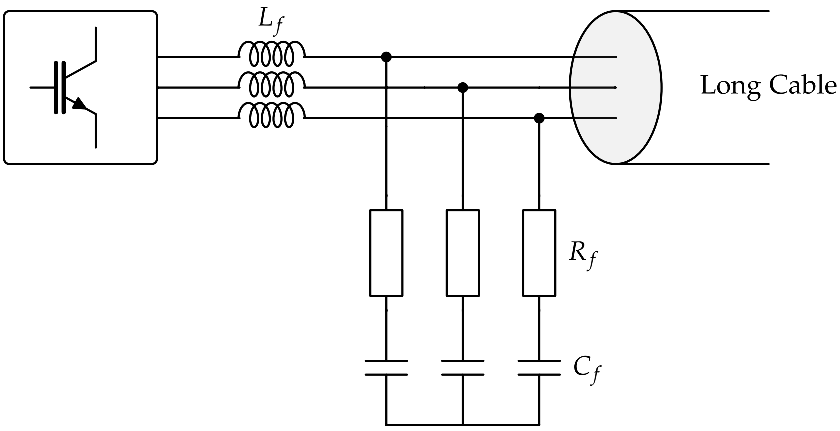

Figure 4.5: Implemented topology of LCR filter

The principle of *dV/dt* filters is, to increase the rise time of PWM voltage pulses. Consequently, the destructive common mode current amplitudes [cf. section 4.1] are reduced, too. For the LCR-topology these current peaks can be reduced up to 50%. If further reduction of the the common mode current amplitude is desired, it is proposed to use the RLC filter networks and certain manner of connection to the inverter DC bus. [20]

In the LCR topology the resistor in series to the capacitor damps the oscillations of the resonance. The resonant frequency of the filter can be calculated as:

$$f_{res,filter} = \frac{1}{2\pi\sqrt{L_f C_f}} \tag{4.7}$$

When considering components for the filter, it should be given that $f_{res,filter} > f_{sw}$. This is, by placing the cut-off frequency high enough to keep the fundamental PWM signal unaffected. [23]

Following [55, 58] the capacitance can be chosen by:

$$C_f \geq l_c \cdot 9.84 \cdot 10^{-10} \tag{4.8}$$

In order to determine the critical rise time, eq. 2.18 is considered and rearranged, with $v_{o,\%}$ being the per unit voltage overshoot, like:

$$t_{cr} = \frac{2 l_c \Gamma_g}{v_c V_{o,\%}} \tag{4.9}$$

This relates the pre-filter characteristic of cable, generator damping and converter rise time to the chosen filter component values. Since, having the critical rise time determined with desired v_o, the inductance can be calculate like:

$$L_f \geq \frac{t_{cr}^2}{C_f} \tag{4.10}$$

Further, it should be minded, that $L_f \ll L_{d,q}$.

To obtain an overdamped filter, the filter resistance can be determined by considering the damping factor and rearranging it:

$$\zeta = \frac{R_f}{2}\sqrt{\frac{C_f}{L_f}} \tag{4.11}$$

$$R_f \geq \sqrt{\frac{4L_f}{C_f}} \tag{4.12}$$

Despite filter losses, an arbitrary high resistance could be chosen, suppressing the overshoot. However, that is not practical due to economical constraints.

The transfer function in laplace domain is given like:

$$H(s) = \frac{V_o}{V_i} = \frac{1 + sR_f C_f}{1 + s^2 L_f C_f + sR_f C_f} \tag{4.13}$$

Chapter 5

Characterization of the Experimental Setup

The objective of this chapter is to correlate theory explained in the previous chapters and the experimental work considering the laboratory setup, shown in figure 5.1, to validate theory by practice and validate circuit simulation by experiments. First, the parametrization of the cable with its challenges is elaborated, followed by the parametrization of the PMSG. Those two are bundled into the remaining aspects of the laboratory setup, relating into the section of system validation, which shall include appropriate high frequency ringing, damping and response to different rise times. For that, two different lengths of cable is conducted. One, emphasizing on no voltage reflection, the other long enough to provoke reflection.

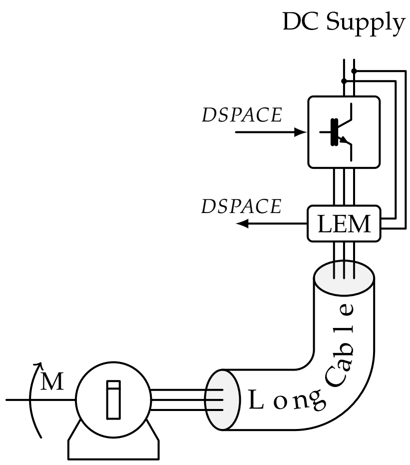

Figure 5.1: Scope of the implemented laboratory setup into Plecs

5.1 The Cable model

The object of investigation is [30], a 6 core cable consisting of 3 phase conductors and 3 PE conductors bounded in a symmetric way as visualized in figure 2.2. In the following sections, the challenges of experimentally determining the cable parameters is elaborated. Here, the two different length of available cable are investigated.

5.1.1 Parametrization of the Cable

As shown in figure 2.1a and explained in section 4.1, the typical switching instance is like two cables are leading in parallel, while the remaining is feeding back. Therefore, reference [39] suggests to measure in this configuration to obtain the short circuit impedance Z_{sc} and the open circuit impedance Z_{oc}.

To obtain suitable parameter for the cable model from the LCR-measurements conducted on the cable, reference [39] provides equations to estimate the parameter for a high frequency equivalent circuit [cf. eq. E.1].

First the open and short circuit impedance is measured with an LCR-meter, where open circuit refers to two lines connected in parallel to one port of the LCR-meter, and the third line connected to the other port of the meter. The far side of the cable is "open circuit" between the two parallel and remaining line, as the test name suggests [cf. figure D.1]. For the short circuit measurement all three lines are connected on the far side [cf. figure D.2].

After obtaining the data, it can be said, that the open circuit impedance should resemble the open circuit characteristic of the model as in Figure 5.2a and the short circuit impedance shapes the short circuit characteristic as it is shown in Figure 5.2b.

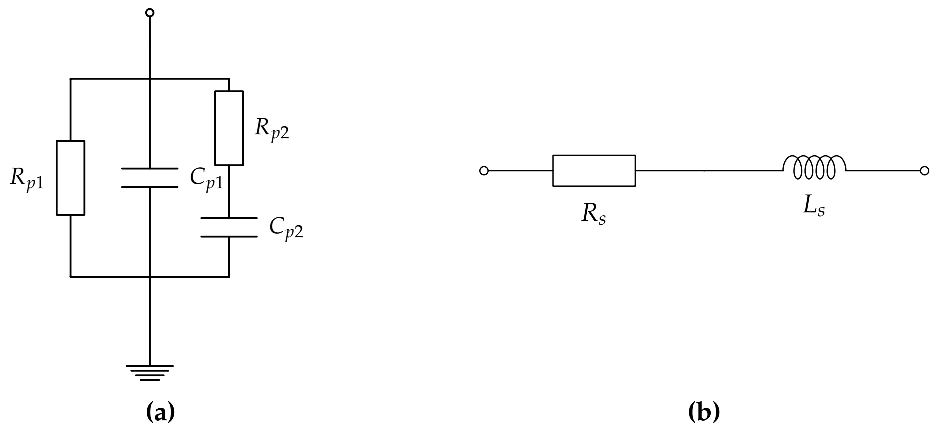

Figure 5.2: Equivalent circuit for the **a)** open circuit impedance **b)** short circuit impedance

When considering the equations E.1 of the reference paper, the parameters for the short circuit behaviour were satisfactory, while the for open circuit behaviour the equations yielded in a bad fit. This is visualized in figure 5.3.

The capacitive behaviour in figure 5.3a of the simulation (——) is significantly higher in magnitude in the low frequency range, compared to the measured impedance (——). Further, the phase of the simulation presents a mismatch between the calculated capacitances and the measured characteristic.

The phase plot of figure 5.3b however, presents a considerably better correlation between simulation and experiment. Yet, looking at the magnitude at the high frequency region a difference is easily apparent. The values can be compared later in table 5.1.

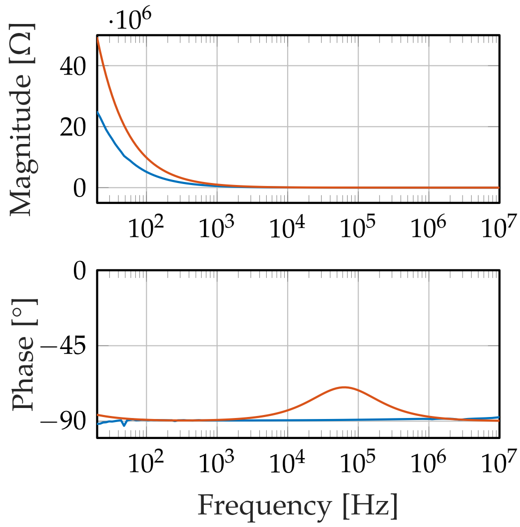

(a) **(b)**

Figure 5.3: Comparison between experimental (——) obtained impedance and simulation (——) with calculated circuit parameter for **a)** open circuit and **b)** short circuit

In order to improve the accuracy of the frequency response of the simulation, the circuit parameter were numerically fitted to the HF-model of the cable. With the obtained parameter the frequency response of the cable model is satisfactory.

To further put the obtained values into a scope, the geometrical derived values from equations 2.9 and 2.10 were used. Having $a = 1.7\,\text{mm}$ as conductor diameter and $b = 3.3\,\text{mm}$ as insulation diameter, while using the given values for copper and XLPE results in $L^{'} = 0.133\,\mu\text{H}$ and $C^{'} = 188.71\,\text{pF}$.

The parameter obtained through the different methods and measurements are compared per meter in Table 5.1. In order to scale the measured impedance to per meter and per phase, following equations are true:

$$Z^{'}_{OC} = \frac{2}{3} \cdot Z_{OC,meas} \cdot l_c \tag{5.1a}$$

$$Z_{SC}^{'} = \frac{2}{3} \cdot \frac{Z_{SC,meas}}{l} \tag{5.1b}$$

where Z_{OC} and Z_{SC} denote the open and short circuit impedance respectively and l_c the length of the cable. The subscript *meas* refers to the measured impedances.

Picking up the geometrically calculated inductance parameter and comparing it to the equations from reference [39], it can be seen, that for the long cable a high correlation is apparent. However, as seen in figure 5.3b, this is not in correlation with the measured impedance. While the fitted parameter for the long cable (—●—) is 67 % higher than the geometrical parameter, the fit gives a better match in the magnitude plot, shown in figure 5.4b.

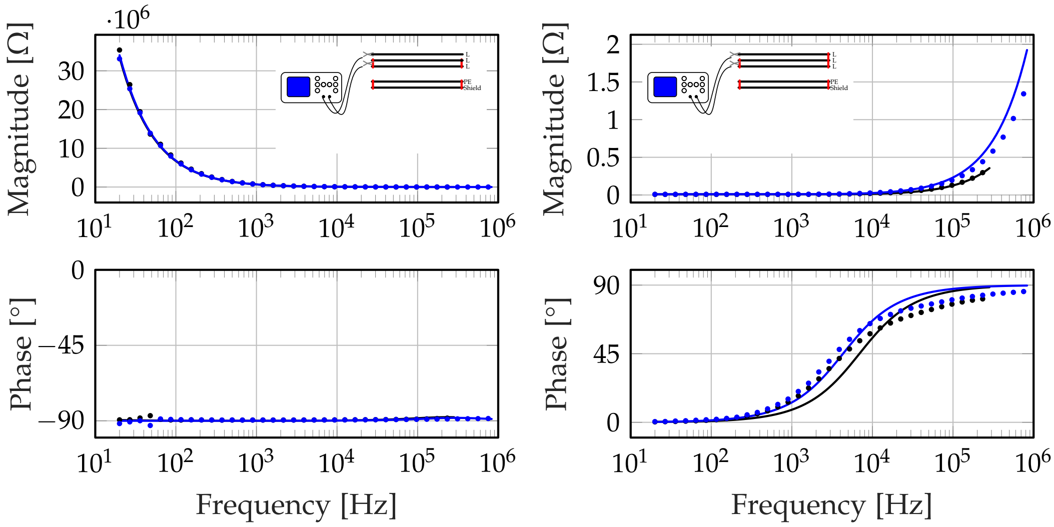

(a) **(b)**

Figure 5.4: RLC measurements for short (—●—) and long (—●—) utilized cable vs. circuit simulation (short: —— and long: ——) following section 3.1. **a)** represents the open circuit impedance and **b)** visualizes the short circuit impedance

Examining the the capacitive behaviour, it is apparent, that the calculated parameters of reference [39] does not correlate to the remaining parameters, as seen in figure 5.3a. Nonetheless, the capacitance, calculated with the geometrical characteristics, is with 16 % difference compared to the fitted values a good indicator for the right range of values. The reliance on the fitted data can however be explained by considering figure 5.4a. This applies for the long, as well as for the short cable.

Therefore, the required characteristic impedance, as explained in eq. 2.1, can be calculated. This is done by correlating the open and short circuit impedance, as:

$$Z_0 = \sqrt{Z_{OC} \cdot Z_{SC}} \tag{5.2}$$

Length	$R_s^{'}$ [mΩ/m]	$L^{'}$ [μH/m]	$R_{p1}^{'}$ [MΩ/m]	$C_{p1}^{'}$ [pF/m]	$R_{p2}^{'}$ [kΩ/m]	$C_{p2}^{'}$ [pF/m]
EQ 2.9 & 2.10	-	0.133	-	189	-	-
2 m EQ. E.1	7	0.182	1110	52.5	65	55.3
40.4 m EQ. E.1	6	0.136	962	0.067	134	2.86
2 m fit	10.7	0.280	402.5	220	40.4	12.5
40.4 m fit	9.16	0.222	282.8	220	40.4	16.7

Table 5.1: Experimentally obtained parameters for utilized cable per unit meter

The calculated characteristic impedance for both fitted parameters and the measured data is visualized for the short and long cable in figure 5.5. This plot does not show any surprises, since we have already seen a good fit for the OC and SC impedance. Following eq. 3.1 and rise times in the μs, the pulses bandwidth would be in the MHz range. Considering that in the calculated characteristic impedance, it would related to around 40 Ω. This value can be used to calculate the reflection factor Γ [cf. eq. 2.3].

Further, following eq. 2.7 and 2.8 and using the 40.2 m fit values of table 5.1, the traveling time for 40.2 m cable is calculated as $t_t \simeq 0.281\,\mu\text{s}$. By comparing experimental recorded waveform on both sides of the cable, the traveling time could be extracted as $t_t = 0.283\,\mu\text{s}$. This results in an error of 0.7 %. It is assumed, that a good fit of the traveling time is a good indicator to the effetely model voltage doubling.

Though, comparing the normalized parameters for the 40.2 m long and a 2 m short cable, differences are clearly evident. Since the fit to its corresponding measurement is matching, some further behaviour is not considered. The thoughts, treating the missing behaviour is explained in the following sections.

5.1.2 Identifying inaccuracies in the cable model

In the following section the inaccuracies of the proposed cable model in comparison with the experimental results are explored.

To identify these additional parasitic components, the cable model is compared to the physical cross-section of the cable, where all possible linkages between conductors are investigated. The capacitive cross couplings are represented in figure 5.9.

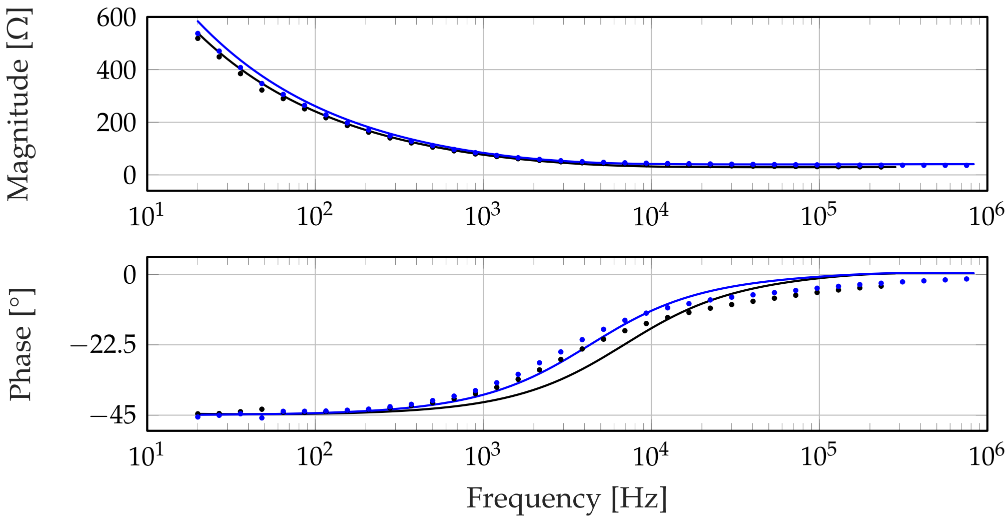

Figure 5.5: Calculated characteristic impedance with HF-model including fitted parameters (short: —— and long: ——) and measured impedance (short: —●—) and long: (—●—) investigated cable

For the open circuit representation, as shown in figure 3.1, it catches the eye, that the presented model not includes a circuit element for line to line.

In order to identify the influence of this coupling capacitance, an additional impedance measurement was conducted. It was measured by measuring 3 phase to ground [cf. figure D.3]. The Open circuit measurement is shown in figure 5.6.

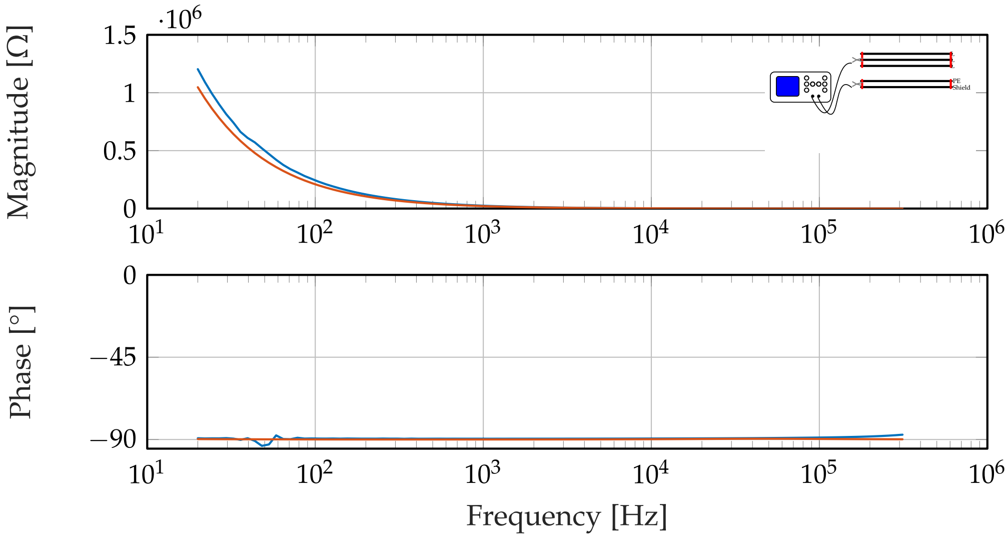

Figure 5.6: Fitted open circuit 3 phase to ground impedance (——) with RLC measurement (——)

From the fit (——), a line to ground capacitance of 160 pF can be extracted. Thus, a line to line capacitance of 60 pF can be calculated.

However, the additional circuit element discarded, because splitting the capacitance into line to line and line to ground components does not include additional behaviour of the cable, when analyzing voltage reflection followed by a pulse between line to line.

Considering the fitted values of the inductance for the long and short cable [cf. table 5.1] an approx. 20% difference of the per meter line inductance attracts attention. This difference might be related to additional parasitic components of the cable not considered yet. The authors considerations lead to a mutual inductance between line to line and line to ground and shield.

In order to verify this thesis, additional measurements were conducted. In figure 5.7 the standard 2 line to line measurement is compared to a similar setup, with the difference, that both ends of the ground and shield combination are connected to each other at the floating ends [cf. figure D.4]. This is done to change the coupling inductance between the wires and thus get an estimate on the magnitude and relation to length of it.

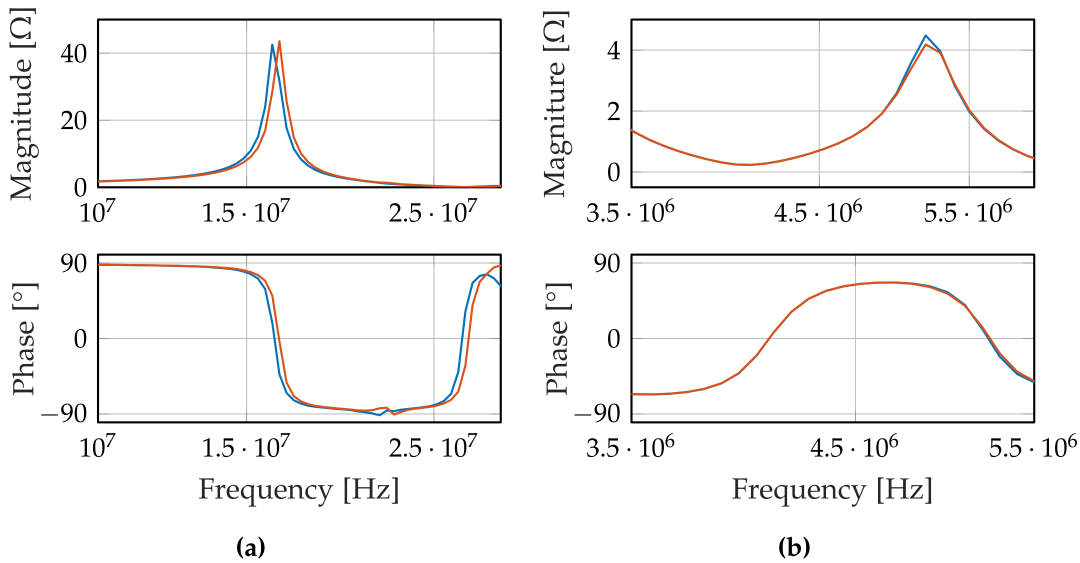

Figure 5.7: Influence of the coupling inductance between phases and ground in a 2 line to line RLC-measurement where both ends of the ground are not connected (——) and connected (——) for **a)** the short cable and **b)** the long cable

As it can be seen in figure 5.7a this change of configuration does convey a small frequency shift for the short cable, while the long cable seems unaffected between configurations, figure 5.7b.

This further proves the consideration of a mutual coupling, which the model should include as a reactive component, an inductor. This would be scaled differently to the length than the current model.

Because this effect is not visible anymore for the long cable, it is assumed that the effect reduces with cable length and is negligible for long cables. It is recommended to consider this behaviour when measuring a short cable and scaling it to length.

Further, inductance of the ground wire and shield is not fitted nor modelled. This may result in an inaccurate behaviour of the ground path in the simulation. For the analysis of the common mode current additional components for the ground wire will increase the accuracy and should thereby be considered. [5]

5.1.3 Scalability of the model

As it can be seen in figure 5.8 the frequency response of the chosen cable model is considered to be a good fit up to and above 10 MHz.

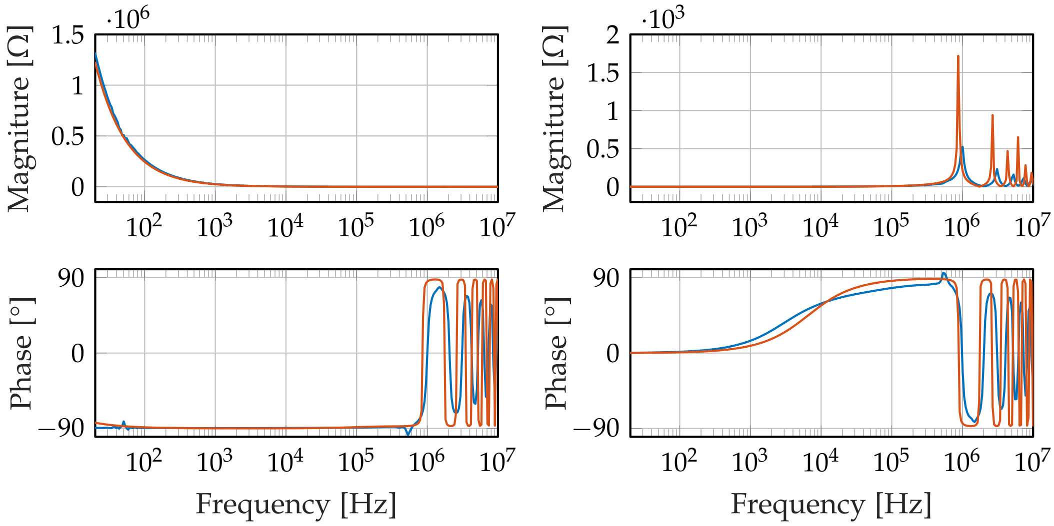

(a) **(b)**

Figure 5.8: Comparing the high frequency response of experimental RLC measurements (——) and a simulated multi section response (——) for **a)** open circuit and **b)** short circuit

The bandwidth of the signal can be estimated with eq. 3.1 and leads with a rise time of 0.24 µs to approximately $f_{BW} \simeq 1.3$ MHz. Comparing the bandwidth and frequency plot of figure 5.8 the HF-model gives a considerable good fit. However, when considering higher frequencies, it is again apparent, that an effect is not quantified.

Generally it can be summarized that the cable model is scalable to length, where the open loop behaviour of the model includes all important length related behaviours of the cable which results in consistent per meter parameter between the long and the short cable [cf. table 5.1].

For the short circuit impedance a mismatch for the line inductance between the long and short cable was identified. This additional unknown influence seems to decrease with cable length. It is assumed that if the measured cable is of sufficient length inhibiting the unknown influence, this effect does not significantly change the cable parameters if scaled longer.

When measuring an unfamiliar cable in order to obtain a parameters cable model the following measurements are recommended to be conducted:

- For the Open Circuit parameter:
  - 2 line to line configuration
  - 3 line to ground configuration when the line to line capacitance is interesting
- For the Short Circuit parameter:
  - 2 line to line configuration
  - additional measurement to identify the missing behaviour

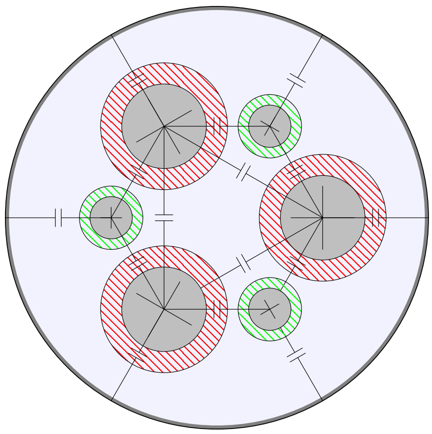

Figure 5.9: Cable cross section including possible capacitive couplings between phase, ground and shield among each other

5.2 Parametrization of PMSG model

The reflection phenomena in long cables is caused by the characteristic impedance mismatch between cable and generator. Thus, to accurately simulate the waveform deterioration through the cable, the generator needs to be modeled accurately. The implemented PMSG-model is described in section 4.2.

For simplification purposes it is assumed that the inductance of the Generator is independent of the rotor position and distributed symmetrical for all phases. The inductance, which is obtained from the data sheet of the PMSM can be transferred to the abc reference frame by following equation 5.3.

$$L_d = L_q = \frac{3}{2} \cdot L_{a,b,c} \tag{5.3}$$

After initial tests it was found that the fundamental model, consisting of an LR-branch for each phase, does only model the generator accurately up to around 25kHz. Because the voltage pulses has a bandwidth of multiple MHz, it is obvious that the high frequency model proposed in section 4.2 is required.

In order to obtain parameters for the generator, similar to the methodology of the cable, an impedance measurement at the generator terminal is conducted. Again the measurement is conducted as 2 line to line in parallel and one as return path. The impedance response is visualized in figure 5.10. The parameters were fit in accordance to this measurement.

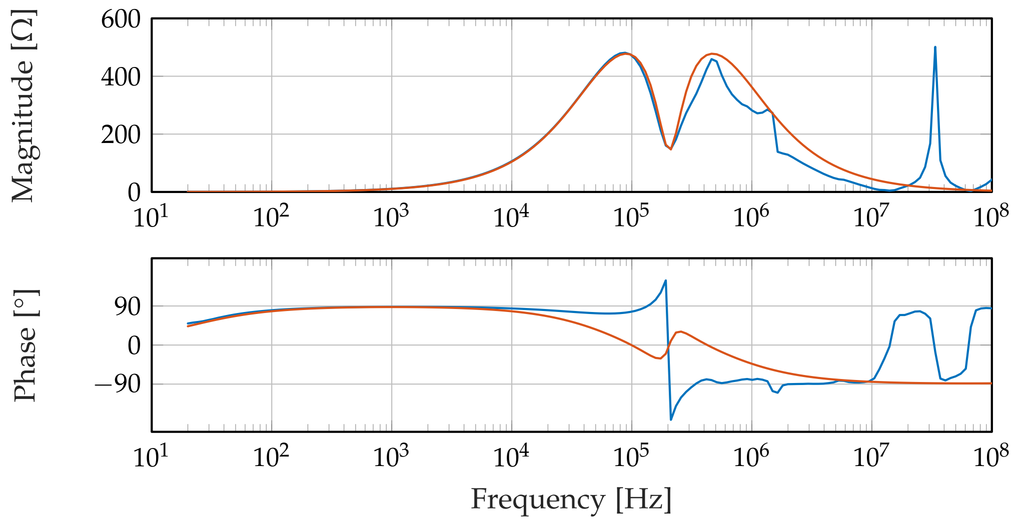

Figure 5.10: Comparison of generator impedance's between measured (——) impedance and simulated (——)

It catches the eye, that at the resonance point in the phase plot at around 200kHz changes from 90° through 180° to -90 degree, while the parameterized model changes through 0°. The authors of this thesis could not explain the behaviour captured in the measurement, nor correlate it to a generator model.

The peak at 25 MHz could be captured with an additional parallel LRC branch in the model per each phase [cf. figure 4.3], but simulations showed, that this additional branch would only have minor impact on the reflection factor. Hence, due to computing power of the circuit simulator, it is discarded.

Referring again to eq. 3.1 and knowing by know the frequency spectrum of the voltage pulse, it can be seen at around 1.3 MHz in impedance response, that the magnitude is around 300 Ω. This value can be used to calculate with eq. 2.3 the reflection factor Γ_g.

When looking at the LR branch of the HF-PMSG-model in figure 4.3, which represents the fundamental behaviour of the generator, a difference between the data sheet values and the numerical fitted parameters was detected. This difference can be explained by iron core saturation.

An further possibility to validate the parameters is possible by looking at the current slopes of the current ripple in the experiment. With the relation:

$$V_{l-l} = L_{calc} \cdot \frac{di}{dt} \tag{5.4}$$

the inductance of the overall system can be extracted from the experimental current and voltage waveforms. Because the cable inductance is very small in comparison to the generator's, it is assumed that the resulting inductance is equal to the generators inductance.

To converter the calculated inductance to the inductance of one phase the relation

$$L_g = L_{calc} \cdot \frac{2}{3} \tag{5.5}$$

can be used. It results, for the conducted laboratory setup, in $L_{g,di} = 2.33\,\mathrm{mH}$, while the fit results in a $L_{g,fit} = 1.688\,\mathrm{mH}$. The data sheet value is $L_{g,specification} = 1.666\,\mathrm{mH}$. It is expected that the value obtained with eq. 5.4 include saturation effects, and reflect the actual setup running at nominal operation point. Therefore, this value is choosen for further reference. However, this is a limitation of the conducted model, since it estimates the fundamental waveform.

Finally all obtained parameters are given in table 5.2.

L_g [mH]	R_g [mΩ]	R_e [Ω]	L_t [µH]	C_t [pF]	R_t [Ω]	C_{GND} [pF]	R_{GND} [Ω]
2.33	225	500	654	916	200	355	0.1

Table 5.2: Parameter for high frequency Generator model

The accuracy of the model in common mode configuration could be increased by conducting a 3 phase to ground RLC measurement on the generator terminal and use it to identify the to ground parameters from a separate measurement.

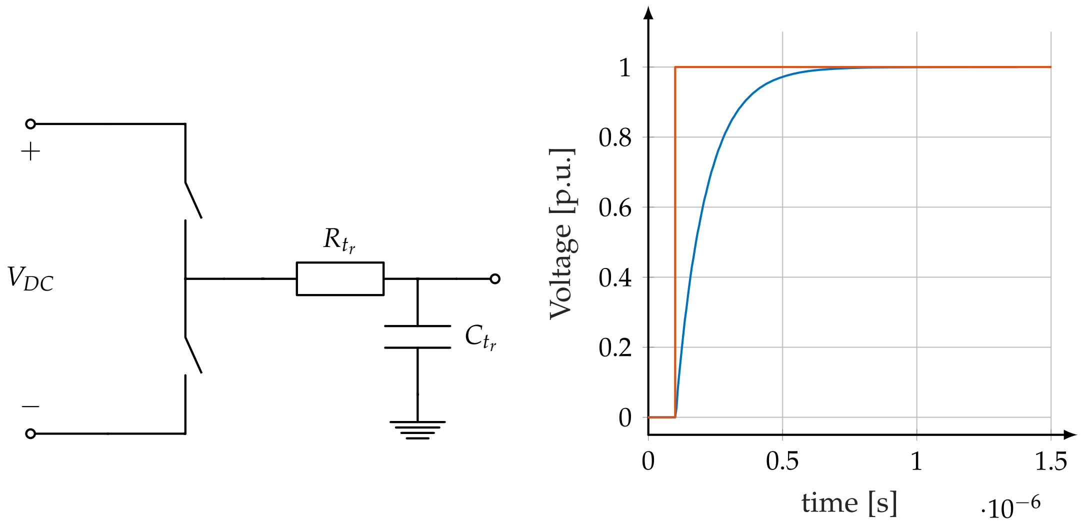

(a) **(b)**

Figure 5.11: Implemented rise time emulation, while **a)** represents the per phase equivalent schematic and **b)** represents an ideal step (——) and a step with the implemented rise time emulation (——)

5.3 Further Considerations

Since the system under investigation in AAU's drive laboratory consist of real components, those needs to be considered.

The idea of emulating the rise time behaviour came from the reference [59]. The approach is, to use capacitive charging and discharging between conductor and ground/low potential rail. The charging/discharging of the capacitor can be described by using the time constant τ, which is related as:

$$\tau = R_{t_r} C_{t_r} \tag{5.6}$$

revealing a resistance, limiting the current. The resistor, compared to the reference, is moved to the AC side of the converter, see figure 5.11, due to the 3 phase implementation.

The above equation gave an estimate, while fine tuning of the RC circuit took place. The draw back of this implementation is, that the current distribution at the DC side of the converter are immature.

Further, to emulate the laboratory setup, the modulation technique is adopted from the experimental setup with space vector modulation. This is mentioned for the sake of completeness. The modulation was just utilized to run the simulation, no further considerations were put in here. This also means, that no control for the rotor speed is implemented.

5.4 System Validation

Now, that all sub-components of the systems are modeled, the overall behaviour of the system driven by the interaction between components is compared to reality, as prove of concept. While correlating circuit simulation to the experimental test setup, following qualities are considered:

- The "operation point" of each pulse can be described with
  - phase currents
  - rise and fall time
- the time between "double pulses" is long enough for all remaining oscillations to be damped. No overvoltages > $2V_{DC}$ [cf section 2.2]

With these considerations, two different simulations were conducted. This is, one light simulation (figure 5.12) focusing on the wave reflection and correlated overvoltage behaviour, the other (figure 5.13) including the same parameters for cable and generator but also the 2 level 3 phase converter, fixing an operation point, being thereby heavier in calculations. This means, that the operation point is floating for the light simulation. However, between light and heavy simulation, the voltage reflections are of comparably nature. This leads to the establishment, that the simulations can be used interchangeable. Which one is used is, depends on the purpose.

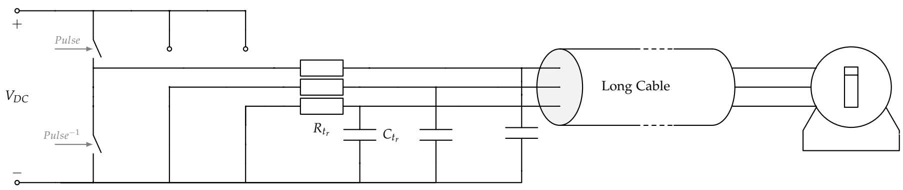

Figure 5.12: Light (double pulse) simulation with floating operation point

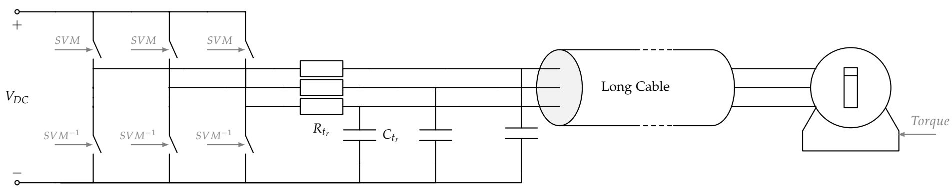

Figure 5.13: Heavy simulation, including fixed operation point by means of current due to implemented Torque

The predominant effect of voltage reflection in relation to the system is the damping factor. In section 4.2 the influence on the damping behaviour is explained. While section 5.2 adopts the theory and parameterizes the measurement to the equivalent circuit of the generator shown in figure 4.3. When the simulated waveform with the experimentally measured waveforms were compared, with the component parameters from section 5.1.1 and 5.2, the damping behaviour did not correspond.

As explained in section 2.3 the damping behaviour can be explained by two mechanisms: the frequency dependent AC resistance, as well as the damping factor due to impedance mismatch.

Trying to explain the difference of damping, the AC resistance was further analyzed. The eq. 2.23 and 2.24 were utilized with the parameters from table 5.1 for 40.2 fit. The oscillation frequency relates thereby to $f_0 = 0.8725\,\text{MHz}$. The related conductor diameter is $a = 1.7\,\text{mm}$, giving an AC resistance of $R_{AC} = 1.6\,\text{m}\Omega$, leading to a damping factor of 0.999. Hence, firstly, the AC resistance is not the missing damping influence, further, for this application it is reasonable to neglect the AC resistance.

Since the rise time of the experimental measurements cannot be determined accurately. Further, with the knowledge of section 2, where it is stated that the rise time has an additional effect on the damping,

Since the utilized parameters results in a missmatch of damping behaviour, eq. 2.3, determining the reflection factor analytically and thereby the damping factor of characteristic impedance difference of generator and cable, cannot be utilized. Therefore, the damping factor can be read from the waveform. However, as stated before, does the rise time also have an influence on the overshoot and thereby the first reflection at the generator terminal cannot be considered to determine the reflection factor.

Cable Parameter							
$R_s^{'}$ [mΩ/m]	$L^{'}$ [μH/m]	$R_{p1}^{'}$ [MΩ/m]	$C_{p1}^{'}$ [pF/m]	$R_{p2}^{'}$ [kΩ/m]	$C_{p2}^{'}$ [pF/m]	-	
9.16	0.222	282.8	220	40.4	16.7	-	
Generator Parameter							
L_g [mH]	R_g [mΩ]	R_e [Ω]	L_t [μH]	C_t [pF]	R_t [Ω]	C_{GND} [pF]	R_{GND} [Ω]
2.33	225	300	654	916	200	355	0.1
Rise time emulation parameter							
C_{t_r} [μF]	R_{t_r} [mΩ]	-					
8	14	-					

Table 5.3: Utilized component values in simulation

In order to separate the behaviours of rise time and characteristic impedance difference, the theory about damped oscillations were considered, as explained in section 2.3.

Applying the theory to the obtained waveforms, a mean value has to be decomposed from the peaks. For that, eq. 2.26 is modified. Still, two peaks of the oscillatory motion is chosen. Though, now the associated minimum to the peak (half a period further) is subtracted from the peak, like:

$$x_{pp}(t, t + m\tau) = max(f_{osci}) - min(f_{osci}) \tag{5.7}$$

With $x_{pp}(t)$ and m periods late $x_{pp}(t + m\tau)$. This relates to the adjusted eq. 2.26, as:

$$\sigma = ln(\frac{x_{pp}(t)}{x_{pp}(t + n\tau)})/n \tag{5.8}$$

Having determined the logarithimc decay σ, the damping factor ζ is calculated following eq. 2.27.

Following the procedure, it relates to a damping factor $\Gamma = 0.75$ for the experimental setup. In order to come closer to this value, the generator parameters were analyzed again. And, it was worked out, when varying the eddy current loss resistance R_e, it has the most influence on the damping factor. Therefore, against the fitted parameter from section 5.2, R_e was chosen to be equal $300\,\Omega$. This leads to a mismatch in frequency plot of figure 5.10 resulting in higher max and min of the peaks at around 200 kHz.

However, with this move, the missing damping could be compensated. This relates to the conducted values in table 5.3, while a voltage waveform of experiment and simulation, related to the damping behaviour is visualized in figure 5.14.

The enclosing function of eq. 2.26 for the simulation is plotted into figure 5.14. This gives prove, that the method described in section 2.3 gives a good estimate of the damping factor. For the simulation, with the values from table 5.3, the damping factor $\Gamma = 0.79$ is calculated.

There is still a difference between simulation and experiment. However, the error is of around 5 %. Considering the characteristic impedance of the cable and generator for the bandwidth of the pulse, deducted in section 3.1 and 5.2, respectively, the following reflection factor Γ_g, with eq. 2.3 is calculated:

$$\Gamma_g = \frac{Z_{0,g} - Z_{0,c}}{Z_{0,g} + Z_{0,c}} = \frac{300 - 40}{300 + 40} = 0.76 \tag{5.9}$$

This calculated reflection factor with the characteristic impedance responses of the measurements and fitted data, lies in between experimental waveform and simulation waveform reflection factor, which further validates the simulation.

Further in this figure 5.14, it is apparent, that between the simulation model with the chosen parameters and experiment a difference in oscillation is apparent.

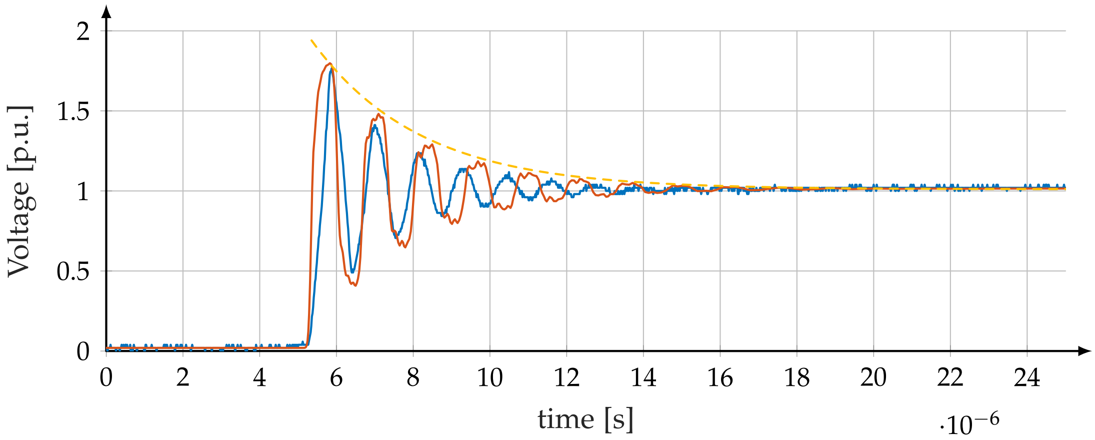

Figure 5.14: Experiment (——) vs. Simulation (——) l-l voltage with the fitted damping coefficient (- - -)

Despite that, it is considered to be reasonable and a good fit, when conducting analyses for the filter and later for the up-scaled simulation.

The damped oscillation following eq. 2.29 for the chosen parameters of table 5.3, resulting in $\zeta = 0.0746$ and $f_d = 760\,\text{kHz}$, is visualized in figure 2.5.

Since the simulation is established and the parameters are determined, it can be analyzed whether theory complies with practice. Measurements of the experimental setup are conducted by measuring right after the LEM box for the converter side measurements, while a measurement box was installed right before the generator terminal in order to measure voltages and currents at the generator terminals [cf. figure 5.1].

Following the employed theory of chapter 2, no or minor overshoot shall occur, when conducting the test setup with a cable shorter than l_{cr}. In figure 5.15 is a line to line voltage of a short cable for the experiment (——) and simulation (——) presented.

While figure 5.15a represents the initial pulse at the converter side, does figure 5.15b represent the voltage at the generator terminal. For both sides it can be concluded, that theory applies and comparably no overshoot occurs. Oscillation at the generator terminal is present. Due to the shorter cable, the travelling time is short, which relates to a higher oscillation frequency. The minor overshoot at the generator terminal can be explained with eq. 2.16 and the related figure 3.5, since $t_t < t_r/2$ and the relation of those two is a high value.

Comparing simulation to the experiment, it can be seen, that a similar behaviour is present. Though, the extent of the overshoot of the is not represented by the simulation as it is in real life.

Though, considering the case of investigation, a long cable between converter and generator, the correspondence between simulation and experiment is closer. In

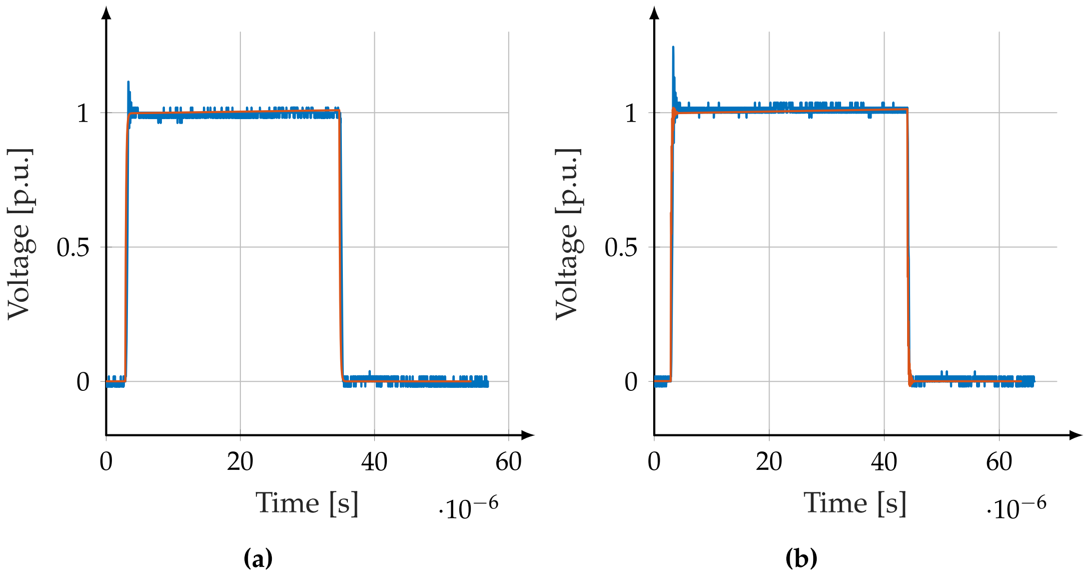

Figure 5.15: Comparing the simulation (——) with the experimental results (——) for the short cable at a) the converter and b) the generator terminals

a detailed look, figure 5.14 confirms that. However, figure 5.16 compares converter terminal to generator terminal of both experiment (——) and simulation (——).

The oscillatory behaviour at the converter side, presented in figure 5.16a, is again not fully represented in the simulation. Nonetheless, comparing the referred figure to figure 5.16b it can also be seen, that theory complies to practice and the simulation complies to a great fit to the experiment.

Wave reflection, as shown in figure 2.1, is clearly present for simulation and experiment at the generator terminal. Considering theory further, the overshoot seen at the generator terminal is not present at the converter terminal, due to its comparably low impedance for high frequencies. Also at the generator terminal, the reflection factor Γ_g shows its influence with the decay down to V_{dc}.

Now having confirmed the theory quantitatively, a qualitative view on the fundamental waveforms is given. It should be denoted, as said in section 5.3, the modulation was not part of the simulation effort. This is clearly evident in the following analyzes. However, the conclusions are draw in regard to wave reflection theory, where the modulation has no influence, when not entering overvoltages > $2V_{DC}$ [cf. section 2.2.2]

First, in figure 5.17, the fundamental line to line voltage of a short cable is shown. In figure 5.17a, the experimental voltages of converter and generator terminal are overlayed, the same for the simulation is shown in figure 5.17b. For both the drawn conclusion from earlier is true, no or minor overshoot due to reflections is visible, since both converter and generator terminal voltage waves are on top of each other. This is different, when looking at the long cable in figure 5.18. Here,

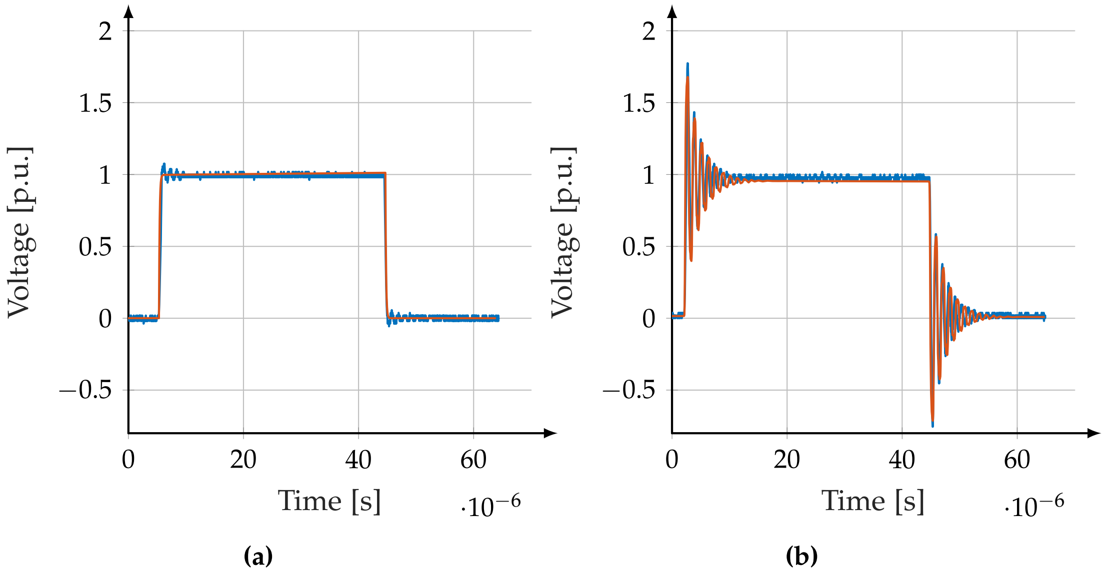

Figure 5.16: Pulsed long cable of simulation (——) vs experiment (——) for **a)** converter and **b)** generator side

the experimental converter and generator voltage waveforms are presented in figure 5.18a, while for the simulation in figure 5.18b. For both figures, it is clearly evident, that the reflection due to characteristic impedance mismatch and travelling time is present, since the voltage at the generator terminal is greater than the initial converter side voltage.

With these assumptions the requirement for the simulation are to recreate a double pulse for a given operation point. With such a double pulse simulation the two parameter which are important to determine the waveform quality, max(dV/dt) and V_O are recreatable.

5.5 Waveform Quality Deterioration

The waveform quality is interesting in two regards. On the one hand The current is measured at the converter terminal to control the active rectifier and through that the generator. On the other hand the waveform quality can be used to determine the stress on the generator.

Additionally the question is raised, if the deterioration through long cables does change the efficiency of the generator/losses in the generator.

Following the inverse behaviour between current and voltage as discussed in Chapter 2 regarding the position of overvoltage the influence of the long cable on the current waveform takes effect on the converter side. There, the sampling for the converter control is taken. Looking at figure 5.19, it can be seen for the short

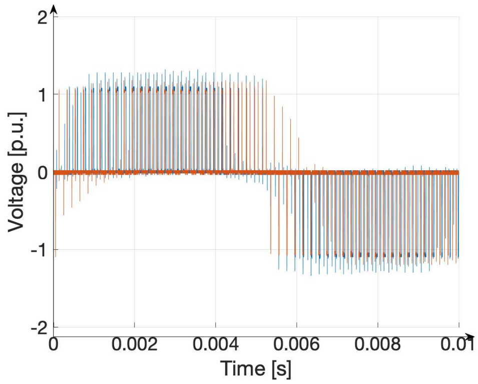

(a)

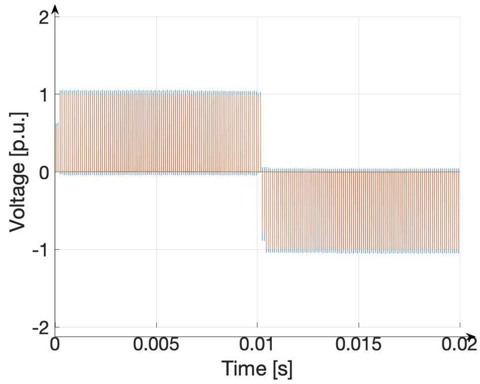

(b)

Figure 5.17: Fundamental voltage of short cable of converter (——) vs generator side (——) for **a)** experiment and **b)** simulation

cable in figure 5.19a, that no great deterioration between converter and generator is given. Though, for the long cable in figure 5.19b, the distortion at the generator is of great influence compared to the generator terminal. This gives a first insight of the requirement to consider deterioration, when conducting senseless control of the generator.

Often, the current for the converter control is sampled approximately in the center between two pulses. With other words, the sampling point is at the peak and valley of a triangular carrier. Further, that reflects, that the sampling is twice the sampling frequency. [12].This results in the fact, that the sampled value is very close to the average of this period.

As seen in the figures before, the long cable consist of noise. As it can be seen in figure 6.6, the introduced noise can be at the sampling instance, which expected to disrupt the accuracy of the control. The noise level, by means of the high frequency ringing, could introduce an error of up to 40 %.

Following the previous argumentation, when looking at the generator stress level, the distorted and dues investigated parameter is the generator terminal voltage. For

- Fourier transform distribution
- max(dV/dt)
- V_{over}

The last two can be obtained form the a pulse and the resulting parameter are described in table 5.4

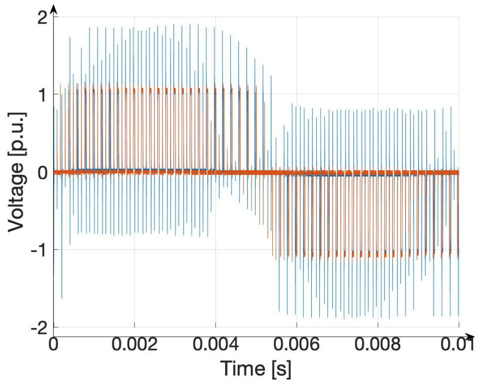

(a)

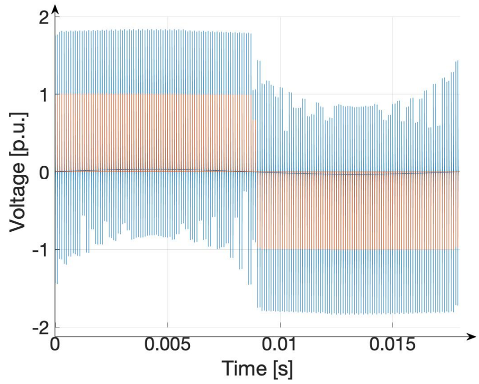

(b)

Figure 5.18: Fundamental voltage of long cable of converter (——) vs generator side (——) for **a)** experiment and **b)** simulation

Method	max(dV/dt) in V/ns	$V_{O,abs}$ in V	V_{rise} in µs
short cable	3.0	520	0.213
long cable w/o filter	5.5	905	0.24

Table 5.4: Voltage waveform parameter comparison to characterise the deterioration

It is expected, that introducing a filter will solve these concerns of control and stress level by improving the current and voltage waveform quality.

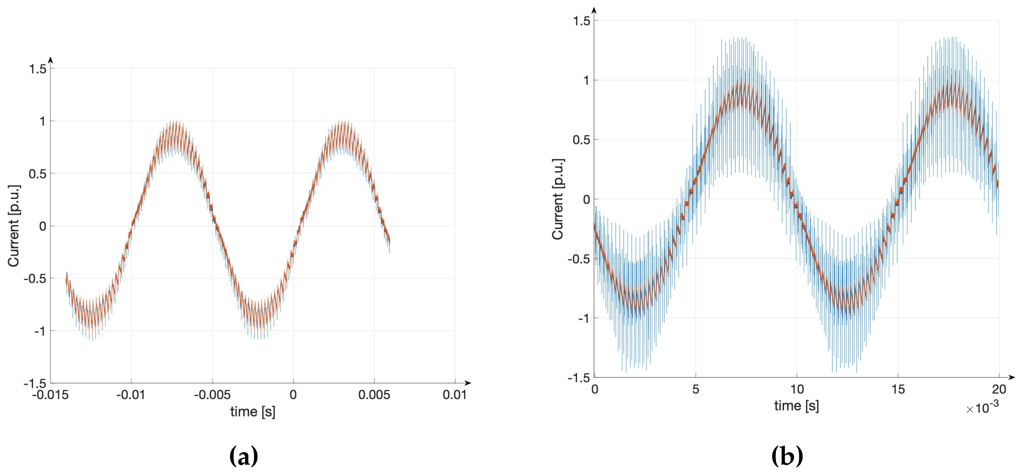

Figure 5.19: Fundamental current of converter side (——) vs generator side (——) for **a)** short and **b)** long cable

Chapter 6

Filter Implementation

In this chapter the impact of a filter on the waveform quality is analyzed. First the design methodology established in section 4.3 is utilized and some simple considerations regarding filter losses are taken into account. Then experimental waveforms are compared to the simulation results. Finally the impact of the filter on the waveform quality is discussed, considering the previous results.

6.1 Filter Design

Following the in section 4.3 established methodology, the different component sizes for the filter are determined. This is by choosing an appropriate overshoot and hence a critical rise time. The chosen values are displayed in the first column of table 6.1.

Taking eq. 4.8 to determine the filter capacitance, an approximate safety margin of 20% was added to the cable length. This relates to a length of 50 m and $C_f = 49.2\,\mathrm{nF}$

Further, when considering eq. 4.9 with $v_c = 150\,\mathrm{m/\mu s}$, $\Gamma_g = 0.74$, $l_c = 41\,\mathrm{m}$ and a $v_o = 0.2$ it relates to a critical rise time $t_{cr} = 3\,\mathrm{\mu s}$.

Now, continuing with the established methodology by using eq. 4.10 and 4.12 the filter inductance of $L_f = 0.187\,\mathrm{mH}$ and $R_f = 123\,\Omega$ can be calculated. To R_f a 20% margin was added, leading to $150\,\Omega$. The values are summarized in table 6.1.

The methodology is conducted for different overshoots to see a range of filter options, limited to the topology. For the last two rows of table 6.1 the rise time is kept constant and the capacitance is changed in correspondence to the resonance frequency depending on the inductance.

Now, to estimate the behaviour of the filter, the frequency response and step response [cf. eq. 4.13] with the component values in the 2. row of table 6.1 are plotted in figure 6.1. In 6.1a it can be seen, that the cut frequency is present at around 155 kHz. The resonant frequency, following eq. 4.7, relates to 52 kHz.

t_{cr} [µs] for $V_{o,\%}$ [%]	L_f [µH]	C_f [nF]	R_f [Ω]	Filter Losses w/o gnd [W] ([%])	Filter Losses with gnd [W] ([%])
6 for 10	732	49.2	292	8 (0.8)	222 (21.0)
3 for 20	187	49.2	150	23 (1.8)	328 (22.8)
2 for 30	81.3	49.2	97	37 (2.5)	434 (27.9)
1.5 for 40	45.7	49.2	72	68 (4.2)	532 (33)
3 for 20	20	182	210	30 (1.8)	- (-)
3 for 20	200	18.2	210	16 (1.0)	177 (11.4)

Table 6.1: Filter component size. Nominal power is 1.5 kW

Thereby both the cut and resonant frequencies are above the switching frequency.

The figure 6.1b shows the step response of this transfer function. Here, it is already visible that the filter will, besides slowing down the rise time, introduce an overshoot at its output. Still, the slower rise time will suppress the voltage doubling effect. This behaviour is more desirable than no filter.

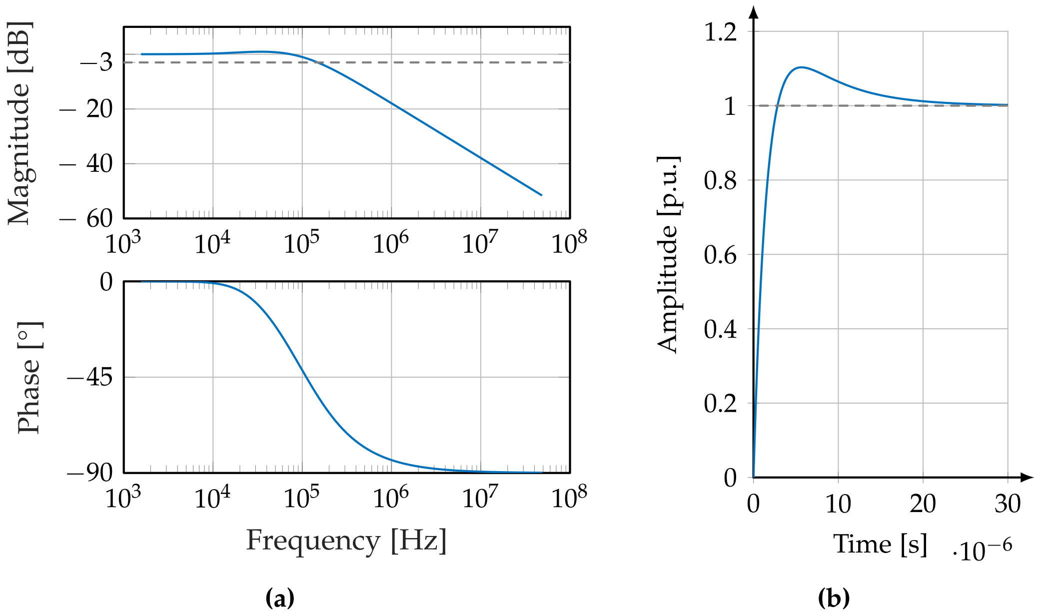

Figure 6.1: Presentation of transfer function of chosen LCR filter **a)** frequency response **b)** step response

The influence of the filter on the overall system, exemplary shown for the parameters of row 2, is visualized in figure 6.2. Examining the generator side (figure 6.2b), where the overshoot and its high frequency ringing due to the reflection has its mayor impact, it is visible that the overshoot with the selected filter could be suppressed by 57% points and lies after reducing the dV/dt at 20% overshoot, as it had been tuned for. The reduced rise time to 3 µs is apparent in figure 6.2a.

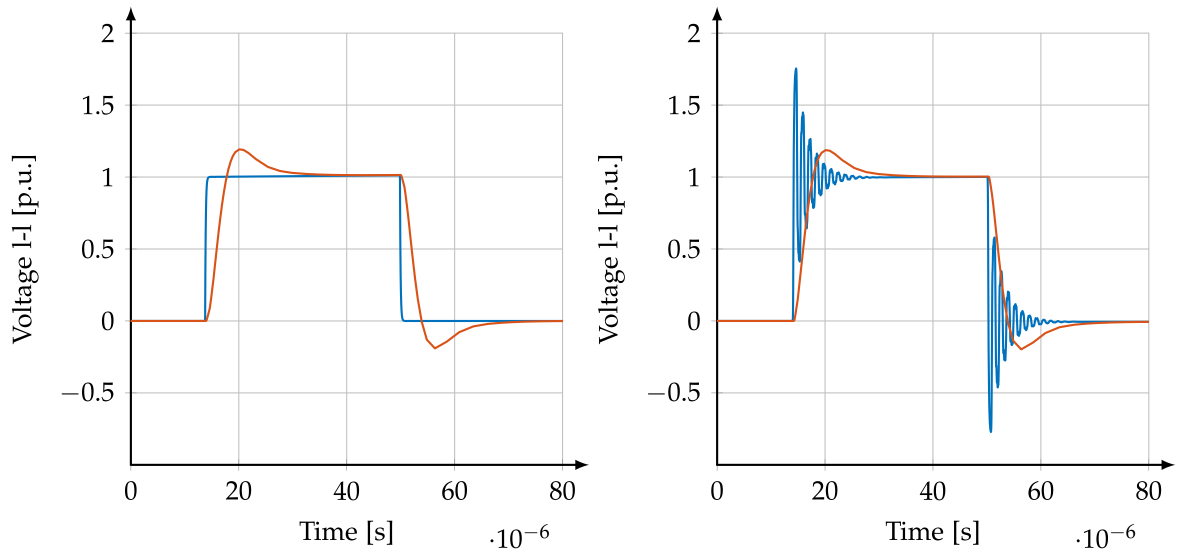

(a)

(b)

Figure 6.2: Circuit Simulation behaviour of filter (——) vs no filter (——) at **a)** converter side and **b)** and generator side

For all suggested parameter combinations, the filter resistor losses are estimated through circuit simulation. These estimated values are compared in table 6.1. There it can be seen that the resistor losses are smaller for bigger inductance, or smaller capacitances.

Additional losses will be present in the experimental setup, which could be model by an ESR. It can be assumed that the losses in the inductor will increase with increasing inductance. Because of that, the inductance should be kept small.

The overall power loss of a filter should be very small. In this case it was tried to minimize the resistor power loss to 0.1%. It was not possible for the authors to archive this goal by tuning this filter topology. That was, because the overall inductance of the system should stay in an acceptable range.

Even though grounding the filter star point reduces additional common mode current and voltage the loss increases by a factor 10, making this not a viable option.

6.2 Experimental filter validation

Even though it was not possible to design an satisfactory economical efficient LRC filter in the previous section, this section will experimentally verify the expected behaviour observed in the simulation.

The components for the experimental setup were selected to have a low overshoot and thereby a relatively long critical rise time to ensure the suppression of the voltage doubling effect, but on the other hand as low losses as practicable using this simple LRC topology. The utilized parameters are given in table 6.2.

L_f [µH]	C_f [nF]	R_f [Ω]
120	22	220

Table 6.2: Component values used for the experimental filter

Implementing the constructed filter into the laboratory setup results in waveforms as presented in figure 6.3. Pictures of the laboratory setup, including the filter, are presented in appendix G.

Comparing the converter side with the generator side, again, a similar waveform shape, due to the filters oscillation is present. At the same time, it can be said that the voltage doubling effect is successfully suppressed. This behavior can also be seen for the simulated waveform.

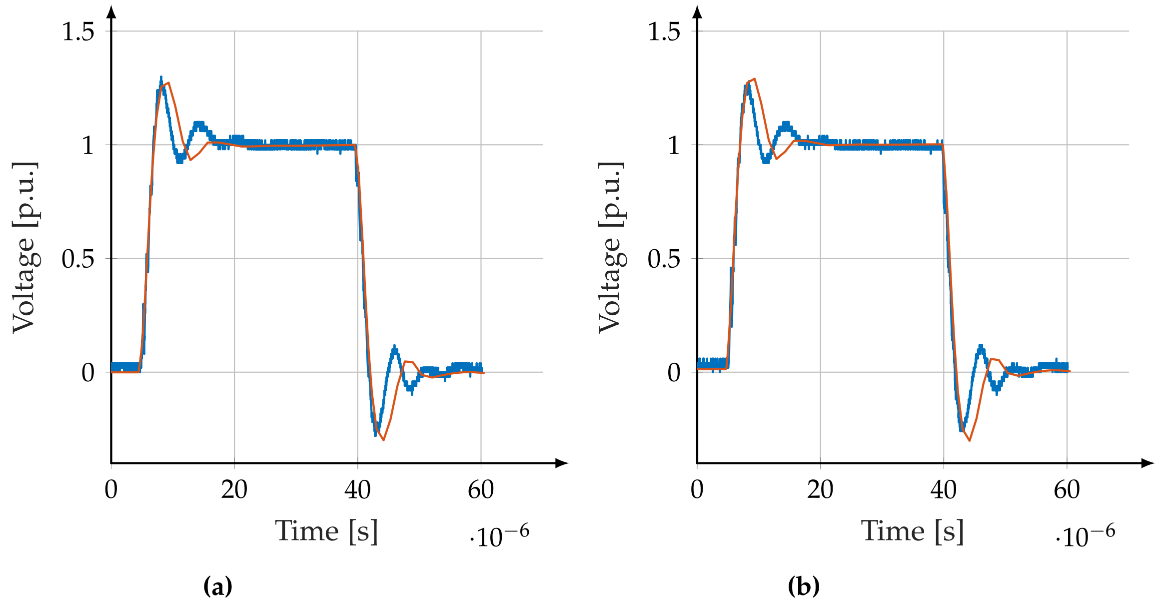

Figure 6.3: Experimental data including the proposed filter. The simulation (——) is compared with the experimental (——) result. The **a)** converter side is compared to **b)** generator terminal waveforms.

Comparing the experimental double pulse with the simulated, the difference is, again, in the oscillation frequency of the overshoot. Apart from this known issue, the magnitude of the overshoot and the damping behaviour are a good fit. Thus, it can be said that the simulation also captures the behaviour of the cable and system, when including a filter.

The experimental data can be used to determine the resistor losses by measuring the voltage drop over the resistor and the current through it. The results can be seen in table 6.3.

Operation point [N · m], [Hz]	P_n [kW]	$P_{filter,R}$ [W]([%])
7, 50	1.96	40 (2.04)
14, 50	4.38	41 (0.94)
14, 23, Simulation	1.72	22 (1.31)

Table 6.3: Experimental measured resistor losses

When comparing the two operation points it seems like the filter losses are operation point independent. It seems that the percentage of power looses drops by increasing the power level. This behavior can be explained with the fact, that the cut frequency of the filter is designed to be above the switching frequency. Because of that, the magnitude of the fundamental frequency should have a small impact on resistor losses.

In figure 6.4 the appearance of the fundamental waveforms are compared. Besides the previously mentioned difference of the fundamental frequency, which leads to a denser appearance of pulses, the shape of the two sub figures is very similar. Now the main influence on the waveforms is no longer the long cable, but the filter. Even, considering the simulated fundamental, presented in figure 6.4b, the generator terminal voltage can not be seen since they are alike.

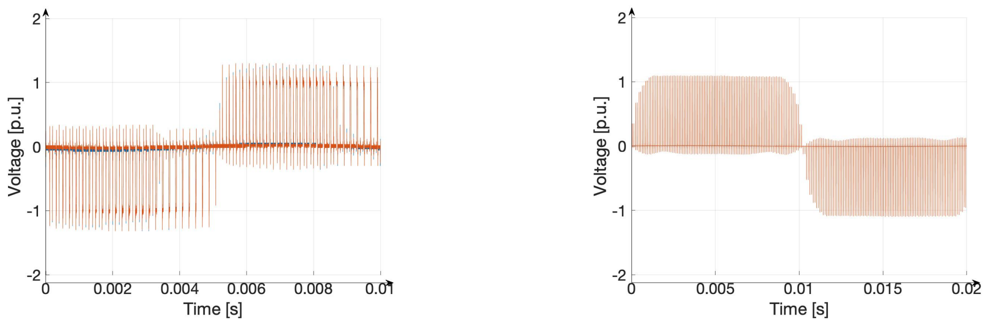

(a) **(b)**

Figure 6.4: Comparison of fundamental waveforms including a filter, for the converter (——) and generator (——), for **a)** the experimental setup and **b)** circuit simulation

Concluding, it can be said that the filter behaviour behaves as expected in the experimental setup. Also, the simulation still represents the cable behaviour when included filter as modeled. With the filter topology chosen it was not possible to have reasonable losses in the damping resistor, but it is expected, that the loss percentage decreases with increasing power. Therefore, both a more advanced filter topology, as well as an higher power level could be beneficial, which is in corresponds to reference [23].

6.3 Waveform Quality Improvement

In section 5.5 the attention is attracted to two areas of concern, the control of the converter and generator stress level. In order to reduce the stress level of the converter, it was suggested that a filter could solve both problems.

Due to theory [cf. figure 2.1], it is assumed, that the filter has a similar suppressing effect on the current high frequency ringing at potential sampling intervals for the control, as seen for the long cable.

In figure 6.5, the fundamental currents at converter and generator side are presented. Comparing the sub-figures, it is apparent, that the filter reduces also in the current the overall noise and thereby the high frequency ringing(figure 6.5b), when comparing it to the long cable without filter (figure 6.5a).

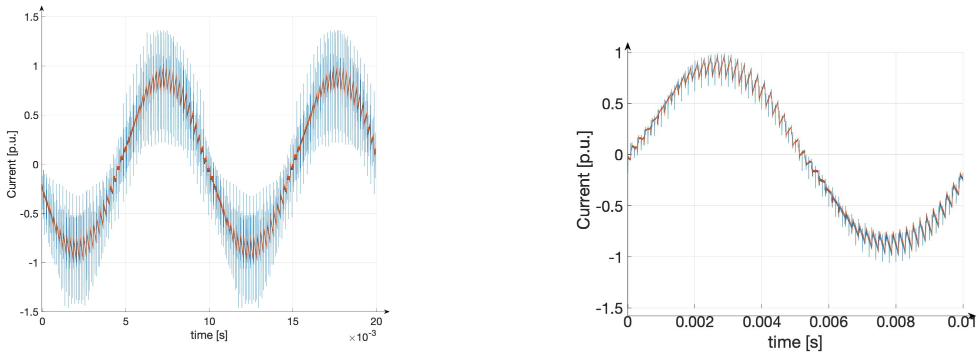

(a) **(b)**

Figure 6.5: Fundamental current of converter side (——) vs generator side (——) for **a)** long cable and **b)** long cable with filter

In regards of the waveform quality, affecting the sampling of the control, this means, as visualized in figure 6.6b, that the overshoot is suppressed to a similar level as measured with a short cable.

put percentages

In the previous section 6.2 it was shown, that by utilizing a simple *dV/dt* filter it is possible to suppress the overvoltage effect, when reducing the rise time. The resulting waveform has an reduced impact on the generator stress, when compar-

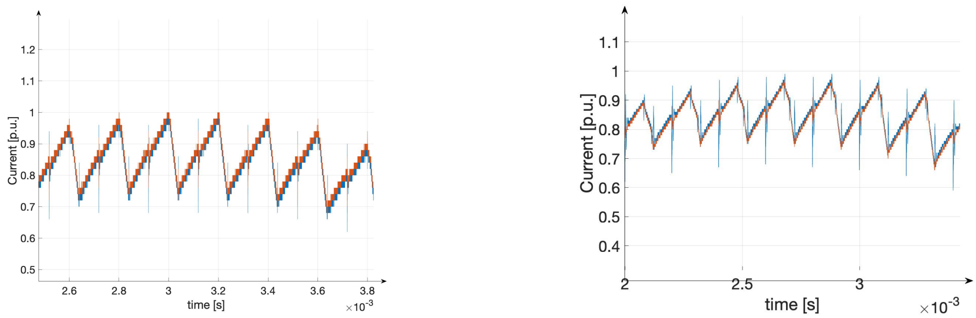

(a) **(b)**

Figure 6.6: Magnitude reduction of high frequency ringing at converter terminal due to *dV/dt* filter for **a)** short cable and **b)** long cable with filter (Zoomed image of figure 6.5b)

ing the values of table 6.4. The rise time is approximately prolonged with a factor of 10 compared to the non-filtered rise times. This has an effect on the max(dV/dt), which is reduced below the 0.5 V/ns [cf. section 4.3]. Thereby, it is concluded, that the *dV/dt* filter has a positive effect on the voltage stress.

Qualitatively an influence of common mode reduction is apparent. Because the common mode paths in the experimental setup were not very defined [cf. figure 1.4] and thus not further measured.

Method	max(dV/dt)[V/ns]	$V_{O,abs}$[V]	t_r[µs]
short cable	3.0	520	0.213
long cable w/o filter	5.5	905	0.24
long cable w filter	0.265	620	2.25

Table 6.4: Voltage waveform parameter comparison to characterize the deterioration

Chapter 7

Case study: 10 MW Up-scaled Wind Turbine

In this chapter the gained knowledge of the impact of long cables in a generator converter setup is used to estimate its influence in a high power medium voltage environment. First, a case is proposed which could outline a future scenario in which long cables implemented. This means, the conversion stage is located at the tower base. All relevant parameter for a operation environment, cable and generator are estimated for the proposed case and a statement about the expected resulting waveform quality is made. Finally a filter design to improve this quality is introduced, to give an estimate of filtering effort needed.

7.1 Up-scaling the model

The proposed case is a wind turbine with nominal power of 10MW. A medium voltage level is amongst others desireble to reduce the cable diameter compared to the same power level for low voltage.Hence, the case for $V_n = 4\,\mathrm{kV}$ is considered. The cable length is investigated for 100 m and 200 m to cover the expected range. The authors of this thesis did not have any data or parameter at for the medium voltage high power setup available at the stage of submitting the thesis. Thus, all implemented parameters are estimates.

For the cable parameter estimation the cable type WINDLINK® (N)TSCGEHXOE is considered as reference. Following section 2.2, the cable parameter can be estimated using the geometric information of the cross-section with eq. 2.9 and 2.10. The conductor and insulation diameter are respectively 10 mm and 20 mm per phase. The insulation is unknown and thus estimated as a worse case scenario. The resistance is estimated using the following relation.

$$R = \rho \cdot \frac{l_c}{A}, \tag{7.1}$$

where ρ is the resistivity of copper, l_c is the cable length and A is the conducting area. The calculated parameters are displayed in table 7.1. One has to be cautious with these estimates, because, as it can be seen in table 5.1, these estimation differ for the in this thesis conducted experiments by 40%.

length [meter]	L_s [µH]	R_s [mΩ]	C_{p1} [nF]	t_t [µs]
1	0.138	0.273	0.180	0.005
100	13.8	27.3	18.0	0.498
200	27.7	54.6	36.0	0.997

Table 7.1: Estimation of cable parameter the proposed MW and kV turbine arrangement

Because the parameter are only estimated the high frequency components are not included into the model. The same approach is taken for the generator. The stator branch (R_g and L_g) is used to model the fundamental behaviour of the generator, a parallel resistor (e.g. R_e) is used to adjust the reflection factor.

The reflection factor for a typical cable generator system can be estimated based on the nominal power, following [14]. The corresponding parallel resistance R_{damp} is obtained through trial. The resulting parameters are given in table 7.2.

Because the lack of data, the stator inductance L_g and resistance R_g are scaled to the power level using the following calculations. This is firstly obtain the per unit values of the characterized lab setup, as:

$$\begin{aligned}
P_N &= 7.2\,\text{kW} \\
V_{base} &= 500\,\text{V} \\
I_{base} &= \frac{P_N}{V_{base}} = \frac{7.2\,\text{kW}}{500\,\text{V}} = 14.4\,\text{A} \\
Z_{base} &= \frac{V_{base}}{I_{base}} = \frac{500\,\text{V}}{14.4\,\text{A}} = 35.7\,\Omega \\
R_{g,pu} &= \frac{R_g}{Z_{base}} = \frac{0.225\,\Omega}{35.7\,\Omega} = 6.3\,\text{m}\Omega \\
L_{g,pu} &= \frac{L_g}{Z_{base}} = \frac{2.33\,\text{mH}}{35.7\,\Omega} = 65.3\,\mu\text{H}
\end{aligned}$$

Which then in turn can be converted to the up-scaled parameters, as:

$$
\begin{aligned}
P_N &= 10\,\mathrm{MW} \\
V_{base} &= 4\,\mathrm{kV} \\
I_{base} &= \frac{P_N}{V_{base}} = 2.5\,\mathrm{kA} \\
Z_{base} &= \frac{V_{base}}{I_{base}} = \frac{4\,\mathrm{kV}}{2.5\,\mathrm{kA}} = 1.6\,\Omega \\
R_{g,up} &= R_{g,pu} \cdot Z_{base} = 6.3\,\mathrm{m\Omega} \cdot 1.6\,\Omega = 10.1\,\mathrm{m\Omega} \\
L_{g,up} &= L_{g,pu} \cdot Z_{base} = 65.3\,\mathrm{\mu H} \cdot 1.6\,\Omega = 0.101\,\mathrm{mH}
\end{aligned}
$$

Through a trial and error methodology it is found in the simulation that these stator parameters have nearly no influence on the reflection factor.

With the relation:

$$P_{mech} = T\omega, \tag{7.2}$$

the mechanical operation point of the simulation can be estimated and set. Finally the rise time is chosen to be of the same value as measured in the experimental low voltage setup. With that, all parameter, considered relevant, are selected.

L_g [mH]	R_g [mΩ]	Γ [-]	R_{damp} [Ω]
0.101	10.1	0.6	93
V_{DC} [kV]	T [kN $\cdot$ m]	ω_g [1/s]	
4	31.8	$2\pi \cdot 50$	

Table 7.2: Estimation of generator parameter for the proposed MW case and resulting operation point

With these parameters a simulation for 100m and 200m is conducted. A double pulse for both length is visualized in figure 7.1. These figures, as well as the table 7.3 seem to suggest that the waveform deterioration is in a similar range than the experimental obtained values, considering the higher voltage level and bigger conductor diameters. The lower reflection factor results in a smaller percentage of overshoot, and the higher voltage level obviously increase the absolute *dV/dt*.

Also the increased cable length increase the absolute traveling time.

Concluding it can be said, that the relative voltage overshoot decreases for the higher power level. The percentage of overshoot goes down, and thus with

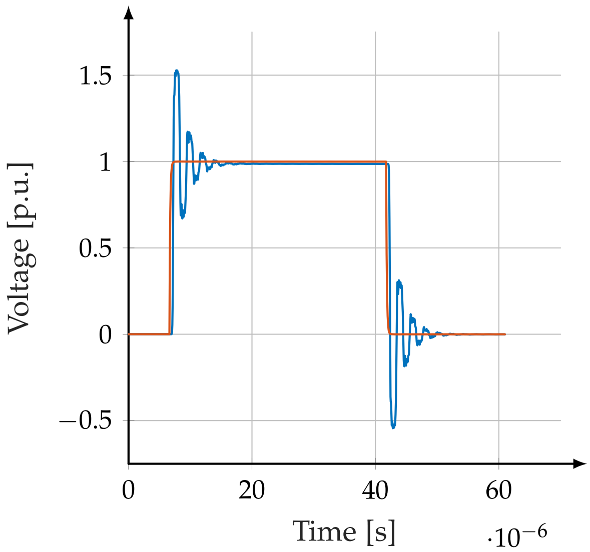

(a)

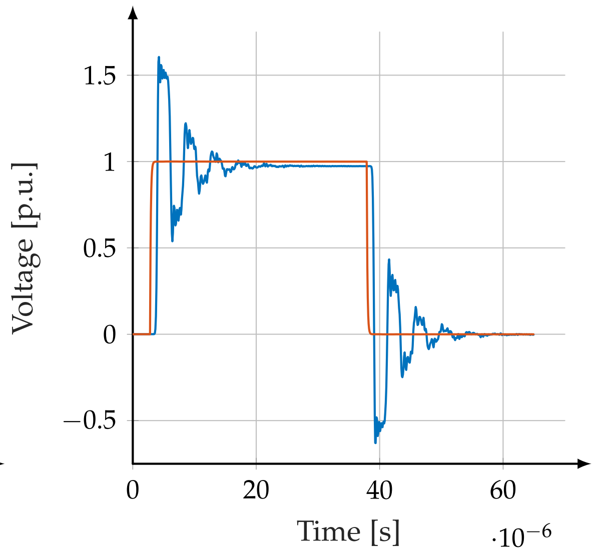

(b)

Figure 7.1: Visualization of voltage deterioration, between converter (——) and generator (——) terminals, for a MW and kV level case, and a cable length of **a)** 100 m and **b)** 200 m

Method	max(dV/dt) [V/ns]	$V_{O,abs}$ [V]	t_r [µs]
100m cable	30	6050	0.24
200m cable	19	6420	0.24

Table 7.3: Waveform quality parameter from the up-scaled model

constant rise time the rate of voltage change also decreases. The fact, that the rate of change for the 100 m cable is faster than for the 200m cable is related to the higher oscillation frequency in the shorter cable. Despite that, the shorter cable will need less filtering effort to avoid the voltage doubling effect. The fundamental waveform could not be analyzed because the simulation did not reach a usable steady state operation.

For the estimation of the cable parameter it can be said that a big variance is expected. E.g. for the experimentally validated methodology [cf. 5.1], a difference of traveling time of around 40 % between geometrical and measurement was seen. It is expected that the estimated cable parameters in this section are in a similar range. As the travelling time is directly linked to the length, the investigated 100 m and 200m can be seen as a best case - worst case scenario of a 150 m long cable.

The biggest influence of the generator on this reflection behaviour is the resulting reflection factor. The authors expect, that a medium voltage multi megawatt generator results in a even lower reflection coefficient in comparison to the here chosen. Thus, the damping is expected to be better than the here shown behaviour.

It should not be forgotten that the rise time will influence the overshoot.

7.2 Impact of a Filter

To obtain the filter parameter, again the equations 2.8, 4.8, 4.9 and 4.10 can be followed. As before, for the length a safety margin of 20% is included. this results in the two parameter sets displayed in table 7.4.

$t_{r,crit}$ and V_O [µs] and [%]	l_c [m]	L_f [µH]	C_f [nF]	R_f [Ω]
3.59 and 20	100	110	120	61
7.18 and 20	200	220	236	61

Table 7.4: Filter parameter for the Upscaled simulation

In figure 7.2 it can be seen that the filter has a similar effect on a voltage step as seen in the low voltage investigation. Thus the general behaviour is expected to be similar.

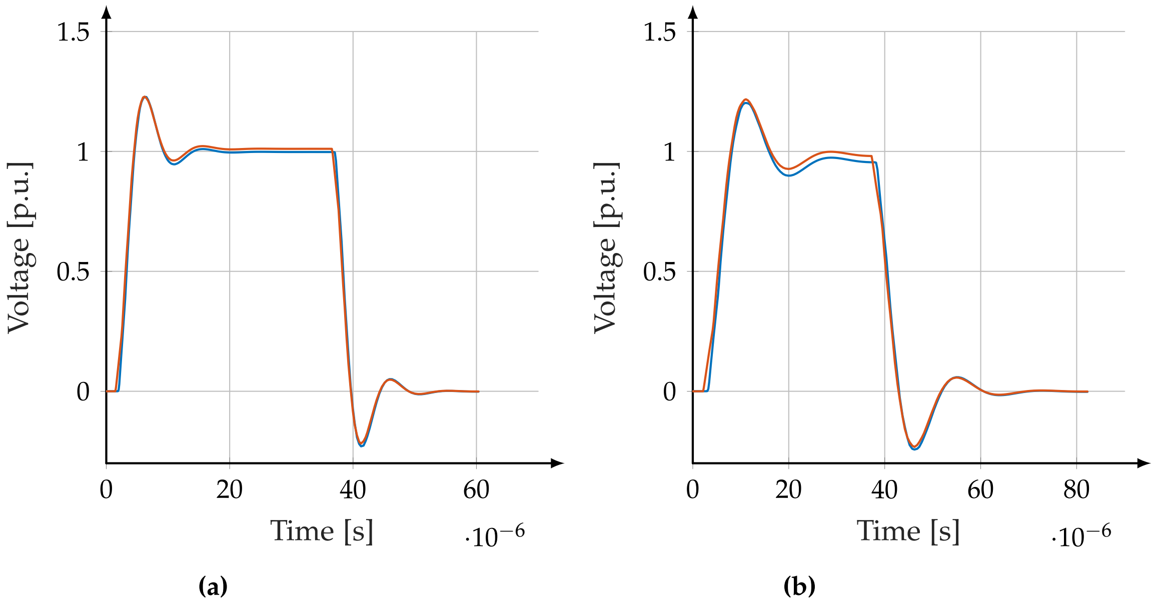

Figure 7.2: Visualization of voltage deterioration including a filter, between converter (——) and generator (——) terminals, for a MW and kV level case, and a cable length of **a)** 100 m and **b)** 200 m

Again, the characteristic parameters, to determine the voltage waveform quality can be seen in table 7.5 and a the waveform improves in the expected way.

Due to the fact that the fundamental simulation did not include control structures of any kind, it was not possible to reach steady state at a realistic fundamental

Method	max(dV/dt) [V/ns]	$V_{O,abs}$ [V]	t_r [µs]
100m cable	1.52	4850	0.24
200m cable	1.15	5110	0.24

Table 7.5: Waveform quality parameter from the up-scaled model including a filter design

frequency. Due to time limitations the control was not implemented. This leads to the facts, that the filter design could not be investigated further. The open topics include the impact on the current quality and the fundamental voltage behaviour. However, due to the presented effects of the up-scaled investigation, as well as the gained knowledge throughout the process researching this topic, the authors believe that the effect of the filter will result in a similar conclusion as for the low voltage investigation.

Overall it can be concluded, that it is expected, that the issue of voltage reflections lessens with increasing power due to the lower reflection factor. A *dV/dt* filter is needed to avoid the voltage doubling effect.

Chapter 8

Discussion

Having established the simulation model and correlated it to the experimental test setup, this section will give an overview of the discrepancies discovered throughout this process. This will include the modeling aspects, the parametrization of components, a system discussion concluding in the *dV/dt* filter implementation and the correlated waveform quality influence.

The cable model showed some variance compared to the distributed characteristics of the cable. In section 3.2.1 it was assumed that the usage of 10 model sections of the cable model is sufficient for an accurate simulation representing the range of investigation. This was validated by an impedance analysis of the implemented cable simulation. It has been seen, that including more cable sections results in additional higher frequencies behaviour. That means, the frequency response below that "cut"-frequency determined by the section number stays unaffected. Albeit, in figure 5.8 the experimentally measured cable shows in the phase plot for higher frequencies a damped behaviour, not represented in the implemented model. Despite that, by determining the bandwidth of that pulse [cf eq. 3.1], a range where the model should be accurate can be established. Considering the frame of this investigation the bandwidth was below the divergent behaviour of measurement and simulation. And, the bandwidth relates a model with 10 cable sections as sufficient.

The cable was modeled as a transmission line model modified for the high frequencies, following the suggestion of reference [39]. Fitting the component values to the experimental data with one section of the cable model yielded a good fit. Though, comparing the modified high frequency and the normal transmission line model for 10 sections a difference between those two is barley apparent [cf. figure 3.3]. While this suggests that the high frequency modification is of minor influence, the authors of this thesis concluded that higher accuracy is desirable, since the reflection is high frequency phenomenon. Although higher frequency cross couplings in a cable could not be fully excluded, it is assumed, that by best prospects the high frequency modification accounts for that.

The noticed inaccuracies of the cable model were further discussed in section 5.1.2. For the open loop model, all coupling capacitance of the cable are modeled as a line to ground representation. Though, the physical structure of the cable indicates line to line coupling capacitances. The presence of the coupling capacitance was experimentally proved. This relates to, that the simplification made for the model is only valid for line to line pulses. Since all pulses in the investigation are line to line this assumption represents the to investigated behaviour accurately. When investigating common mode currents line to line capacitances are needed and should be associated.

When investigating the cable's scalability to length, an inductive coupling between conductive elements of the line inductance of the investigated cable was experienced. This leads to an difference of inductance of approx. 20 % between short and long cable measurements. However, the influence of the coupling decreases with increasing the cable length [cf. figure 5.7]. This relates to that it is assumed to have no influence, when the parametrization measurements are conducted on a cable of sufficient length. Thus, the equations 5.1 can be used to scale the measured impedance to per meter.

Due to the pulses bandwidth, Similar considerations as to the cable model were drawn for the converter. A high frequency model was deemed necessary, because this thesis mainly investigated the high frequency ringing at the generator terminals [cf. Ch. 2].

The main simplifications used for the generator model [cf. section 5.2] are that neither iron core saturation nor the angular dependency of the stator inductance were modeled. This simplification was done, because the fundamental current does not directly influence the reflection behaviour. An observed mismatch of generator inductance between LCR-meter measurement and inductance obtained from the fundamental's current ripple [cf. eq. 5.4] could be caused by one of the two unidentified phenomena. Because a try and error analysis of the fundamental parameter suggested that the influence of this parameter is relatively small on the impedance mismatch, no further investigation was conducted.

The frequency response of the generator's impedance shows difference between fit and measurement [cf. figure 5.10]. This is due to the structure of the chosen high frequency generator model which is not compatible with the measured data. The phase shape of the measurement around 200kHz suggests that a different model type is required to described the obtained impedance measurement. Hence, it could not be verified, if the measurement can be fully trusted. However, around the pulses bandwidth reasonable data of the generator model can be extracted. A fully accurate model of the generator and thus representation of the reflection factor was not completely achieved.

Nevertheless, the reflection behaviour is operation point independent. Thus, the influence of the generator on the damping is described by the impedance mismatch between generator and cable characteristic impedance. While conducting simulations with the above explained inaccuracies, the observed reflection factor could not be obtained [cf. section 5.4]. The authors of this thesis suggest as possible reasons with descending probability:

- the previously mentioned inaccuracies of the generator model,
- the not included ac resistance,
- general inaccuracies in the model structures.

To counteract the discrepancies, the damping factor was adjusted. This was done with the modeled resistor between line and neutral point. This resistor represents the eddy current losses of the generator. Unfortunately, this does not fully represent experimental impedance measurements. However, this might compensate the established model. This is, because a damping factor with around 5 % deviation between experimental ans simulated waveforms could be obtained.

As last simplification, it needs to be mentioned, that the heavy simulation does not include any kind of control of the converter. Only a default space vector modulation, in which the rotational angle of the generator is fed as reference signal was conducted. This was done due to time constraints. The generator is connected to a mechanical torque and rotation source. That means, the operation point of the simulation is not directly adjustable and thereby dependent on extrinsic influences. This results in a different pulse distribution and fundamental current in comparison to the experimental waveforms[cf. figure 6.4]. Still, the general fundamental waveform shape can be reproduced, which makes this simulation a great and fairly accurate tool to estimate the fundamental behaviour of the setup and cable. Because of that, for pulse comparison this thesis used a separate simulation, [cf. figure 5.12].

Analyzing the implemented filter's power losses estimation, an approx. 50 % difference between measured and simulated power loss is noticeable [cf. table 6.3]. The heavy simulation was used for estimations. As said, the operation point was not controllable. This means, the fundamental operation point between simulation and experimental data differs, thus the $P_{filter,R}$ differs. Also, the equivalent series resistance of the filters' inductor and capacitor was not considered in the simulation. However, since the relative filter loss to its corresponding operation point is in a reasonable range, the filter loss estimation but also the overall simulation can be stated as an useful tool to investigate the filters effect.

In addition, it was not possible to tune a LRC-filter with power losses smaller than 0.1% which is a desirable value, especially for industrial applications [cf. Chapter 6]. The tuned filter exceeded this limit by at least 1.2 percentage points. In addition, the losses of the inductors equivalent series resistance were not even considered and should thereby be added to the calculated losses. This means, the overall losses are even higher. However, the filter losses are mostly related to the switching frequency, and not so much on the amplitude of the fundamental current [cf. section 6.2]. Thus it is expected that the filter resistor losses decrease with increasing power. Alternatively it is suggested to use more advanced filter typologies to avoid this issue.

Further, current deterioration through a long cable might influence sensorless control. This is, the location of the current noise ripple is at times in the middle of a continuing slope [cf. 5.19]. This is caused by the switching of a parallel phase. Thus, the instance of the sampling and/or switching could be controlled in such a way, that this noise does not effect the control, while considering the mean value estimate.

Else, it was also found that a filter suppresses this current noise to a similar level as in the short cable. Thereby, by protecting the generator of high stress, the current noise could be resolved [cf. section 6.3].

Finally, the question is raised, how the voltage waveform deformation has a negative impact on the generator, e.g. on the efficiency of the generator or its insulator stress. This thesis focuses mainly on the cables effect and the waveform deterioration. Thus, the analysis of the waveform quality is based on estimates of which parameter may have the biggest influence.

Due to the lack of actual data many assumptions were made to estimate the parameters of a medium voltage multi megawatt wind turbine generator arrangement [cf. Chapter 7]. Thus, the meaningfulness of the conclusion is vague. It is reasonable that the two given cases give a range of how a cable could behave. It is expected that an actual 150 m long cable behaves somewhere in the given range. An impedance measurement of a cable would greatly improve the accuracy and thereby the conclusion.

A major limitation of the up-scaling is that the fundamental waveform could not be simulated due to a constrain in the simulation. Thus, the impact of the cable on the current and the fundamental voltage could not be examined, which limits the value of the obtained results. This can be overcome by introducing a control structure into the simulation and thus improve the usability.

No experimental investigation on a medium voltage high power setup was conducted. Because the used model was developed in a low voltage - low power environment, it is uncertain if further effects will be dominant in a different environment, which is not represented by the up-scaling. This has to be considered when taking the results into account.

Chapter 9

Conclusion

Concluding this work, it can be said that this thesis succeeded its goal of investigating the impact of long cables between a generator and a converter on waveform deterioration. Thereby, with a focus on wind turbine applications investigation was based on experimental and stimulative analysis. This following chapter will give the highlights on how the goal was achieved.

Literature research guided to a transmission line model including high frequency components. The requirement was that it should represent a waves travelling time, dependent on the cable length. The cable model must thereby consider wave reflections at its points of discontinuities, as a cable end and generator terminal junction. Harmful voltage reflection does occur, when the waves travelling time is twice as fast as a pulse' rises.

Component values are parameterized based on an impedance characterization. The establishment of a high frequency cable and as generator model with the parameters was successful. By impedance fitting of the investigated cable the traveling time could be calculated to an accuracy of 0.7% in comparison to the experimentally measured. Thus it can be said that the cable behaviour is modeled very accurately by it self.
The cable model is scalable to length. For a very short cable a not quantified influence is seen, introducing an 20% error when scaling the line inductance between the two measured lengths.

The interaction of system components by means of the reflection factor could be modeled with an 5 % error compared to the experimental extracted reflection factor. This result is in correspondence with the noticed inaccuracies of the generator modeling. Calculating the reflection factor theoretically based on the characteristic impedance resulted in Similar results.

Generator stress is quantified with waveform quality considering max(*dV/dt*), the rise time and overshoot.

A cable exceeding the critical length with respect to a travelling-rise time relation increases the stress level experienced by the generator. For the measured setup, an overvoltage of 1.75 p.u. and an increase of max(*dV/dt*) of 1.8 is noticed.

However, the long cable introduced also high frequency ringing in the current waveform. It was observed, that this ringing is located at a typical sampling instance for sensorless generator control. It was further observed, that the peak of the ringing of the investigated setup can have a magnitude of up to 40 % above the mean value. Thus the long cable could introduce disturbances for the control performance, if the issue is not addressed.

To counter this unwanted behaviour, a filter was introduced. Besides the fact that the power losses in the introduced filter were not economical, it was possible to limit the overvoltage by 57% leading to 1.2 p.u. overshoot. It needs to be pointed out, that the remaining overshoot is related to the damped resonance behaviour of the LRC filter.

It was noticed, that the filer with a long cable also suppressed the current ripple to a similar level as operating the system with the short cable.

Also, with the implemented filter the fastest rate voltage change could be slowed down to 0.265 V/ns, which is beneath the typical suggested limit of 0.500 V/ns to ensure the longevity of the generator insulation. The filter improves the waveform quality again to a level where it is similar or better as the system operated with a short cable.

In the end it is was possible to estimate parameters for an expected future application of long generator cables in a medium voltage multi mega watt environment. The expected behavior was analyzed for two different length (100m and 200m), which can be seen as borderline results for a 150m cable. Thus the expected impact of a long cable on the generator is given. With this information the simple LCR - filter was tuned, to give an estimate of how much filtering would be required to suppress the voltage doubling effect. Even though the estimates are vague, it is assumed that a *dV/dt* filter has a similar effect as in the low voltage environment.

In general it can be said: long cables introduce negative effects in a converter - cable - generator system. These effects can be well described and was throughout the process very predictable. The initial unknown filtering effort can be concluded, as: slowing down the pulses' rise time has a suppressed effect on the overvoltage, and thus the introduced problem is avoided. Therefore, in the scope of this thesis, the authors conclude that the converter stage of a wind turbine can be moved down tower.

Finally it is proposed for future work, that a control structure needs to be included into the simulation to fix an operation point. This would greatly improve the usability of the simulation, especially for the analysis of filter losses and the change of nominal power.

Further analysis of influence of the waveform deterioration on the generator insulation stress and efficiency would give further insight on a desirable filter size.

To enrich the conclusions, especially on harmful stress on the generator windings and filter design, further determination of common mode paths should be investigated.

Bibliography

[1] ABB Drives. Technical Guide No. 5 - Bearing Currents in Modern AC Drive Systems, 2011. URL http://www05.abb.com/global/scot/scot201.nsf/veritydisplay/8c253c2417ed0238c125788f003cca8e/$file/abb_technical_guide_no5_revc.pdf.

[2] ABB Wind. Low voltage wind turbine converter ACS880, 800 kW – 8 MW, 0.

[3] ABB Wind. PCS6000 wind turbine converter - Medium voltage, full power converter, up to 12 MW, 2016.

[4] ABB Wind. ACS880-87LC-4000A / 4132A-7 wind turbine converters Hardware manual, 2018.

[5] Ali Ahmed Adam and Kayhan Gulez. High frequency modeling of PMSM connected to long cable. In *SICE Annual Conference 2007*, pages 1662–1669. IEEE, 9 2007. ISBN 978-4-907764-27-2. doi: 10.1109/SICE.2007.4421251. URL http://ieeexplore.ieee.org/document/4421251/.

[6] Alstom. Haliade 150-6MW Overview, 2014. URL http://pdf.archiexpo.com/pdf/alstom/haliade-150-6mw/88574-242448.html.

[7] B. Basavaraja and D.V.S.S.Siva Sarma. Application problem of PWM AC drives due to long cable length and high dv/dt. In *2006 International Conference on Power Electronic, Drives and Energy Systems*, pages 1–6. IEEE, 12 2006. ISBN 0780397711. doi: 10.1109/PEDES.2006.344380. URL https://ieeexplore.ieee.org/document/4147875/.

[8] C. Batunlu and A. Albarbar. Strategy for enhancing reliability and lifetime of DC-AC inverters used for wind turbines. *Microelectronics Reliability*, 85 (April):25–37, 2018. ISSN 00262714. doi: 10.1016/j.microrel.2018.04.006. URL https://doi.org/10.1016/j.microrel.2018.04.006.

[9] Frede Blaabjerg and Ke Ma. Future on power electronics for wind turbine systems. *IEEE Journal of Emerging and Selected Topics in Power Electronics*, 1(3): 139–152, 2013. ISSN 21686785. doi: 10.1109/JESTPE.2013.2275978.

[10] Frede Blaabjerg, Marco Liserre, and Ke Ma. Power Electronics Converters for Wind Turbine Systems. *IEEE Transactions on Industry Applications*, 48(2): 708–719, 3 2012. ISSN 0093-9994. doi: 10.1109/TIA.2011.2181290. URL `http://ieeexplore.ieee.org/document/6112212/`.

[11] A.H. Bonnett. Analysis of the impact of pulse-width modulated inverter voltage waveforms on AC induction motors. *IEEE Transactions on Industry Applications*, 32(2):386–392, 1996. ISSN 00939994. doi: 10.1109/28.491488. URL `http://ieeexplore.ieee.org/document/491488/`.

[12] Fernando Briz, David Diaz-Reigosa, Michael W. Degner, Pablo Garcia, and Juan Manuel Guerrero. Current sampling and measurement in PWM operated AC drives and power converters. In *The 2010 International Power Electronics Conference - ECCE ASIA -*, pages 2753–2760. IEEE, 6 2010. ISBN 978-1-4244-5394-8. doi: 10.1109/IPEC.2010.5543175. URL `http://ieeexplore.ieee.org/document/5543175/`.

[13] Filipe Faria da Silva and Claus Leth Bak. *Electromagnetic Transients in Power Cables*. Power Systems. Springer, London, 4th edition, 2013. ISBN 978-1-4471-5235-4. doi: 10.1007/978-1-4471-5236-1. URL `http://link.springer.com/10.1007/978-1-4471-5236-1`.

[14] Danfoss. Output Filters Design Guide, 2011. URL `http://files.danfoss.com/download/Drives/doc_MG90N502.pdf`.

[15] Delta Electronics. Delta Wind Turbine Converter, 0. URL `https://www.deltaelectronicsindia.com/wp-content/uploads/2018/11/Delta_wind_turbine_introduction.pdf`.

[16] Enercon. Enercon Grid Technology, 0. URL `https://www.enercon.de/en/technology/grid-technology/`.

[17] Enercon. ENERCON wind energy converters Technology & Service, 2010. URL `http://www.enercon.de/p/downloads/EN_Eng_TandS_0710.pdf`.

[18] S. Faulstich, B. Hahn, and P. J. Tavner. Wind turbine downtime and its importance for offshore deployment. *Wind Energy*, 14(3):327–337, 4 2011. ISSN 10954244. doi: 10.1002/we.421. URL `http://doi.wiley.com/10.1002/we.421`.

[19] FeCon GmbH. FEC1900 - HIGH EFFICIENCY 1900 KVA BACK-TO-BACK CONVERTER, 0. URL `https://www.wstech.com/en/products/wind-technologies`.

[20] Camila C. Flavio, Vitor R. Diab, Charles Bruno C. Assuncao, and Alessandro F. Moreira. PSCAD/EMTDC® model for overvoltage and common mode current analysis in PWM motor drives. In *2010 9th IEEE/IAS International Conference on Industry Applications - INDUSCON 2010*, pages 1–6. IEEE, 11 2010. ISBN 978-1-4244-8008-1. doi: 10.1109/INDUSCON.2010.5739978. URL `http://ieeexplore.ieee.org/document/5739978/`.

[21] Freqcon. NGC-Wind, 0. URL `https://www.freqcon.com/products/wind-energy/power-converter-ngc-wind/`.

[22] Marcelo Gustavo and Juan Gimenez. Technical and Regulatory Exigencies for Grid Connection of Wind Generation. In *Wind Farm - Technical Regulations, Potential Estimation and Siting Assessment*. InTech, 6 2011. ISBN 9783834814609. doi: 10.5772/16474. URL `http://www.intechopen.com/books/wind-farm-technical-regulations-potential-estimation-and-siting-assessment/technical-and-regulatory-exigencies-for-grid-connection-of-wind-generation`.

[23] T.G. Habetler, Rajendra Naik, and T.A. Nondahl. Design and implementation of an inverter output LC filter used for dv/dt reduction. *IEEE Transactions on Power Electronics*, 17(3):327–331, 5 2002. ISSN 0885-8993. doi: 10.1109/TPEL.2002.1004240. URL `http://ieeexplore.ieee.org/document/1004240/`.

[24] Berthold Hahn, Michael Durstewitz, and Kurt Rohrig. Reliability of Wind Turbines. In *Wind Energy*, pages 329–332. Springer Berlin Heidelberg, Berlin, Heidelberg, 2007. ISBN 3540338659. doi: 10.1007/978-3-540-33866-6{_}62. URL `http://link.springer.com/10.1007/978-3-540-33866-6_62`.

[25] Siegfried Heier. *Grid Integration of Wind Energy - Onshore and Offshore Conversoin Systems*. Wiley, 3rd edition, 2014. ISBN 9781119962946.

[26] Ingeteam Power Technology S.A. READY FOR YOUR LCoE OPTIMIZATION, 2018.

[27] Florin Iov and Frede Blaabjerg. Power electronics and control for wind power systems. In *2009 IEEE Power Electronics and Machines in Wind Applications*, pages 1–16. IEEE, 6 2009. ISBN 978-1-4244-4935-4. doi: 10.1109/PEMWA.2009.5208339. URL `http://ieeexplore.ieee.org/document/5208339/`.

[28] Md Rabiul Islam, Youguang Guo, and Jianguo Zhu. A review of offshore wind turbine nacelle: Technical challenges, and research and developmental trends. *Renewable and Sustainable Energy Reviews*, 33:161–176, 5 2014. ISSN 13640321. doi: 10.1016/j.rser.2014.01.085. URL `https://linkinghub.elsevier.com/retrieve/pii/S1364032114001087`.

[29] Jenkins, O'Malley, Fox, Bryans, Anaya-Lara, Milborrow, Watson, and Flynn. *Wind Power Integration: Connection and system operational aspects*, volume 12. Institution of Engineering and Technology, 1 2007. ISBN 9780863414497. doi: 10.1049/PBPO050E. URL https://digital-library.theiet.org/content/books/po/pbpo050e.

[30] Kabeltec GmbH. Technical data - Control Cables 2XSLCHK-J 3PLUS VFD, 2013. URL https://www.kabeltec.de/templates/cable_detail_pdf.php/2XSLCHK-J3PLUSVFD.pdf?cableid=666&lang=_en&color=FFC109&firstdata=&seconddata=497423921-0&thirddata=kabeltec@kabeltec.de.

[31] R Kerkman, D Leggate, and G Skibinski. Interaction of drive modulation and cable parameters on AC motor transients. In *IAS '96. Conference Record of the 1996 IEEE Industry Applications Conference Thirty-First IAS Annual Meeting*, volume 1, pages 143–152. IEEE, 1996. ISBN 0-7803-3544-9. doi: 10.1109/IAS.1996.557008. URL http://ieeexplore.ieee.org/document/557008/.

[32] Fried Lauha, Shukla Shruti, Sawyer Steve, and Teske Sven. Global Wind Energy Outlook 2016, 2016. URL http://www.apren.pt/fotos/newsletter/conteudos/globalwindenergyoutlook2016_1483545282.pdf.

[33] Jaroslaw Luszcz. Modeling of common mode currents induced by motor cable in converter fed AC motor drives. In *2011 IEEE International Symposium on Electromagnetic Compatibility*, pages 459–464. IEEE, 8 2011. ISBN 978-1-4577-0812-1. doi: 10.1109/ISEMC.2011.6038355. URL http://ieeexplore.ieee.org/document/6038355/.

[34] J. F. Manwell, J. G. McGowan, and A. L. Rogers. *Wind Energy Explained*. John Wiley & Sons, Ltd, Chichester, UK, 12 2009. ISBN 9781119994367. doi: 10.1002/9781119994367. URL http://doi.wiley.com/10.1002/9781119994367.

[35] R. Mini, S. R. Resna, and M. N. Dinesh. LC clamp filter for voltage reflection due to long cable in induction motor drives. In *2014 Annual International Conference on Emerging Research Areas: Magnetics, Machines and Drives (AICERA/iCMMD)*, pages 1–6. IEEE, 7 2014. ISBN 978-1-4799-5202-1. doi: 10.1109/AICERA.2014.6908272. URL http://ieeexplore.ieee.org/lpdocs/epic03/wrapper.htm?arnumber=6908272.

[36] Ned Mohan, Tore M. Undeland, and William P. Robbins. *Power Electronics: Converters, Applications, and Design*. Wiley, 3rd edition, 2002. ISBN 9780471226932.

[37] A.F. Moreira, T.A. Lipo, Giri Venkataramanan, and Steffen Bernet. High-frequency modeling for cable and induction motor overvoltage studies in

long cable drives. *IEEE Transactions on Industry Applications*, 38(5):1297–1306, 9 2001. ISSN 0093-9994. doi: 10.1109/TIA.2002.802920. URL http://ieeexplore.ieee.org/document/1035183/.

[38] Alessandro F. Moreira, Thomas A. Lipo, and Giri Venkataramanan. Modeling and Evaluation of dv / dt Filters for AC Drives with High Switching Speed. In *9th European Conference on Power Electronics and Applications*, pages 1–14, 2001. ISBN 1608265382.

[39] Alessandro F. Moreira, Thomas A. Lipo, Giri Venkataramanan, and Steffen Bernet. High-frequency modeling for cable and induction motor overvoltage studies in long cable drives. *IEEE Transactions on Industry Applications*, 38(5): 1297–1306, 2002. ISSN 00939994. doi: 10.1109/TIA.2002.802920.

[40] Erik Persson. Transient effects in application of PWM inverters to induction motors. In *Conference Record of 1991 Annual Pulp and Paper Industry Technical Conference*, pages 228–233. IEEE, 1991. doi: 10.1109/PAPCON.1991.239644. URL http://ieeexplore.ieee.org/document/239644/.

[41] Plexim. Plecs The Simulation Platform for Power Electronic Sustems - User Manual Version 4.2, 2002. URL http://www.plexim.com.

[42] J.A. Pomilio, C.R. de Souza, L. Matias, P.L.D. Peres, and I.S. Bonatti. Driving AC motors through a long cable: the inverter switching strategy. *IEEE Transactions on Energy Conversion*, 14(4):1441–1447, 1999. ISSN 08858969. doi: 10.1109/60.815087. URL http://ieeexplore.ieee.org/document/815087/.

[43] Hans-Joachim Pöss and Gary Van Schaick. Overcoming Motor Bearing Failures in AC Motor Drive Systems, 2014. URL http://www.coolblue-mhw.com/wp-content/uploads/2014/09/Overcoming-Motor-Bearing-Failures-in-AC-Motor-Drive-Systems.pdf.

[44] Uha Pyrhöonen, Valeria Hrabovcova, and Scott Semken. *Electrical Machine Drives Control - An Introduction*. Wiley, 2016. ISBN 9781119260448.

[45] D Rendusara and P. Enjeti. A method to reduce common mode and differential mode dv/dt at the motor terminals in PWM rectifier/PWM inverter type adjustable speed drive systems. In *APEC '98 Thirteenth Annual Applied Power Electronics Conference and Exposition*, volume 2, pages 1010–1016. IEEE, 1998. ISBN 0-7803-4340-9. doi: 10.1109/APEC.1998.654021. URL http://ieeexplore.ieee.org/document/654021/.

[46] Joseph Salvatore. *World Energy Perspective - Cost of Energy Technologies*. World Energy Council Regency House, 2013. ISBN 9780946121304.

[47] Osman Selcuk Senturk. *High Power Density Power Electronic Converters for Large Wind Turbines*. PhD thesis, Aalborg University, 2011. URL `http://vbn.aau.dk/files/58604347/osman_selcuk_senturk.pdf`.

[48] Siemens. Simodrive & Masterdrives, 2005. URL `https://cache.industry.siemens.com/dl/files/289/28708289/att_2592/v1/PFT6_1005_en.pdf`.

[49] Siemens AG. Portfolio Wind Equipment. *Order no: E20001-A110-P550-X-7600*, 2013.

[50] Siemens Gamesa. Ertragsoptimierte Betriebsstrategien im virtuellen Kraftwerk, 0. URL `http://spreewind.de/windenergietage/wp-content/uploads/sites/4/2018/01/26WT0911_F11_0935_ABE_SGRE.pdf`.

[51] Siemens Gamesa. Wind Farms, 2016.

[52] Michal Sztykiel. *High Voltage Power Converter for Large Wind Turbine*. PhD thesis, Aalborg University, 2014. URL `http://vbn.aau.dk/files/202390929/michal_sztykiel.pdf`.

[53] The Switch. FPC+ 1000 – 7500 kW, 2015.

[54] Vensys Energy AG. VENSYS Energy AG: Full-power Converter, 0. URL `https://www.vensys.de/en/technology/full-power-converter/`.

[55] A. von Jouanne and P. Enjeti. Design considerations for an inverter output filter to mitigate the effects of long motor leads in ASD applications. In *Proceedings of Applied Power Electronics Conference. APEC '96*, volume 2, pages 579–585. IEEE, 1996. ISBN 0-7803-3044-7. doi: 10.1109/APEC.1996.500499. URL `http://ieeexplore.ieee.org/document/500499/`.

[56] A. von Jouanne and P.N. Enjeti. Design considerations for an inverter output filter to mitigate the effects of long motor leads in ASD applications. *IEEE Transactions on Industry Applications*, 33(5):1138–1145, 1997. ISSN 00939994. doi: 10.1109/28.633789. URL `http://ieeexplore.ieee.org/document/633789/`.

[57] A. von Jouanne, P. Enjeti, and W. Gray. Application issues for PWM adjustable speed AC motor drives. *IEEE Industry Applications Magazine*, 2(5):10–18, 1996. ISSN 10772618. doi: 10.1109/2943.532149. URL `http://ieeexplore.ieee.org/document/532149/`.

[58] A. von Jouanne, D.A. Rendusara, P.N. Enjeti, and J.W. Gray. Filtering techniques to minimize the effect of long motor leads on PWM inverter-fed AC motor drive systems. *IEEE Transactions on Industry Applications*, 32(4):919–926,

1996. ISSN 00939994. doi: 10.1109/28.511650. URL http://ieeexplore.ieee.org/document/511650/.

[59] Peng Wang, Jinquan Li, Jian Wang, Andrea Cavallini, and Jiawei Zhang. A high voltage repetitive square wave voltage generator used for endurance evaluation of inverter-fed motors. In *2017 International Symposium on Electrical Insulating Materials (ISEIM)*, pages 411–414. IEEE, 9 2017. ISBN 978-4-88686-099-6. doi: 10.23919/ISEIM.2017.8088772. URL http://ieeexplore.ieee.org/document/8088772/.

[60] D. J. Willis, C. Niezrecki, D. Kuchma, E. Hines, S. R. Arwade, R. J. Barthelmie, M. DiPaola, P. J. Drane, C. J. Hansen, M. Inalpolat, J. H. Mack, A. T. Myers, and M. Rotea. Wind energy research: State-of-the-art and future research directions. *Renewable Energy*, 125:133–154, 2018. ISSN 18790682. doi: 10.1016/j.renene.2018.02.049. URL https://doi.org/10.1016/j.renene.2018.02.049.

[61] Windpowerengineering. GE MV700, 0. URL https://www.windpowerengineering.com/business-news-projects/ge-provide-5-gw-converters-support-chinas-offshore-wind-market/.

[62] Woodward Kempen GmbH. Concycle - Frequency converters for wind turbines, 0. URL www.woodward.com.

[63] Bin Wu, Yongqiang Lang, Navid Zargari, and Samir Kouro. *Power Conversion and Control of Wind Energy Systems . IEEE Press Series on Power Engineering*. John Wiley & Sons, Inc., Hoboken, New Jersey, 2011. ISBN 9780470593653.

[64] Venkata Yaramasu, Bin Wu, Paresh C. Sen, Samir Kouro, and Mehdi Narimani. High-power wind energy conversion systems: State-of-the-art and emerging technologies. *Proceedings of the IEEE*, 103(5):740–788, 5 2015. ISSN 0018-9219. doi: 10.1109/JPROC.2014.2378692. URL http://ieeexplore.ieee.org/document/7109820/.

[65] Mikel Zabaleta, Eduardo Burguete, Danel Madariaga, Ignacio Zubimendi, Markel Zubiaga, and Igor Larrazabal. LCL grid filter design of a multimegawatt medium-voltage converter for offshore wind turbine using SHEPWM modulation. *IEEE Transactions on Power Electronics*, 31(3):1993–2001, 2016. ISSN 08858993. doi: 10.1109/TPEL.2015.2442434.

Appendix A

Evolving Component Placement in wind turbines

While researching the arrangement, it was only to a certain extend possible to extract the arrangement of the WTG manufacturers. On the other hand, the converter manufacturer were more informative. This can also be seen in the comprehensiveness of the following tables.

Converter Manufactureres	Type	Converter Type	Converter Location	Generator Voltage [V]	Grid Voltage [V]	Filter	[kV/µs]	Implemented in:	References
ABB	ACS880	FS (PMSG, IG)	Tower or Nacelle	0-750	525 -690	dV/dt	1.0 - 1.4	-	[2, 4]
ABB	PCS 6000	FS (PMSG, IG)	Tower base	0-3400 and 0-4300	3300 and 4160	dV/dt	< 1.5	-	[3]
The Switch	FPC+ 1000 - 7000 kW	FS (PMSG, IG)	Tower or Nacelle	-	690	-	-	-	[53]
Delta Electronics	-	FS (EESG)	tower base or nacelle	-	-	dV/dt	-	XE93-2?	[15]
Delta Electronics	-	FS (IG)	tower base or nacelle	-	-	dV/dt	-	XE93-2?	[15]
GE	MV7000	FS (PMSG, IG)	-	-	0-3300 and 0-6600	for 3.3kV dV/dt optional	(l_c [50-200]m; oth. on requ.)	-	[61]
Siemens AG	LOHER Dynavert XL	FS (IG, Direct drive, SG)	Nacelle	-	690	-	-	-	[49]
Siemens AG	SINAMICS	FS (IG, Direct drive, SG)	-	-	-	-	-	-	
Woodward	Concycle	FS (PMSG, EESG, SCIG)	Tower or Nacelle	-	690	-	-	-	[62]
Freqcon	NGC-Wind	FS (PMSG, Direct drive, SG)	-	-	-	-	-	-	[21]
Fecon	FEC1900 (...650, 1150, 1300, 1600)	FS (PMSG, EESG)	Tower base?	-	1550	dV/dt	-	-	[19]
Ingeteam	FS LV 100-10000	FS (PMSG, EESG, IG)	-	-	690	dV/dt	<1	Gamesa & Acciona? 2015	[26]
Ingeteam	FS MV 3000-15000	FS (PMSG, EESG, IG)	Tower or Nacelle	-	3000	dV/dt	1.5 (other on request)	Gamesa Acciona? (2015)	[26]

Table A.1: Wind turbine converter placement sorted by converter manufacturer

Producer	WT - Type	Gear box	Maschine type	Converter loc.	Converter Manufacturer	Converter type	Transformer loc.	Voltages [V]	Hub Heigths [m]	Reference
Siemens Gamesa	SWT-DD-x	No	PMSG - direct drive	Nacelle	-	-	Nacelle	690	-	[50]
Siemens Gamesa	SG 7.0-154 DD	No	PMSG - direct drive	Nacelle	-	-	Nacelle	690	-	[51]
GE wind (former Alstom)	Haliade	No	PMSG - direct drive	tower base	(Alstom?Needs to be checked)	3 * three full-power converters	tower base	900	100 (or site-specific)	[6]
GE wind	2.5MW	-	-	tower base	-	-	-	-	-	-
GE wind	1.5MW	-	-	Tower base	-	-	-	-	-	-
Enercon	All types	No	IG - direct drive	Rectivier - top, Inverter Bottom	Bottom	-	-	-	-	[1 17]
Vensys	All types (representative Vensys 115)	No	PMSG - direct drive	Tower base	Woodward? Needs to be checked	Tower base	-	-	-	[54]

Table A.2: Wind turbine converter placement sorted by WTG manufacturer

Appendix B

Visualization of IEC's Rise Time Definition

The rise time is defined by IEC to the time required for the voltage to rise from 10% to 90% of the peak voltage. This thesis follows this definition.

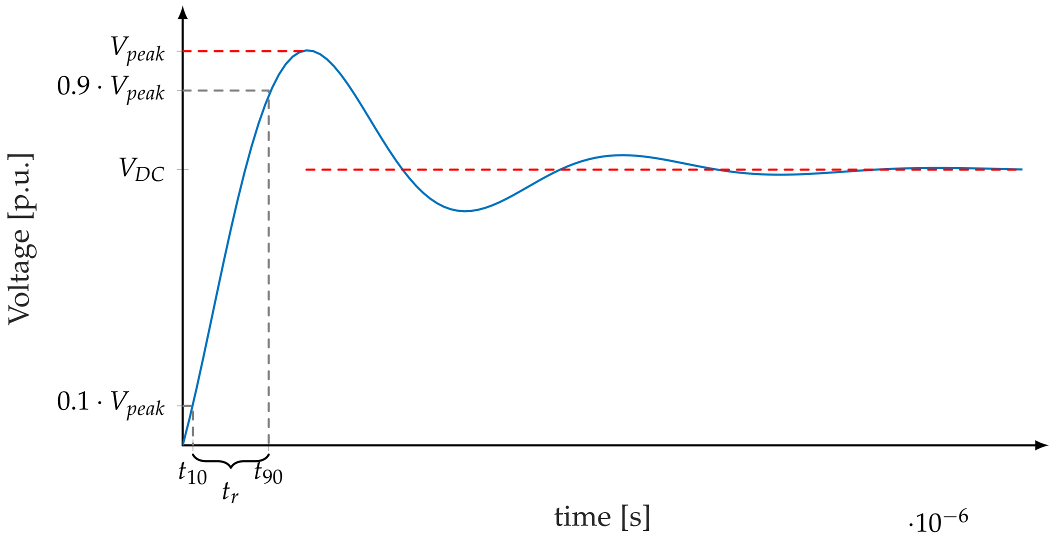

Figure B.1: Visualized definition of rise time t_r following IEC standard

Appendix C

Laboratory setup specifications

In this chapter all information about the used lab setup is displayed, including al component specifications.

C.1 Induction Machine (IM)

Manufacturer	ABB Motors	3~ Motor	
Serial number	MTM100LB28-4 V290-50A		
Voltage	400Y / 230D V	Nominal Power	2.2 kW
Frequency	50Hz	Nominal current	4.7/ 8.1 A
Rotational speed	1450 /min	Power factor	0.80

Table C.1: Name plate information of IG

C.2 Permanent Magnet Synchronous Generator (PMSG)

Manufacturer	Siemens	3~Brushless Servomotor	
Serial number	1FT6084-8SH71-1AA0		
I_N (at 100 K)	24.5 A	M_N (at 100 K)	20.0 Nm
I_0 (at 60/100 K	22.7/28 A	M_0 (at 60/100 K	21.6/26 Nm
n_{max}	7100/min	n_N,n_{opt}	4500/min
P_N	9.4 kW	U_{IN}	281 VY
n_{pp}	4	J	4.8 $\cdot 10^{-3}$kgm^2
Additional Elements			
Optical Encoder	B01 2048 S/R KTY84		
Blower	2CW 1332 1-230V 0.28/0.24 A 50/60Hz		
Machine Parameters:			
L_d, L_q	2 mH	R_{ph}	0.18 Ω
λ_{mpm}	0.123 Wb	J_{synch}	0.0158 kg $\cdot$ m^2

Table C.2: Name plate information PMSG [48]

C.3 Active rectifier (module for IM and PMSG)

Manufacturer	Danfos	AutomationDrive FC302	
Nominal Power	15 kW / 20 HP	Nominal Voltage	400 / 480V
Input:		Nominal Voltage	3*380-500V
Frequency	50/60 Hz	Max. current	20/25A
Output:		Voltage	0-Vin
Frequency	0 - 1000Hz	Max. current	20 / 27 A

Table C.3: Name plate information active rectifier

C.4 Inverter

Manufacturer	Siemens	Rectifier/Regenerating Unit	
Order Number	6SE7028 – 6EC85 – 1AA0		
Type	D380 – 460 – G510 – 620/?? CRUFO		
Operation Mode	Kl. I (Kl.II 78A)	Production State	A2
Input		Voltage	3AC 380 – 460V
Frequency	50/60 Hz	current	74/ 82A
Output		Voltage	DC 510 - 620V
current	86A		

Table C.4: Caption

Appendix D

Schematics of Conducted LCR-meter measurements

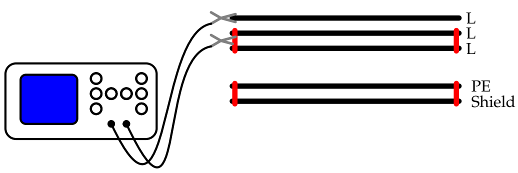

Figure D.1: Measurement setup for open circuit measurements

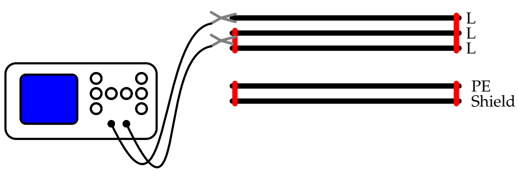

Figure D.2: Measurement setup for short circuit measurements

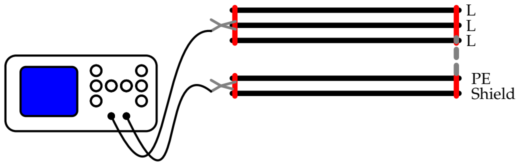

Figure D.3: Three phases to ground measurement. The gray, dashed line indicates the connection for the short circuit measurement

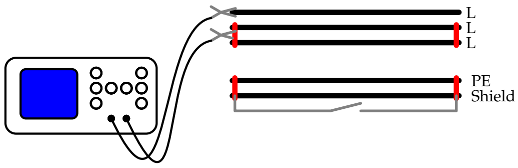

Figure D.4: 2 lines in parallel, one as return path with ground + shield short circuited(gray)

Appendix E

Equations following Reference

Those equations of [39] are presented in the appendix for the sake of completeness. Throughout the process of this thesis, the authors observed an incompleteness of the OC circuit components. The author of the paper did not respond upon asking for typo or incompleteness.

$$
\begin{aligned}
R_s^{'} &= \frac{2}{3} Real\{Z_{sc}^{'}\}_{f_{low}} && \text{(E.1a)} \\
L^{'} &= \frac{2}{3} Imag\{Z_{sc}^{'}\}_{f_{high}} && \text{(E.1b)} \\
R_{p1}^{'} &= 2\left(Real\{Z_{oc}^{'}\}_{f_{low}}\right)\left[\left(\frac{Imag\{Z_{oc}^{'}\}_{f_{low}}}{Real\{Z_{oc}^{'}\}_{f_{low}}}\right)^2 + 1\right] && \text{(E.1c)} \\
R_{p2}^{'} &= 2\left(Real\{Z_{oc}^{'}\}_{f_{high}}\right)\left[\left(\frac{Imag\{Z_{oc}^{'}\}_{f_{high}}}{Real\{Z_{oc}^{'}\}_{f_{high}}}\right)^2 + 1\right] && \text{(E.1d)} \\
C_{p1}^{'} &= \left[\left(2\pi f_{low}\right)\left(\frac{Real\{Z_{oc}^{'}\}_{f_{low}}}{Imag\{Z_{oc}^{'}\}_{f_{low}}}\right) R_{p1}\right]^{-1} && \text{(E.1e)} \\
C_{p2}^{'} &= \left[\left(2\pi f_{high}\right)\left(\frac{Real\{Z_{oc}^{'}\}_{f_{high}}}{Imag\{Z_{oc}^{'}\}_{f_{high}}}\right) R_{p2}\right]^{-1} && \text{(E.1f)} \\
& && \text{(E.1g)}
\end{aligned}
$$

Appendix F

Measurement Results

F.1 Converter behaviour

In table F.1 the measured rise and fall time for different operations modes are documented. The sampling time of the used oscilloscope is $1e-9s$. It can be seen, that the fall time of the different pulses stay very constant for the different operation conditions. It also seems like the Rise time is mostly dependent on the Torque, or on the current throught the IGBT. The measured pulses for low rotational speeds (10Hz) did not reach full voltage amplitude in the recorded data. Because of that the values were not comparable.

Rotor speed (Hz)	Torque (Nm)	Rise time (μs)	Fall time (μs)
10	5	NaN	NaN
10	10	NaN	NaN
30	5	0.472	0.23
30	10	0.330	0.240
50	5	0.447	0.230
50	10	0.323	0.230

Table F.1: Comparison of rise and fall time of converter pulses for different operation points

Appendix G

Images of the Laboratory Setup

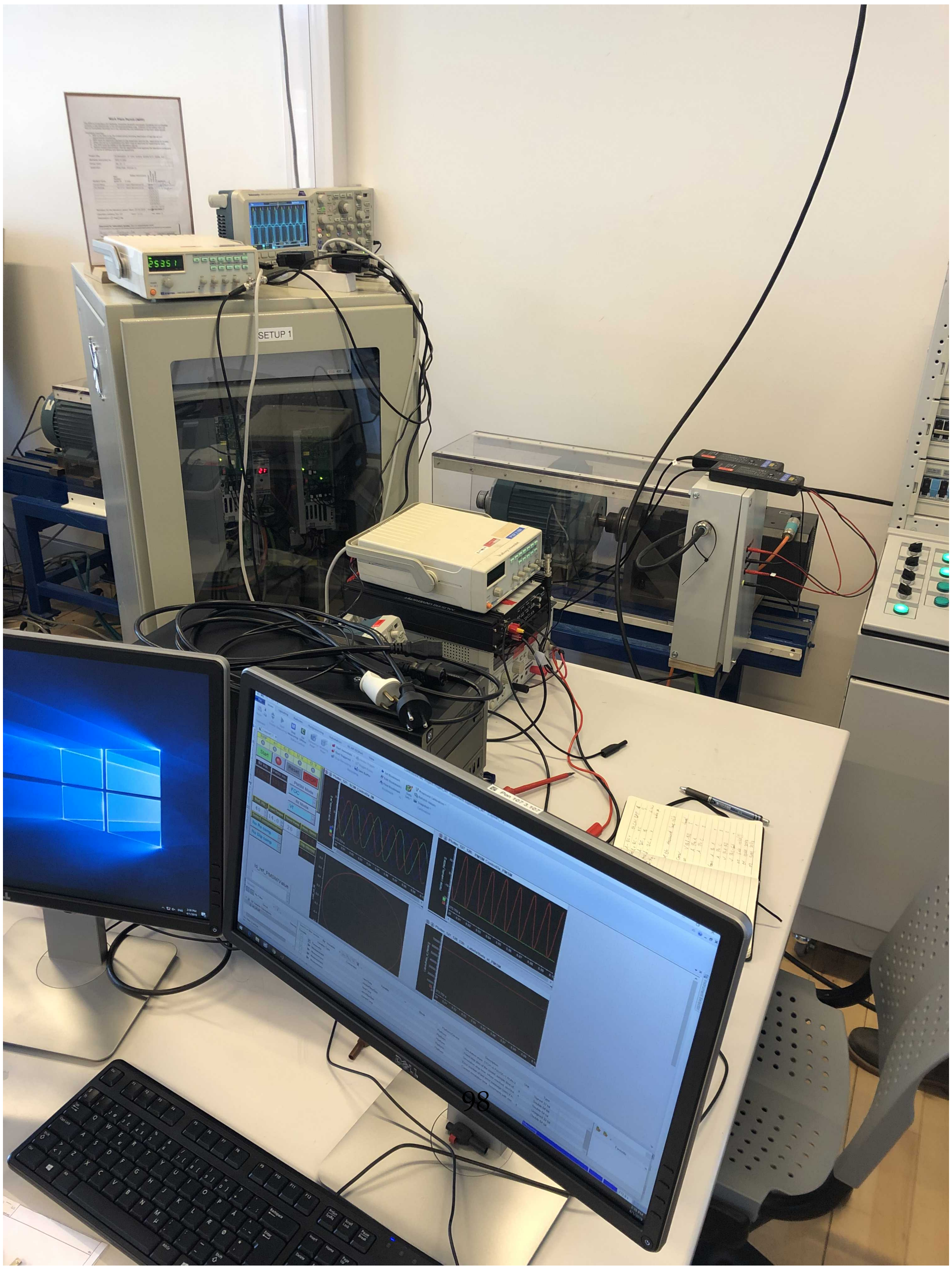

Figure G.1: Overview of laboratory setup with measurement box at lower right corner

Figure G.3: Cable routing return path

Figure G.2: 40 m cable routing around laboratory

Figure G.4: Switching Cabinet

Figure G.5: Converter Cabinet

Figure G.6: Lem Box connection at converter side

Figure G.7: Bidirectional converter supplying all setups in drive lab

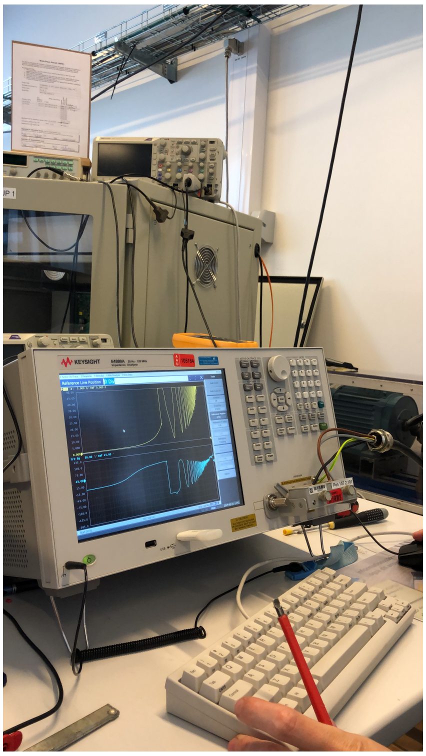

Figure G.8: Cable LRC-meter Measurement

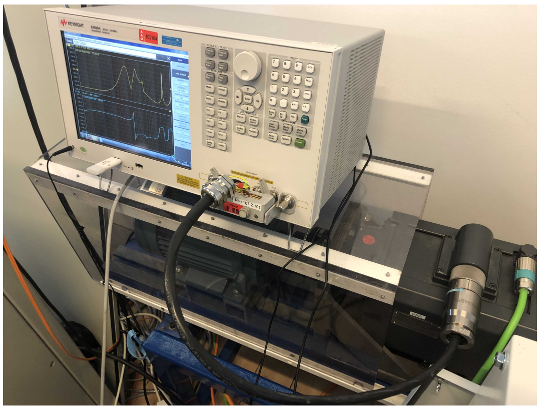

Figure G.9: Generator LRC-meter Measurement

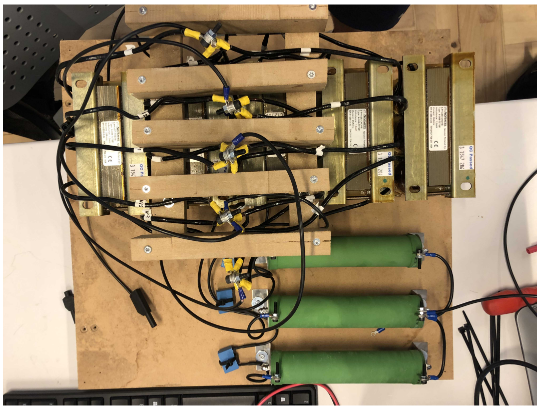

Figure G.10: Implemented filter - topview LRC

Figure G.11: LRC filter implemented into converter Cabinet

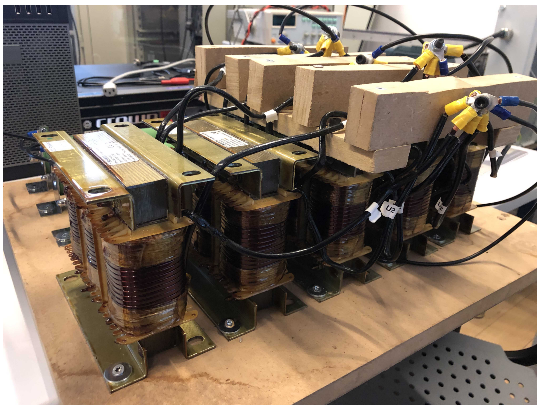

Figure G.12: 5 parallel 600 mH inducotors making 120 mH